A STUDY OF THE USE OF VIBRATION AND STRESS WAVE SENSING FOR THE DETECTION OF BEARING FAILURE

National Aeronautics and Space Administration
Huntsville, AL

Sep 75

N76-15462

ENGINEERING REPORT NO. 75-18 C

A STUDY OF THE USE OF VIBRATION AND STRESS WAVE SENSING FOR THE DETECTION OF BEARING FAILURE

Prepared for:

National Aeronautics and Space Administration, George C. Marshall, Space Flight Center, Huntsville, Alabama 35812

Prepared under:

NASA Contract NAS8-29916

By: L. C. Ensor — C. C. Feng

Approved by: R. M. Whittier — A. D. Diercks

ENDEVCO
San Juan Capistrano
30 September 75

158

ABSTRACT

This report presents the results from an experimental study of vibrations and stress waves emited from ball bearings. Tests were run with both high quality bearings and man faulted bearings, all of one size, the 207. Radial loads varied from 430 pounds to over 2000 pounds so to accelerate fatigue. Speed was either 5400 rpm or 12,900 rpm. Tests were instrumented with different sensors so to detect the noises from 10 Hz to 1 MHz. Frequency spectrum plots are presented. The modulation characteristics of the ultrasonic noises were analyses, and acoustic emission type measurements were conducted.

Results are presented which show that there is usable acoustic signal levels even beyond 500 kHz. These signal levels are modulated by a low frequency carrier which is a function of the stress loading and acoustic transmissibility. As expected the results are significantly weighted by the bandwidth characteristics of the sensor employed.

The results were correlated to fault size in the bearings, although the number of tests was few and therefore the results, statistically limited. The correlation does show that the sensor used for signals from 100 kHz to 1 MHz gave the best sensitivity and detected the generation of very small spalls or pits.

TABLE OF CONTENTS

APPENDIX

LIST OF FIGURES

Page intentionally left blank

LIST OF FIGURES (continued)

I. INTRODUCTION

A controlled bearing test program was conducted by Endevco under NASA Contract NAS8-29916. The overall objective of the test program was to study vibration and/or stress wave sensing techniques and data processing techniques to detect incipient failures of rolling contact bearings. Appendix 1 is a copy of the contractural statement of work. Deep groove radial 207 size ABEC-7 quality bearings were run at two different speeds and with various loads. The measurements were made over the frequency range of from 10 Hz to beyond 1 megahertz. Some of the bearings were in new condition, some had simulated faults of different types and sizes, and some were run to fatigue in accelerated life tests. The simulated faults were placed in the inner race or outer race with sizes ranging from 0.00013" deep x 0.00014" wide to 0.0127" deep x 0.0448" wide. In one case a ball fault was simulated with circumferential grooves.

Different sensors for detection of the mechanical signals were used for frequency ranges of 10 Hz to 50 kHz, 10 Hz to 200 kHz, and 100 kHz to the megahertz region. The electrical signals generated by these sensors were processed by various methods including frequency spectrum analysis, envelope detection and the counting of signals above a threshold level and over various time intervals. Magnetic tape recordings and chart recordings were made to facilitate this study. To accomplish the above tasks the project was divided into different

phases, first analysis and experimentation, second equipment setup and preparation of bearings, third a series of tests to examine faulted bearings, and fourth a series of tests to examine fatigue and fault propagation in bearings. This report summarizes each of these activities and presents the conclusions which have been made from them.

II. BEARING FAULTS, THEIR ASSOCIATED DYNAMIC PHENOMENA, AND THEIR DETECTION

The purpose of this section is to briefly present the technology involved. It will discuss how the physical deterioration of a rolling contact bearing results in vibration and dynamic stress. It will describe the characteristics of these dynamic phenomenon, and review the techniques available to sense and detect incipient failure of the bearing. This text is not meant to be a complete treatise on these subjects, but only a review to provide background and explanation for the test program reported herein.

A. Bearing Failure Modes

Many things can cause a bearing to fail, however improper lubrication and defects in or on the bearing parts are reported to be the primary causes of failure (1) (2). By design, the contact area between a rolling element and a bearing race is small, thus during operation the stress local to that area is high. In fact, the contact area is not actually in contact but is separated by a layer of lubricant which is needed to prevent the contact points from being virtually pressure welded and subsequently pulled apart. Not only lack of lubricant or changes in its quality will initiate bearing degradation, but also lubricant containing solid particles will also defeat the process since a small radius of curvature of a solid particle increases the contact pressure tremendously. Similar increase of contact pressure, or stress,

can be caused by any dimensional upset of the bearing contact surface as a result of improper assembly, corrosion or other environmentally induced changed. A basic material imperfection beneath the surface of contact but still within the high stress field can also cause greatly magnified stress points. These all cause high stress which encourage surface and subsurface microcracks to grow and will accelerate the fatigue process, leading to failure.

A good bearing, that is one not subjected to improper lubrication, one without internal material faults, or one without flawed bearing surfaces, can also be failed by fatigue simply due to excessive repetitive loading. This action has been reported (3) to cause dislocation motion in the material resulting in microcracks. Some short duration stress waves are initiated in this process. This type of stress wave has an energy content which is evenly distributed over the frequency spectrum up to a few tens of megahertz and is generally termed acoustic emission. Acoustic emission phenomena have been investigated widely and is well described in the literature (4).

B. Vibrations and Stress Waves as the Observable Change

When a bearing, in good condition, is assembled properly, it will run smoothly and will exhibit minimal vibration and resultant noise. Experiments have shown that the presence of excessive vibration and noise can likely be traced to a surface fault which causes an impact to occur every time a defect is passed. The impact duration is generally quite short (on the order of 10μ sec for a 207 size bearing with a surface fault of about 10 mil width). The frequency content of this impact extends well beyond the 100 kHz range, and in some cases it

could even extend into the MHz range. This impact initiates a stress wave in the bearing system. Since the bearing system made of steel is a high Q structure, multiple reflection of the stress wave causes the bearing to resonate. Vibration and noise are the end products of this process. Occasionally excessive vibration and noise can also be attributed to the roughness of the contact surface. When two surfaces with irregularities are rolled together, the motion of the rolling element is less well-defined. In addition to irregular impacts, there can also be sliding friction (skidding), jerking, and side-way motions combined with the main rolling motion. This is equivalent to creating random noise sources having a wide frequency bandwidth. The bearing and sensor system, again acting as a high Q filter, rings in response to this excitation.

The stress wave sources due to surface and subsurface fatigue crack growth is termed acoustic emission, and has even a higher frequency content. This occurs whenever the material undergoes a permanent non-elastic change.

As mentioned above, during operation a defective bearing gives out short duration stress waves which, in turn, causes the bearing system to resonate. Thus stress waves, and elastic vibrations are always present in an operating defective bearing. If a sensing device is used to measure the presence of the above mechanisms, theoretically, one can determine the existance of a defect in a bearing. Indeed, an experienced mechanic often can tell which part of an automobile is defective by simply listening to it with his unaided ear. With the help of modern sensors, not necessarily limited to the audio frequency range, a bearing monitor should be able to discriminate between defective

and acceptable bearings, and in addition, identify the nature of the defect.

C. Important Frequencies of Interest

To effectively detect the defects in a bearing, one must know some of the basic characteristics of a bearing. It is well established in the literature (5) that some very useful characteristic frequencies might be employed for bearing defect detection. Those frequencies are the ball pass frequencies for a discrete outer race defect, inner race defect, and ball defect. These frequencies are associated with the number of impacts per unit of time or the number of times a rolling element rolls over a defect either on the races or on the rolling element itself. They are a function of the bearing geometry and the angular speed of the outer race relative to the inner race (bearing rotation speed) (6). The relations are the following for ball type bearings including the 207 size (figure 1) used in this test program:

(A) for fault on outer race

$$f_o = \frac{1}{2} n f_r \left(1 - \frac{BD}{PD}\right) \qquad (1)$$

(B) for fault on inner race

$$f_i = \frac{1}{2} n f_r \left(1 + \frac{BD}{PD}\right) \qquad (2)$$

(C) for fault on ball

$$f_b = \frac{PD}{BD} \left[1 - \left(\frac{BD}{PD}\right)^2\right] f_r \qquad (3)$$

where

f_o = ball pass frequency for fault on outer race

f_i = ball pass frequency for fault on inner race

f_b = ball pass frequency for fault on ball

n = number of balls in the bearing

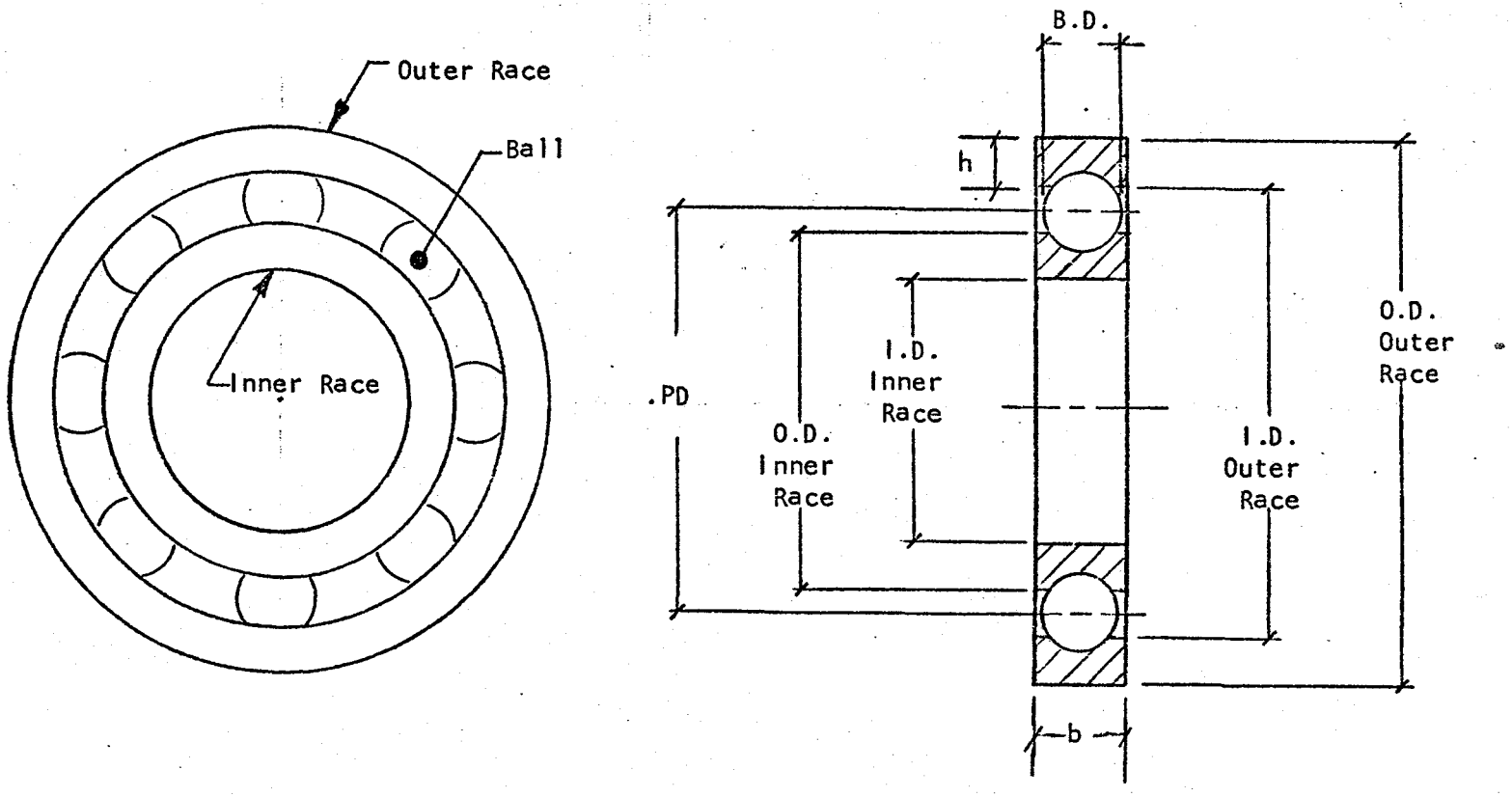

Figure 1 - Basic Dimension of a Fafnir 207 Bearing

f_r = angular frequency of bearing rotation

BD = ball diameter

PD = pitch diameter as defined in figure 1

Figure 2 portrays typical signals in the time domain that would result from a single fault located on a raceway. Notice that in figure 2a the decaying sinusoids repeat according to the ball pass frequency for the outer race fault. The decaying sinusoids relate to a natural resonance, and the individual ring downs are quite alike in both amplitude and time duration. Figure 2b shows the signal caused by an inner race fault. One can see that though the sinusoids occur according to the ball pass frequency for an inner race fault, the individual bursts are not the same in amplitude or time duration. This is due to the fact that when the fault is met by a ball near the maximum load position, the force generated is maximum. For a fault on the ball, a similar result is obtained. For a radially loading bearing, this maximum load on fault phenomenon occurs once per revolution.

Table I gives the calculated ball pass frequencies for a Fafnir 207 bearing for two different rotation speeds. It is clear that these frequencies are generally low. In addition to these frequencies, special attention should be paid to the bearing rotation frequency. The once per revolution frequency can easily be excited by the unbalance, misalignment, or other effects generally associated with a non-ideal set-up. It is also present in the case with a fault on the inner race or a ball as explained above.

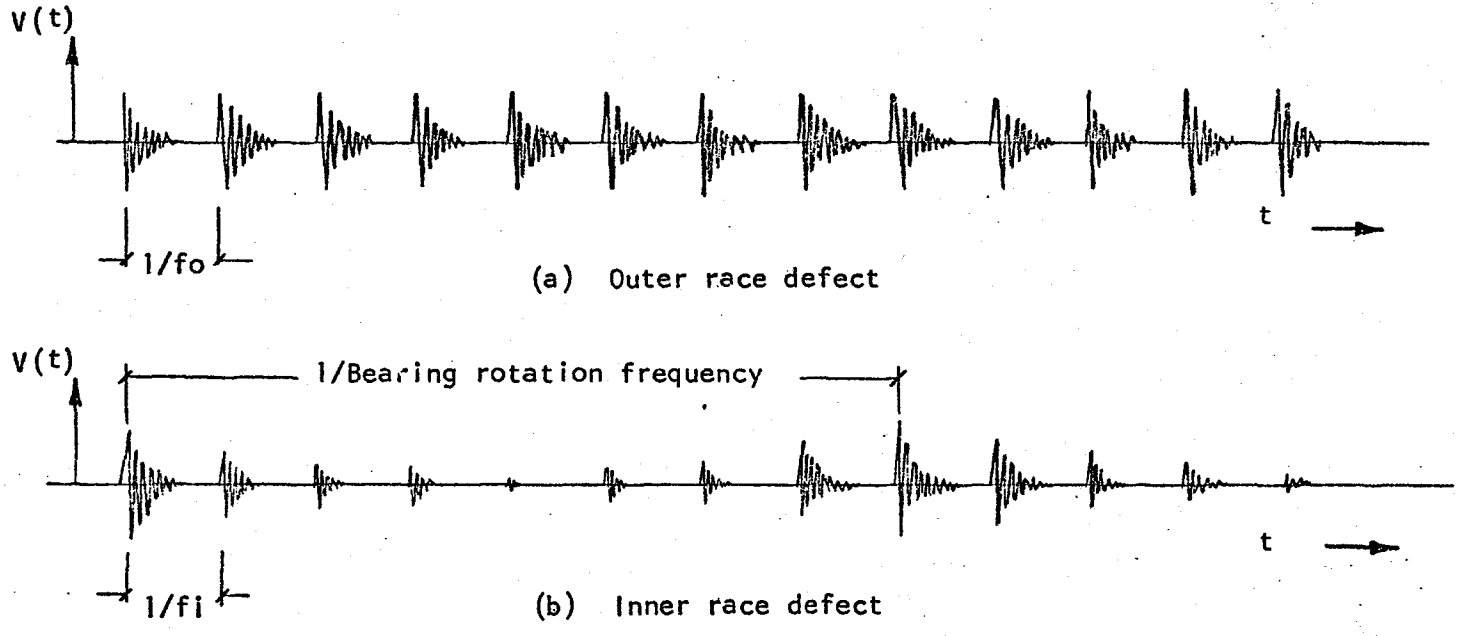

Figure 2 - Typical defect signals for an outer race fault and an inner race fault

TABLE I

BALL PASS FREQUENCY OF 207 FAFNIR ANTI-FRICTION BEARING

Faulted Component	Bearing Rotation Speed	
	12900 RPM (215 Hz)	5400 RPM (89 Hz)
Outer Race	668	281
Inner Race	1052	440
Ball	915	384

Other frequencies of importance are the various resonant frequencies of the bearing parts, such as the radial modes, flexural modes, etc. The following formulas are for those various resonant frequencies (7):

(1) Resonant frequency of a ball

(a) ellipsoidal mode

$$f_{BS} = \frac{0.424}{\frac{BD}{2}} \sqrt{\frac{E}{2\rho}}$$

(b) radial mode: f_{Rr} satisfies the following frequency equation

$$\tan \alpha = \frac{4\mu\alpha}{4\mu - \alpha^2(\lambda + 2\mu)}$$

where

$$\alpha = (BD)\,\pi\, f_{Rr}/c$$

(2) Resonant frequency of races

(a) In-plane flexural modes

$$f_{Ri} = \frac{N(N^2 - 1)}{\sqrt{N^2 + 1}} \cdot \frac{1}{2\pi a^2} \sqrt{\frac{EI}{m}}$$

(b) Transverse flexual modes

$$f_{Rt} = \frac{N(N^2-1)}{\sqrt{N^2 + 1 + \nu}} \cdot \frac{1}{2\pi a^2} \sqrt{\frac{EI}{m}}$$

(c) Radial mode

$$f_{Rr} = \frac{1}{2\pi a} \sqrt{\frac{E}{\rho}}$$

where E = Young's modulus

ρ = density

ν = Poisson's ratio

c = wave speed $= \sqrt{\frac{E}{\rho}}$

λ & μ = Lame's constants

N = number associated with mode order

a = radius of neutral axis

$I = \frac{bh^3}{12}$

b = lateral dimension of the bearing

$h = \frac{1}{2}$ (O.D. - I.D.)

$m = \rho A$

$A = bh$

The different mode shapes are shown in figure 3.

The calculated resonant frequencies for the various modes are given in Table II. As can be seen from the area moment of inertia (I) and the area (A) for the 207 size bearing and races of rectangular cross-sections are assumed. This may introduce some discrepancy between the calculated values and the experimental ones.

D. Resonance Frequency Testing for the Bearing Components

A test was conducted to ring the bearing components artifically by impacting the races with metallic objects of different sizes. Frequency analysis was performed on the signal played back from an ENDEVCO® 2743 Transient Recorder. Figure 4 shows the block diagram for this test. Figure 5a shows a 2 msec signal generated by impinging the inner race of a Fafnir 207 bearing with a 1/16" diameter steel bead. Figure 5b is the corresponding frequency analysis. It can be seen from the frequency spectrum that several sharp peaks exist in the range from 3 kHz to 100 kHz. The 15 kHz and 40 kHz are the highest ones which correspond fairly

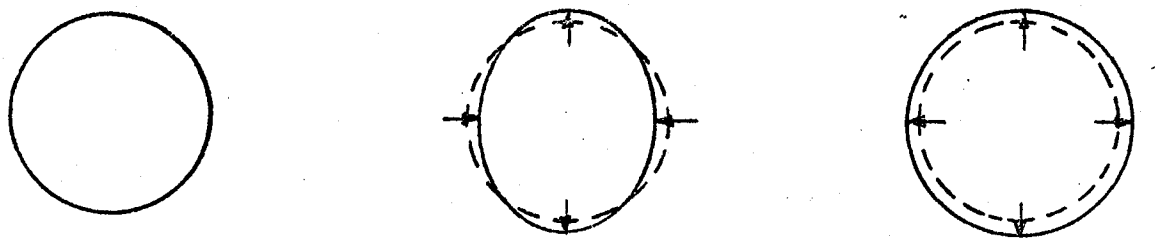

(a) Ball

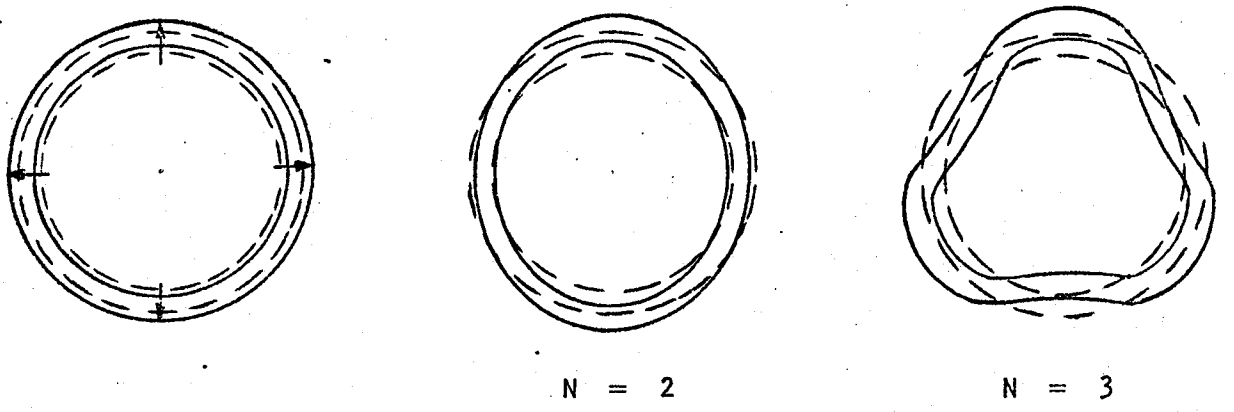

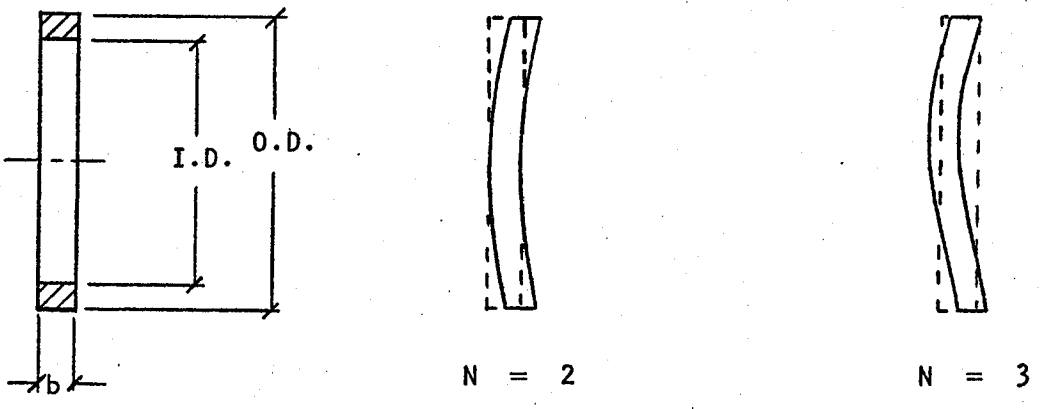

(b) Race

Figure 3 - Different mode shapes for bearing components

TABLE II

CHARACTERISTIC FREQUENCIES (kHz) OF 207
FAFNIR ANTI-FRICTION BEARING

COMPONENTS \ N	IN-PLANE FLEXURAL MODE					TRANSVERSE FLEXUAL MODE					RADIAL MODE	ELLIPSOIDAL MODE
	2	3	4	5	6	2	3	4	5	6		
Outer Race	5.5	15.6	30	48.5	71.1	5.4	15.4	29.7	48.2	70.8	22.5	N/A
Inner Race	13.3	37.6	72.2	116	171	12.9	37.1	71.6	116	170.6	34.9	N/A
Ball	N/A					N/A					HIGH	252.5

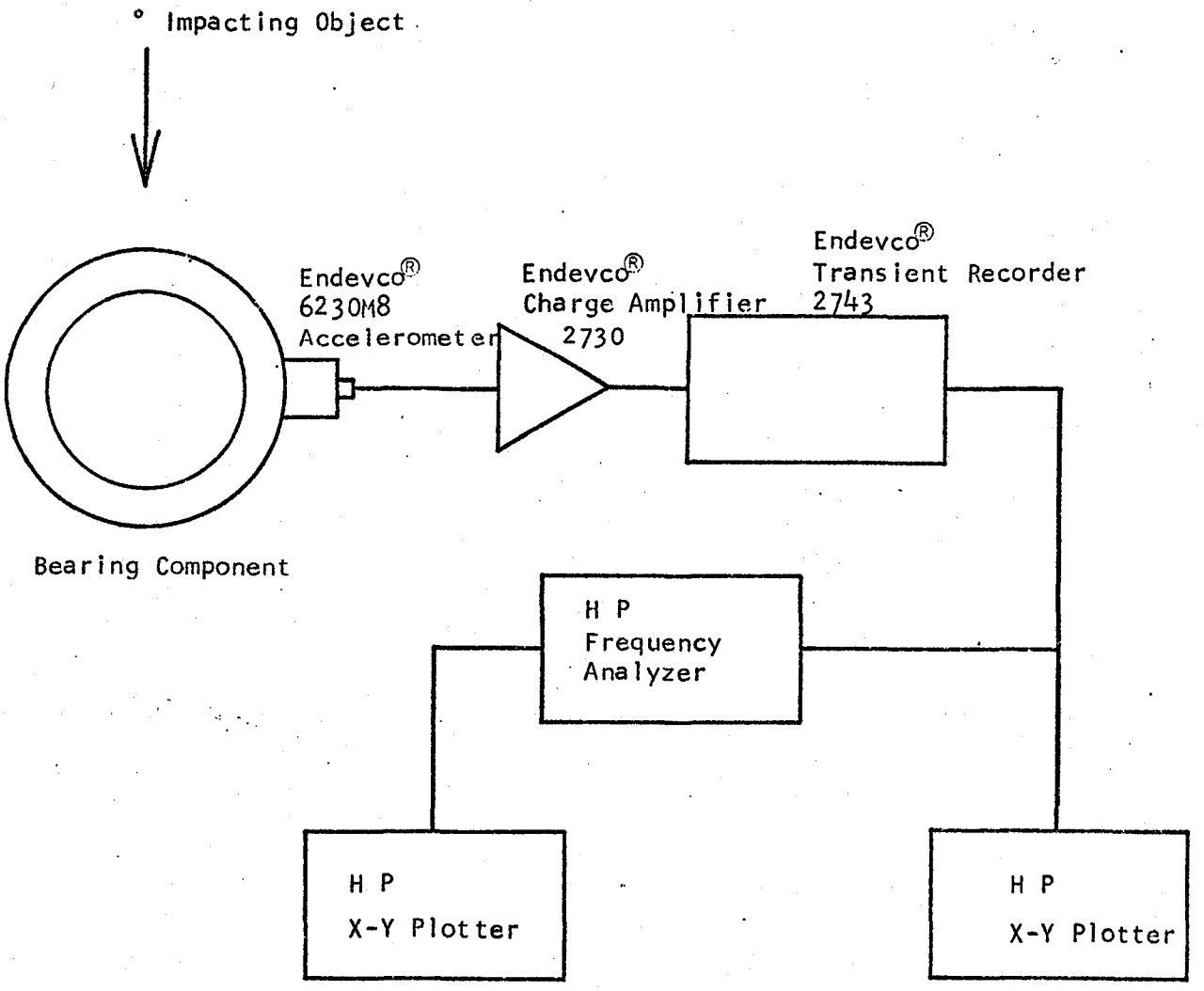

Figure 4 - Block diagram for bearing component ringing test

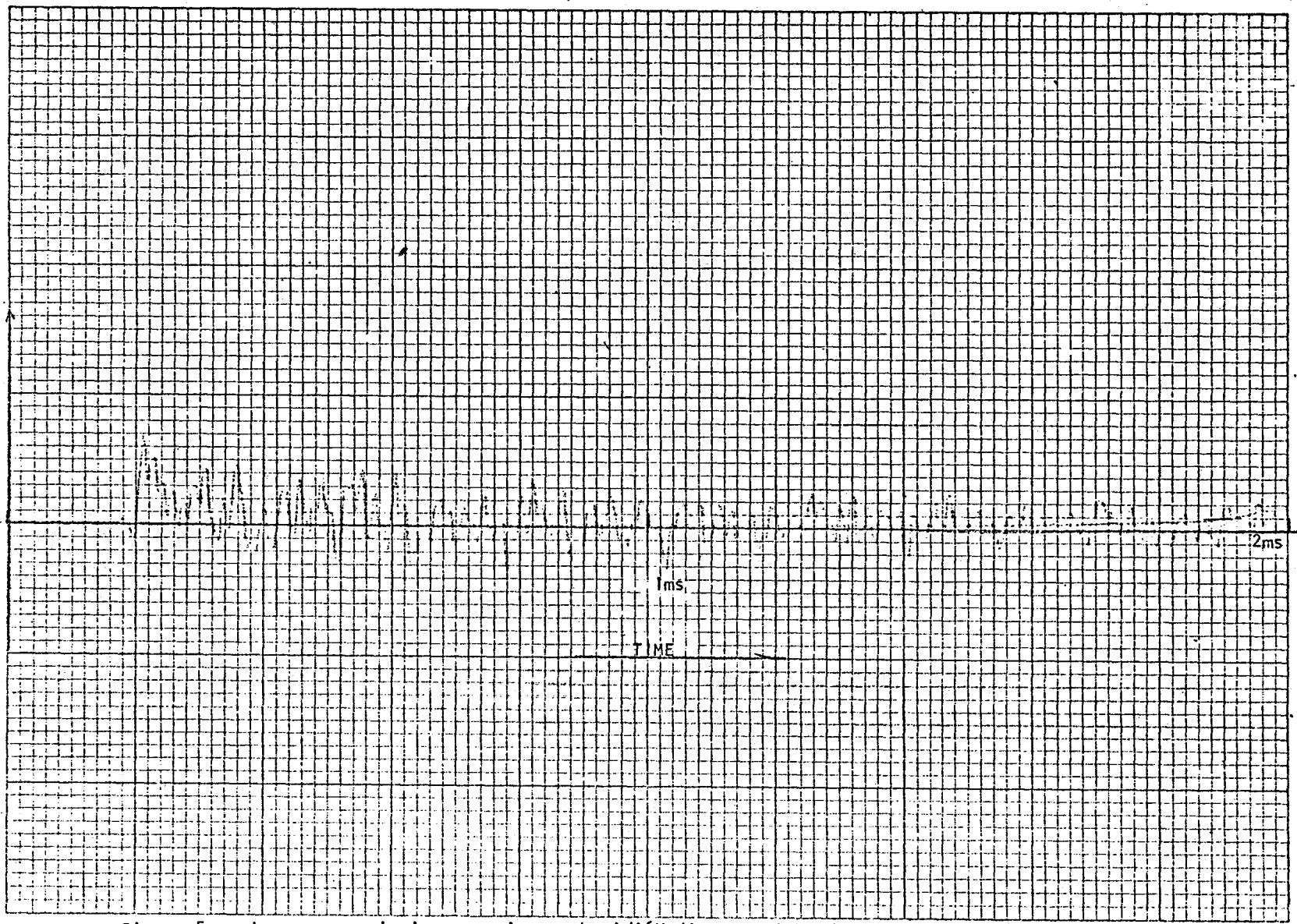

Figure 5a - Inner race ringing upon impact by 1/16" dia. steel bead.

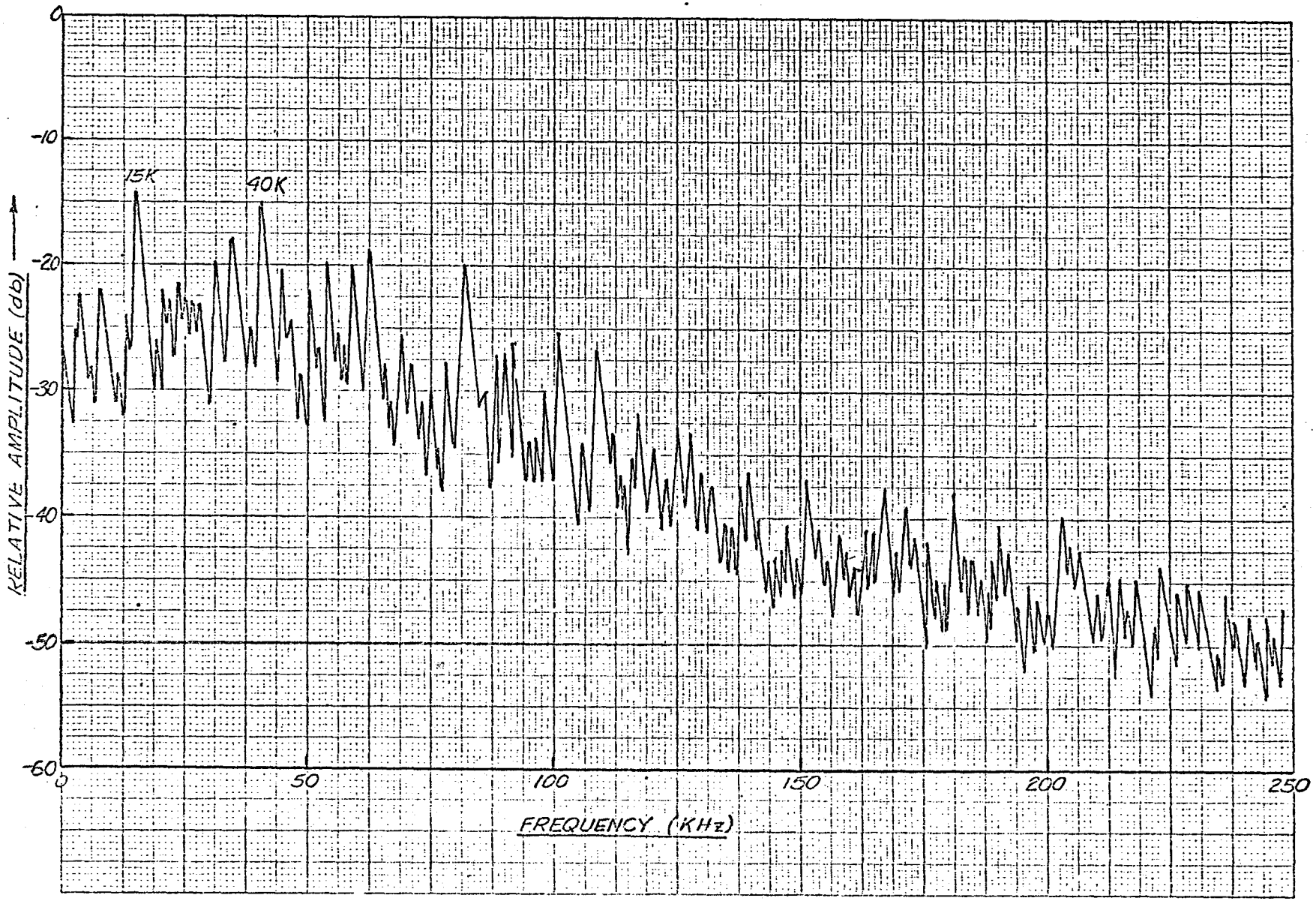

Fig 5b Frequency Spectrum of Fig 5a.

well with the calculated values for the cases N = 2 and N = 3 given in Table II previously. The time history trace presented in figure 5a gives a good picture on how the bearing rings. Bear in mind that the impact duration is less than about 10μ sec. From the length of ringing one can see that the race is really a high Q elastic body. The shape of the traces also shows that it is in a compound mode of vibration. This is also verified by the corresponding frequency spectrum given in figure 5b. Figure 6 shows the in-plane modes of the bearing outer race. The different resonant frequencies can clearly be detected. Those experimental values compared favorably to those of the calculated ones given in Table II. Discrepancies are unavoidable due to the model used for computation. Finally, a test was also conducted on the loading yoke for the test rig. Figure 7 shows that the yoke has resonant frequencies near 30 kHz.

From the above results, one can see that the different modes in a mechanical system can be excited by a short duration impact. The amplitudes of each mode also depend on the frequency content and mode of excitation of the source. This test shows that there are many modes excited in the frequency bandwidth from a few kHz to 50 kHz. This is in agreement with the theoretical calculation. However, the calculated values may not coincide exactly with the experimental ones. This is not surprising since the model used for the theoretical calculation is much simplified from the actual geometry.

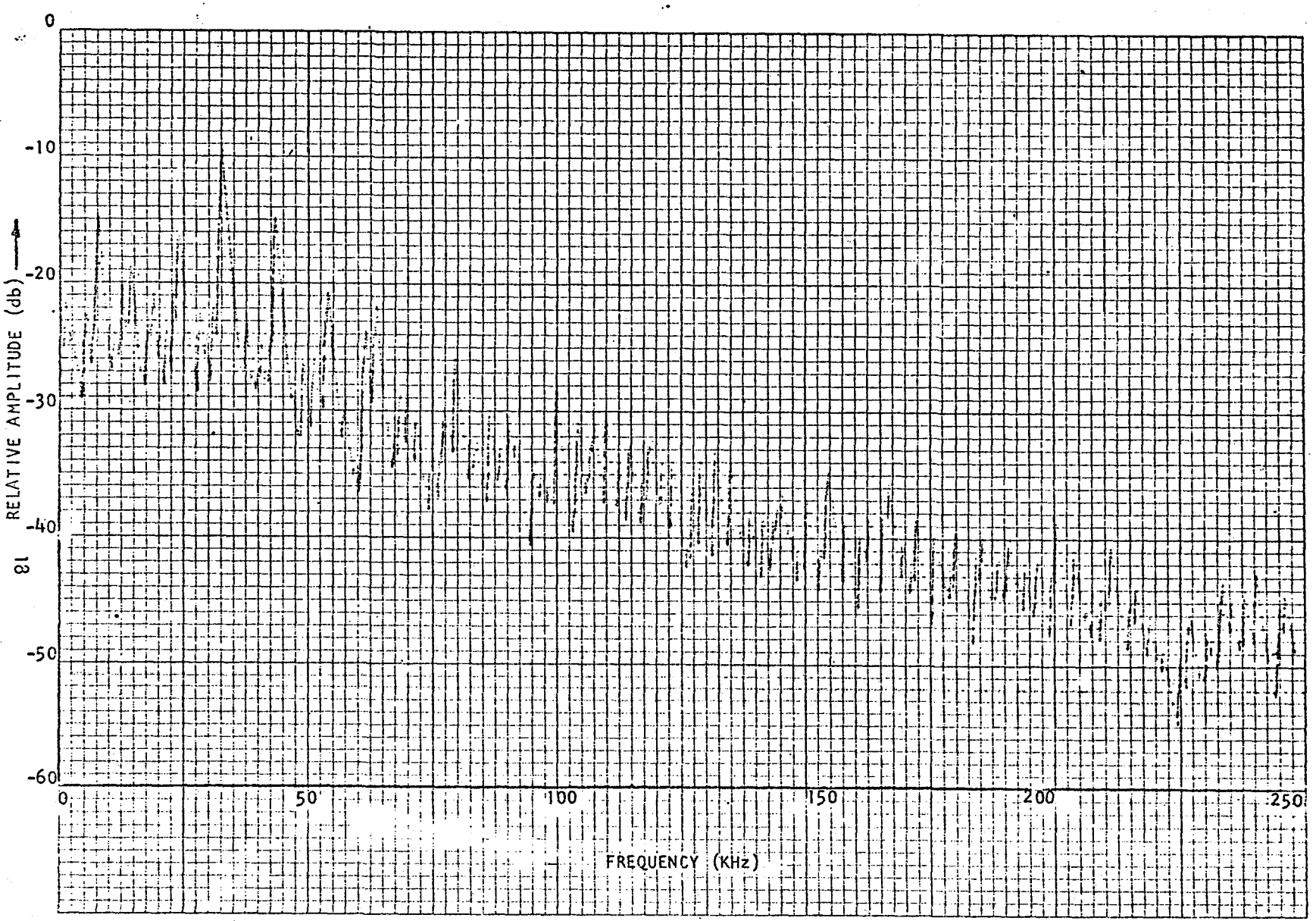

Figure 6 - Outer race in plane ringing Spectrum upon impact by a 1/18" dia. steel bead

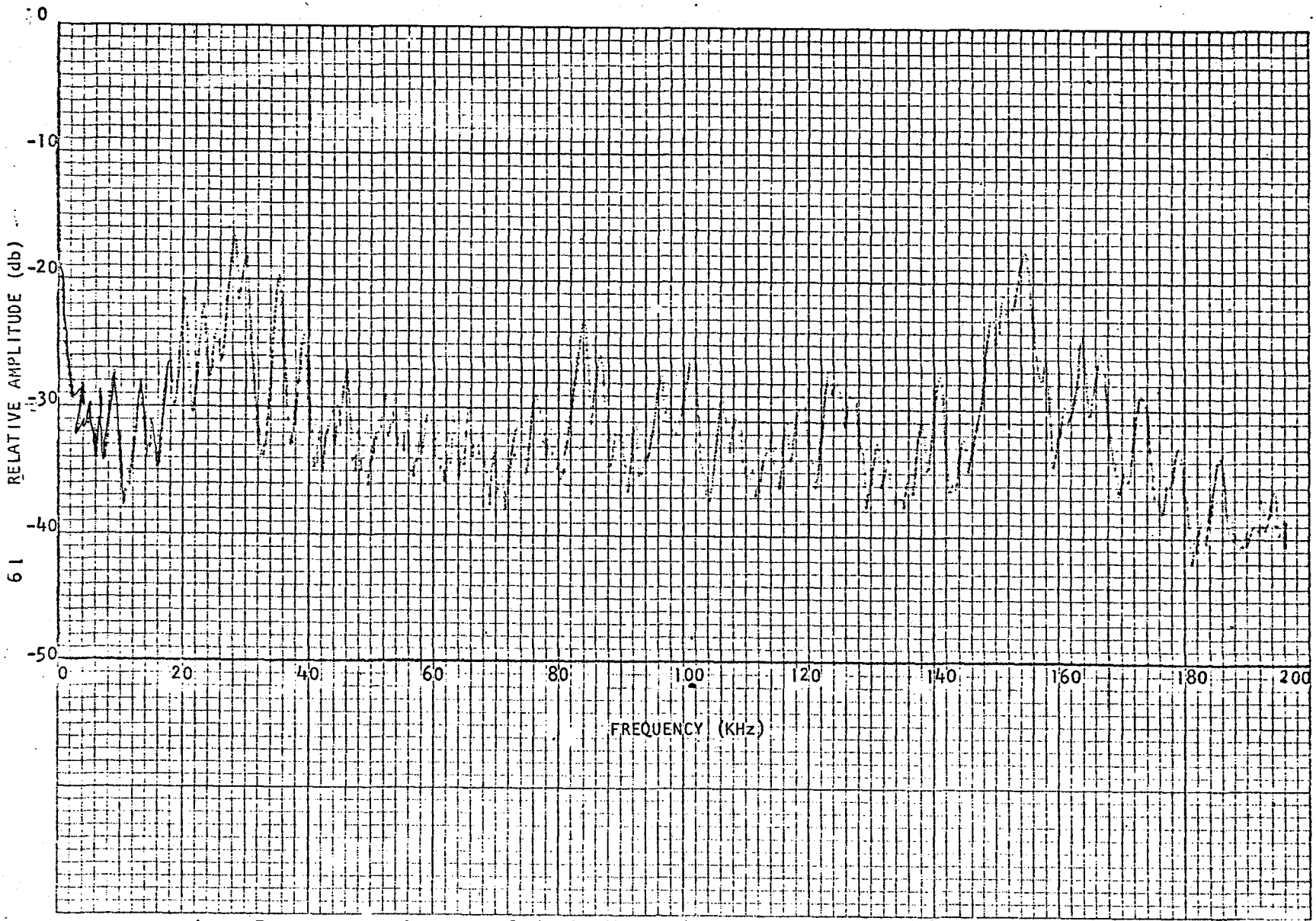

Figure 7 - Frequency Spectrum of the loading yoke upon impact by a 1/16" dia. steel bead.

E. The Structure as an Acoustic Body

The previous sections discuss the various resonant frequencies of the bearing components and showed that they could be excited by an impact or any other equivalent source having energy content in the frequency bandwidth. The resulting amplitude depends on the source characteristics and the transfer function between the source and the receiver for the particular mode involved. Because of the ease by which these modes are excited, a bearing fault detection concept based on the resonance phenomena has been reported in the literature. Data to be presented in Section V seems to confirm that the lower frequency outer race modes of the test bearing are excited. However, there is a strong indication that the inner race resonance modes are not excited. This is not an unreasonable finding. A close examination of the bearing system reveals that the outer race of the bearing is loosely coupled to the system, i.e., it is only supported by the balls at relatively small contact surfaces. It is rather "free" to vibrate. On the other hand, the inner race is assembled on the shaft quite rigidly by a shrink fit. In the process, the inner race and the shaft become an integral elastic body from an acoustical standpoint. The inner race radial and flexural modes are lost in the process. This implies that one should view the whole bearing system and its supporting structure (such as the yoke) as a whole entity in trying to pin-point and use the various modes.

When considering the optimal detection of faults in a bearing system,

one cannot achieve this without considering signal transmission in the bearing system and the optimal detection frequency bandwidth. First of all, the bearing system is made of several components with interfaces and probably some gaps among them. An acoustic signal generated often has to travel across the various interfacres before it can be detected. However, an interface is usually quite lossy, maybe., sometimes on the order of 20 db. Generally speaking, this loss is a function of contact pressure in the interface and of frequency. As frequency increases, the loss is generally higher. Fortunately, in a bearing system, lubrication oil often fills the interface gaps and serves as an effective acoustic couplant and improves the transmissibility markedly.

These aspects point out that a frequency higher than the lower resonant frequency of the bearing system may be desireable for use. As mentioned before, due to the interface loss and the internal damping of the material, the high frequency component of a stress wave does not travel as far as the low frequency component. Furthermore, the generation of noises in a mechanical system generally has more low frequency energy content. Therefore, the noises or other unwanted signals have a frequency spectrum typically heavily weighting the low frequency end. On the other hand, the signal associated with a bearing defect often has quite a wide frequency content no matter whether it it due to the impact of a small discrete fault, friction noise by skidding, or due to acoustic emission. From the above, one can postulate that using a frequency as high as practical may improve the defect detection efficiency. In this test program, a frequency bandwidth as high as 1 MHZ was used.

F. Sensing and Signal Processing

For comparison, different sensors were applied in this experiment. Different signal processing techniques were also used and evaluated for their relative merits. The various sensors and signal processing techniques will be described fully in the next section. One particular technique worth mentioning here is the frequency analysis of the periodic signal as encountered in the test when there is a discrete fault on the outer race.

To simplify the discussion, let's assume that the signal detected is a square burst of duration τ_o of a pure sinusoidal signal of frequency f_o (Fig. 8a). The repetition rate is assumed to be F_o which is the inverse of signal interval T_o. Figure 8b gives the frequency spectrum of a single burst of signal, assuming that $f_o \gg F_o$. The spectrum is centered at the "ringing" frequency f_o with side lobes extending to both the low and the high frequency sides. Figure 8c gives the spectrum for the whole signal train. Note that the envelope of the spectrum amplitude is of the same shape as given in Fig. 8b. The repetition frequency F_o does show up in the figure. However, its height is not very large compared to the peak amplitude near F_o. But, as mentioned previously, it is important to be able to detect the repetition rate F_o since it is associated with the discrete defect. The detection of F_o can possibly tell the operator what kind of defect and which part of the bearing is defective. The following analysis will show that envelope detection can do the trick. Fig. 9a gives the spectrum for the envelope of a single burst. Note that the spectrum has its maximum at d.c. in this case. Fig. 9c is the spectrum for the whole envelope detected signal train. It is clear that besides at $f = o$, the maximum peak now occurs at the repetition frequence F_o. The finite widths of the peaks

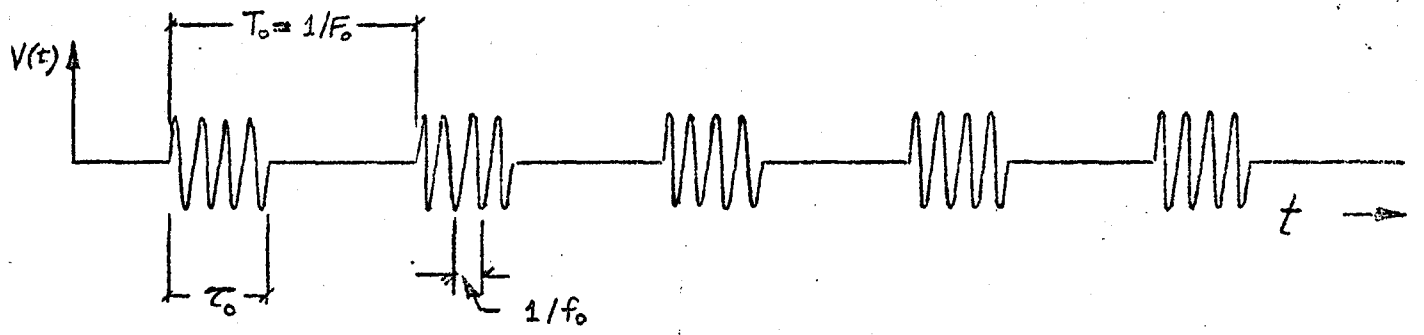

(a) A repetitive signal of frequency fo and repetition rate Fo and single burst duration τ_o

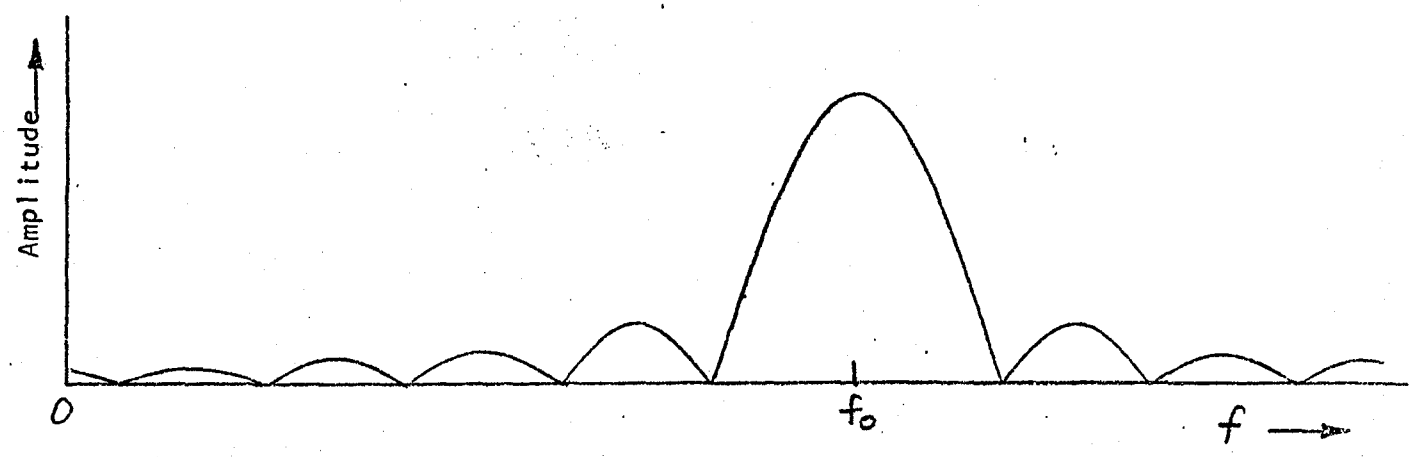

(b) Frequency Spectrum for a single burst signal of (a)

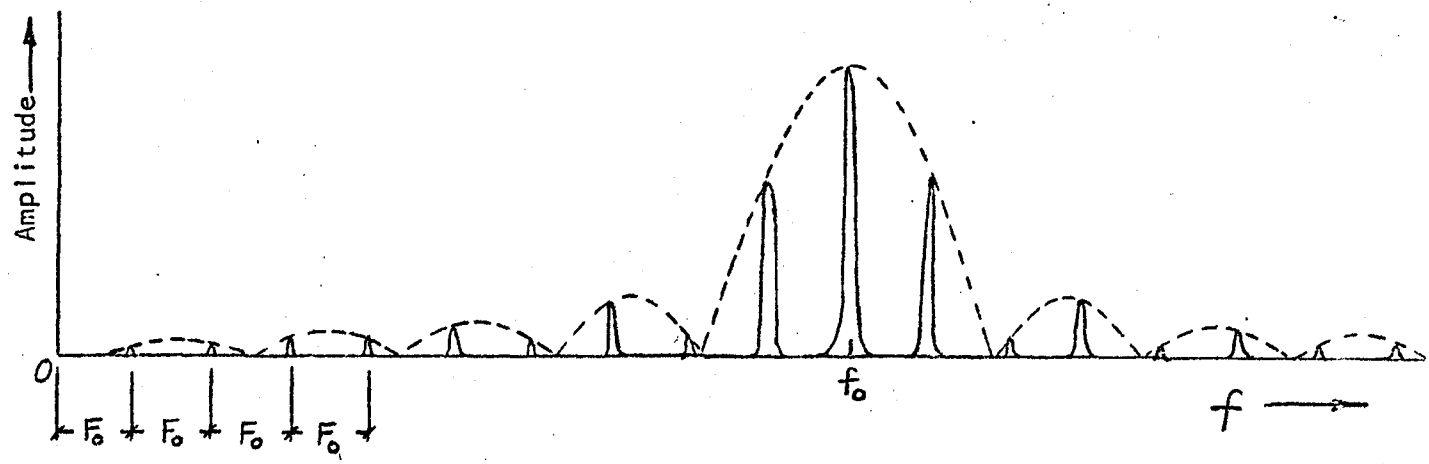

(c) Frequency Spectrum for (a)

Figure 8 - Frequency Analysis of a repetitive signal

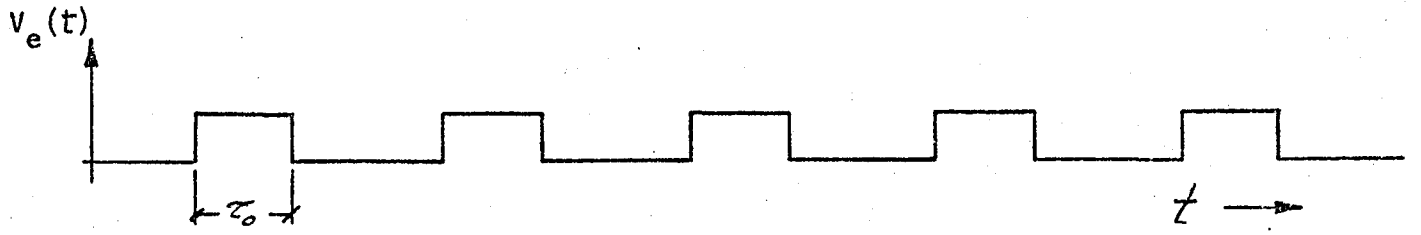

(a) Envelope detected signal of (a)

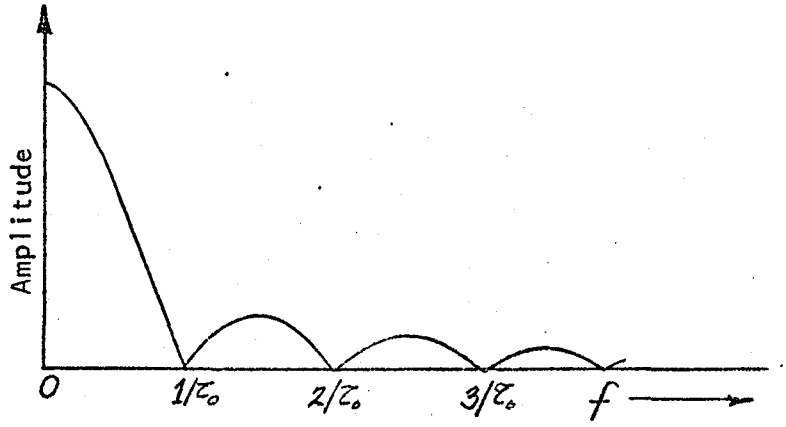

(b) Frequency Spectrum of the envelope detected single burst

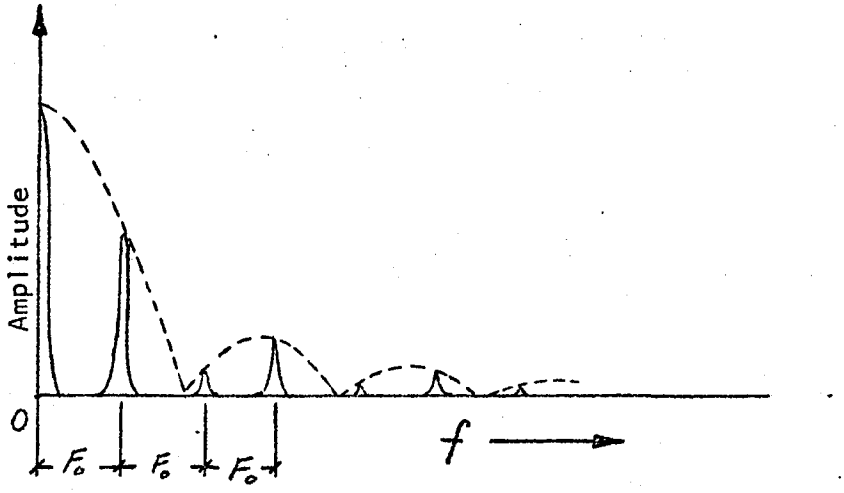

(c) Frequency Spectrum for (a)

Figure 9 - Frequency Analysis of the envelope detected signal of Figure 8..

shown in the above example is due to the finite bandwidth assumed for the spectrum analysis. From the above one can see that it is necessary to envelope detect high frequency signal in order to extract the low ball pass frequencies simply by comparing Fig. 8c to Fig. 9c.

Another signal processing technique to consider for a bearing monitor is the application of the standard acoustic emission measurement techniques. Conventionally, when acoustic emission signal is detected, count or count rate information is obtained by counting the number of times the signal voltage exceeds a preset threshold level. This information is then used to characterize the particular acoustic emission phenomena. More recently, a technique to obtain the relative energy of an acoustic emission was developed by Endevco. This technique was implemented by integrating the square of the acoustic emission signal. It was hoped that the energy method would give more information about acoustic emission than the conventional count method. Subsequent applications of the energy method to acoustic emission testing have been reported by Harris and Bell (9) and showed that while the energy method might be valuable in some cases, it did not seem to give more information in the cracking and fatigue crack growth tests they performed. Specifically, they found that a linear relation between the energy and the count exists. They also showed that mathematical expression could be derived to relate the energy to the count from considering a ring-down type signal.

III EQUIPMENT

A. Bearing Test Rig

The bearing test rig was designed and assembled by Industrial Tectonics Incorporated, Compton, California; they were also responsible for installing all bearings and maintaining the rig during the test program. This equipment was designed so to apply variable radial load, essentially no axial load, and to have a speed capability of up to 13,000 rpm. It was designed specifically to accept the 207 size bearing.

The machine is composed of a spindle, a load mechanism, a lubrication system and an electric drive. The spindle consists of a shaft supported by two side bearings with a radial load applied to a third center bearing through a massive cam shaped housing. As such the center bearing carries twice the load of the side bearings. The shaft protrudes from the test cavity through a labyrinth seal at one end. The housing is in three parts. The center portion, which contains one test bearing, is connected to a pivoting load yoke. The out-board sections are secured to the test stand containing one support bearing each. Figure 10 shows a cross-sectional view of this machine.

The load mechanism consists of a lever and dead weight system with a ratio of 100:1 as shown on the system outline drawing Figure 11. The radial load applied to the yoke is transferred through the load bearing to the shaft.

The yoke was sealed between the outer two bearing housings by rubber "O" rings. The only other mechanical connection between the center bearing housing and the side bearing housing was through the load lever mechanism

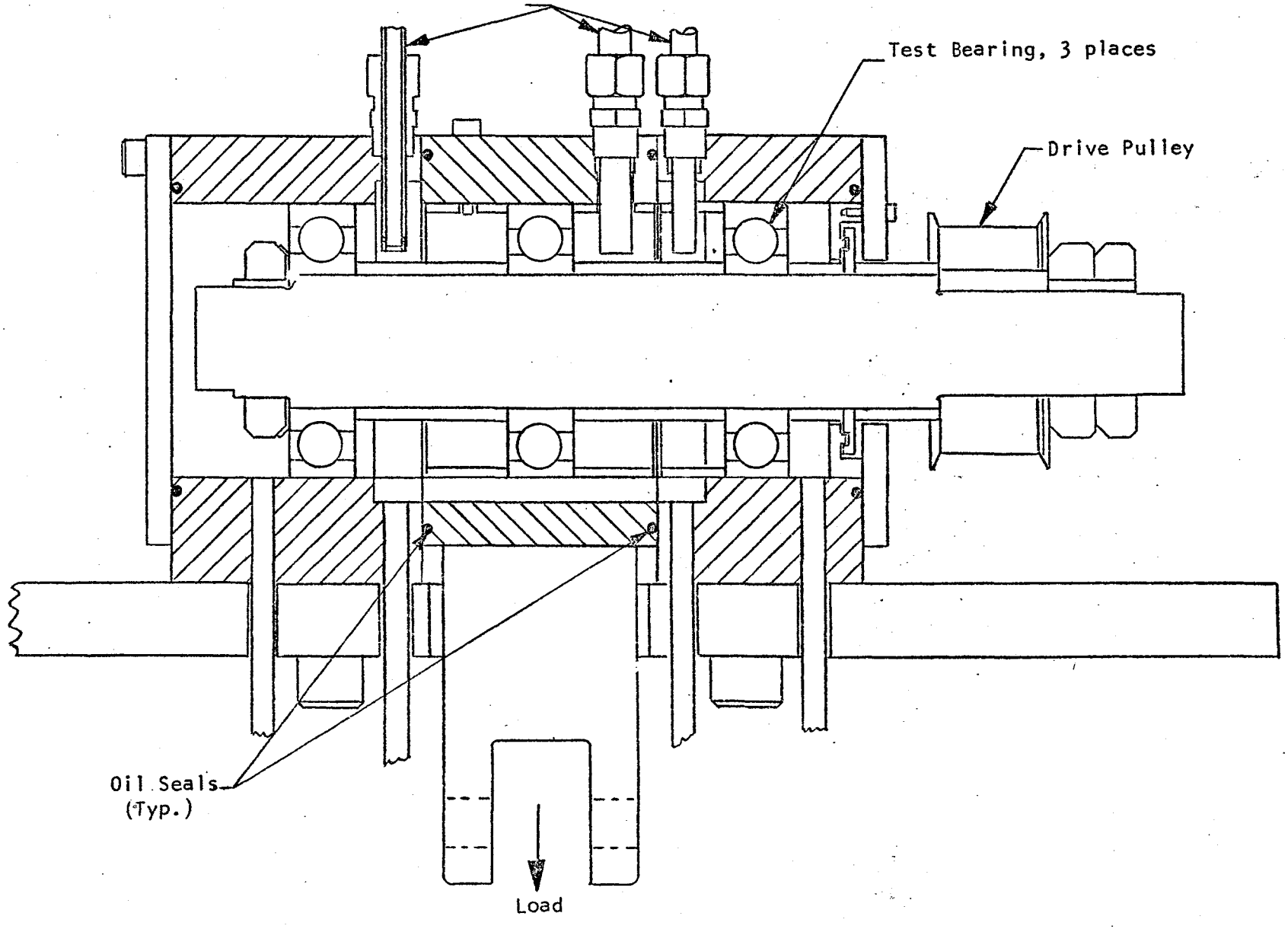

Figure 10 - Cross Section of Bearing Test Machine

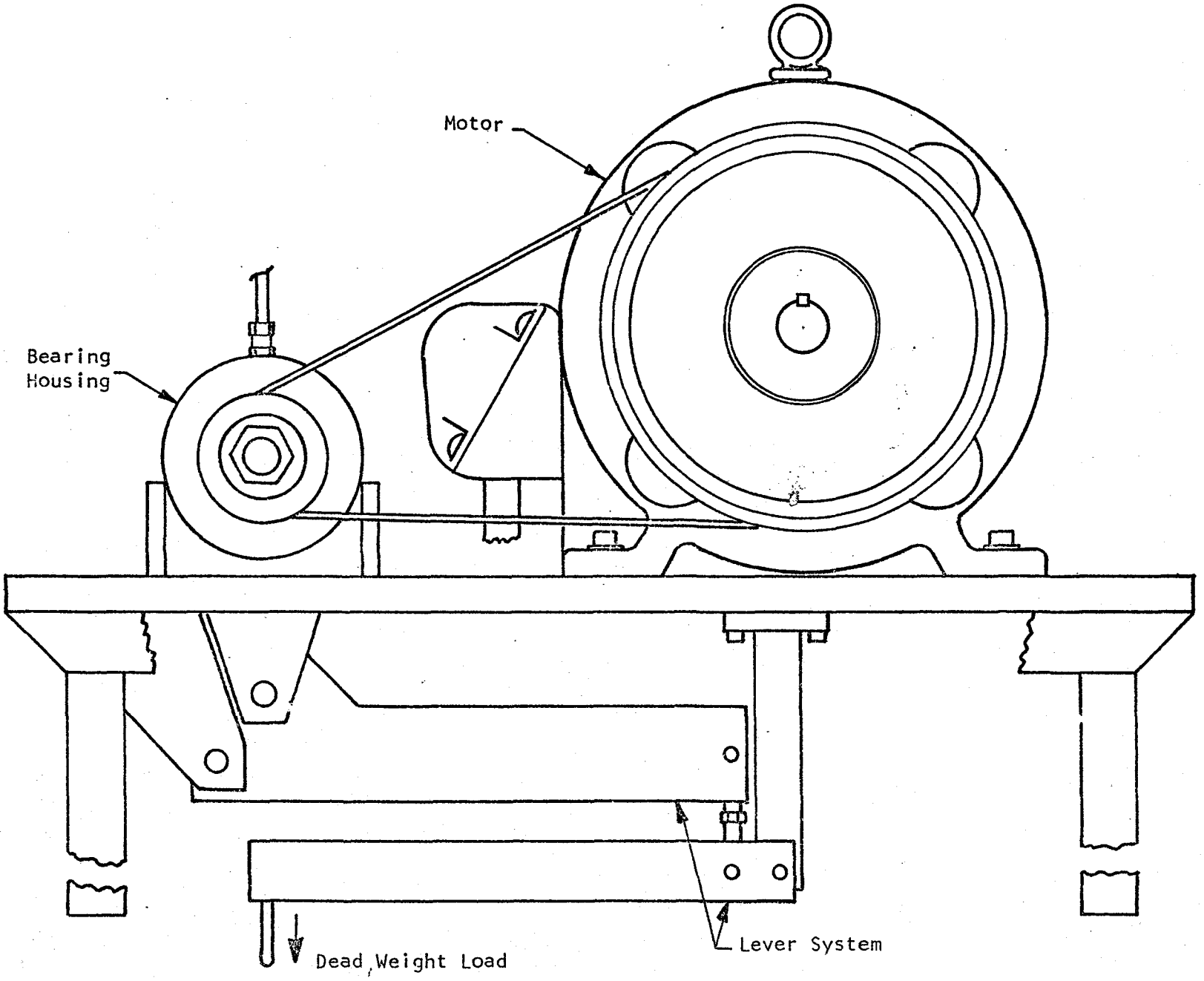

Figure 11 - Bearing Test Machine Assembly

which was attached to the test stand. Therefore, mechanical vibrations from one bearing to another would be attenuated at higher frequencies by the transmission characteristics of the load level mechanism. The other path of transmission between bearings is through the common shaft where the mechanical input is generated in one bearing, transmitted to the shaft, then to another bearing and out to the other housing to be detected. The two out-board bearings support the shaft and transfer the radial load to the structure. This radial load system capacity is from 350 lbs. to 2,580 lbs.

The inner race of these bearings were assembled to the shaft by a light shrink fit in accordance with the Fafnir Catalog Installation Procedure. Spacers over the shaft, bolted in compression between the inner races of the bearing, maintained the position of the bearings on shaft. The outer race was a slip fit clearance in accordance with the recommended installation procedure. Fixed spacers were positioned in the housing to maintain the bearings in position.

This machine is equipped with a 3,600 rpm, 5 hp electric motor which drives the spindle by means of a conventional timing belt and pulleys. Pulleys and belts are provided for spindle speeds of approximately 5,400 rpm and 12,900 rpm. There were 20 teeth on the spindle drive pulley for 12900 rpm speed and 32 teeth for 5400 rpm speed.

Bearing lubrication was accomplished by pumping MIL-L-23699 oil through appropriate feed lines and a 10 micron filter and oil jets to the test spindle and returning to a reservoir.

Three temperature sensors were provided for monitoring the oil inlet temperature, the test bearing outer ring temperature, and the exit oil

temperature. These temperatures were sequentially displayed on a West temperature indicating device that gave an audible alarm should any temperature go above a pre-set value.

A proximity sensor was installed near the shaft to monitor the speed of rotation with a counter. The entire bearing test rig with sensors mounted is shown in the photograph, Figure 12

B. Bearings

The bearings were Fafnir MM 207 KCR which are deep groove (not angular contact) ABEC-7 bearings. The separators are phenolic of two pieces, riveted together. The bearings can be disassembled and re-assembled without damage, if done professionally. The dimensions and specifications for the bearings are as follows:

SIZE	207
BORE	$1.3780\ ^{+.00000}_{-.00020}$ inches (35mm)
O.D.	$2.8346\ ^{+.00000}_{-.00020}$ inches (72mm)
WIDTH	$0.6693\ ^{+.000}_{-.005}$ (17mm)
FILET RADIUS	0.039 inch
BALL DIAMETER	15/32 inch
NO. OF BALLS	8

C. Sensors

One of the objectives of this program was to examine alternative sensing methods for monitoring bearing performance, that is sensing techniques which may permit the earliest detection of incipient failure. Important to this is the selection of a sensing method which best provides a signal which is a manifestation of an event containing information of interest. Information not of interest is considered as noise. Since the

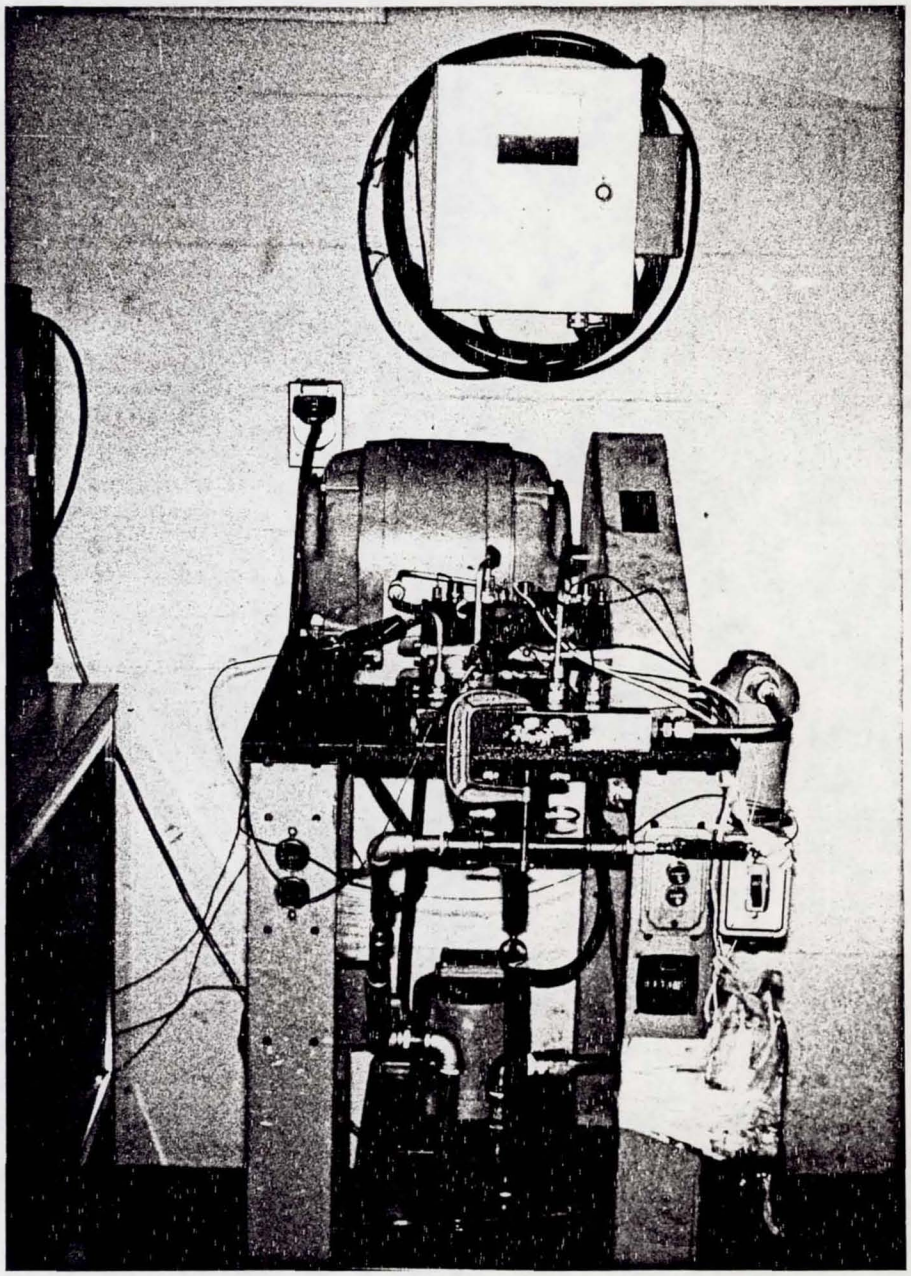

Figure 12 - Bearing Test Machine with Sensors attached.

vibrations internal to the bearing and its supporting structure are caused by several phenomena and all have varying and complex spectral frequency contents, one of the basic needs is to obtain valid measurements over a wide frequency range. To accomplish measurements from 10 Hz to 1,000,000 Hz does require the use of more than one type of sensor. In addition, because of the wide difference in required sensitivities, several sensors were necessary. The selection of these various sensors is discussed below.

In order to obtain maximum sensitivity in the high frequency range of resonances for the bearing outer race, the ENDEVCO Model 2236 Sensor was used. The resonance frequency of these sensors is near 27 kHz and as shown in Figure 13, the amplification factor to forced vibration at this frequency is on the order of 40 dB greater than the low frequency sensitivity. Since the bearing outer race and its holding structure both have resonances in the frequency region, the overall sensitivity to small amplitude impulses should be good. ENDEVCO Model 2730 Charge Amplifiers were used with these sensors to provide a wide dynamic range of acceleration from a fraction of a g to 500 g over the frequency range from 10 Hz to about 50 kHz.

A Model 2236 Accelerometer was also used with ENDEVCO Model 6634 Signal Conditioner as a vibration control for automatic shut down during fatigue testing. This conditioner provides a relay switch with an adjustable level control which may be set at a desired vibration level above the normal bearing vibration for automatic shut down of the test. Bandwidth of this shut down system is from 10 Hz to greater than 10 kHz.

To determine some correlation of how much output actually does come from the bearing and structure, as opposed to sensor resonance response,

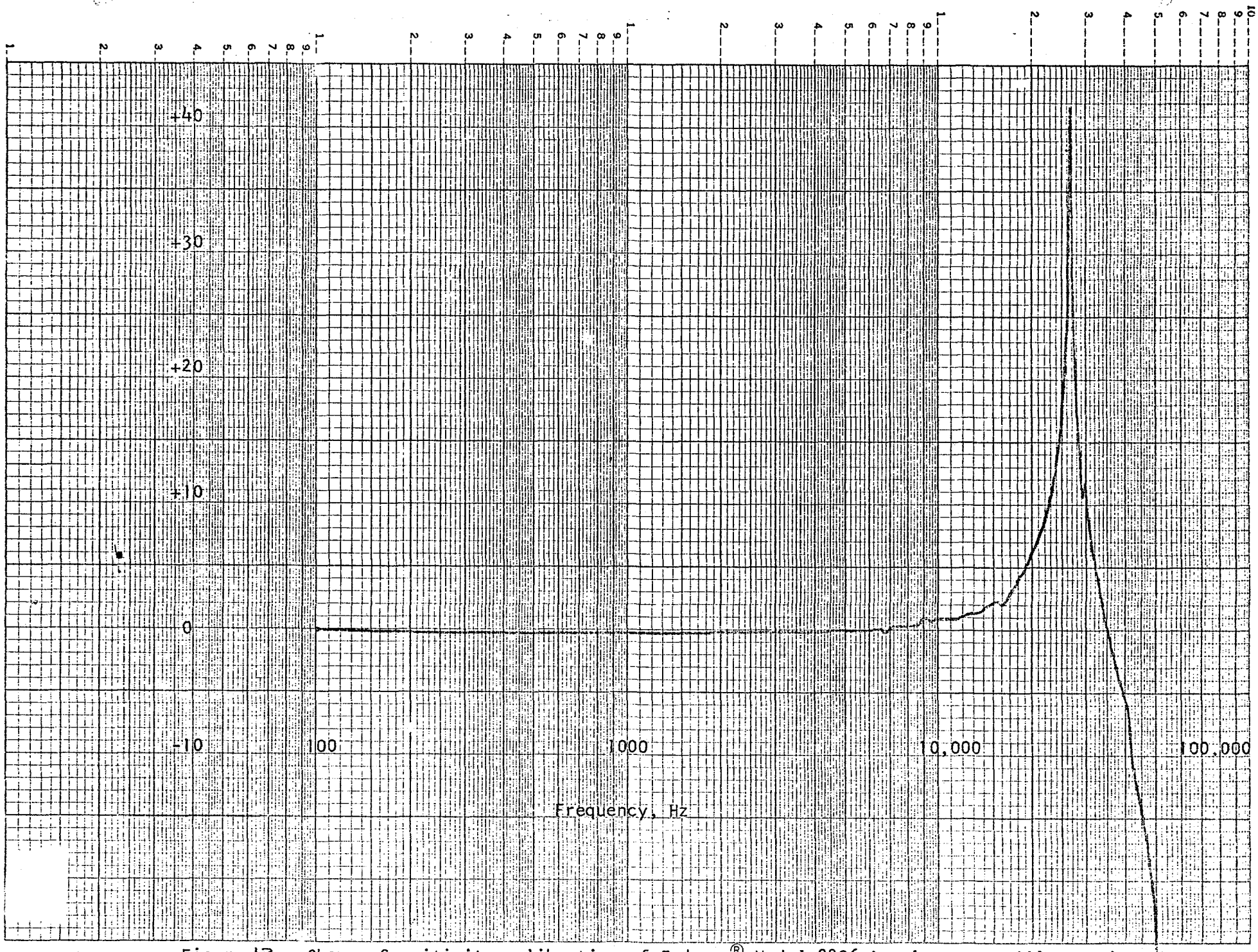

Figure 13 - Charge Sensitivity calibration of Endevco® Model 2236 Accelerometer illustrating the resonance frequency response.

ENDEVCO Model 6230M8 Sensors were also used. These sensors have relatively constant acceleration sensitivity up to 50 kHz as shown by Figure 14 and with a major resonance frequency near 150 kHz. When used with ENDEVCO Model 2740 Charge Amplifier, data may be obtained up to about 200 kHz.

In addition to these vibration sensors, an acoustic emission/stress wave sensor, ENDEVCO Model D9202, was used to extend the frequency measurement capability to the megahertz region. This sensor is only responsive above 100 kHz to allow better recognition of data above 100 kHz. Thereby, outputs from lower frequency vibrations of structures are eliminated from the measurement and only stress wave data is obtained. There are several resonance frequencies in this design such that the output to impulsive acoustic inputs is a shaped response with a peak near 500,000 Hz.

Figures 15 and 16 show the calibration data for the D9202 Sensor used for these tests. This data was obtained by the Spark Calibration Test Method (10). Figure 17 gives the response curve using a random noise input which is provided by shaking many small tungsten beads in an enclosed fixture on which the transducer is mounted. In operation, the transducer will ring when a disturbance with energy in the frequency bandwidth arrives at the transducer. The ringing of the transducer will eventually die off due to the damping of the transducer and the stress wave losses to other structures which are in contact with the transducer. At a high frequency, the damping generally increases very rapidly with frequency (8). Consequently shorter lapse time for the ringing at high frequency is observed. This makes the output of the Model D9202 with Model 801P Preamplifier look like

Figure 14 - Vibration Frequency Response of Endevco® 6230M8

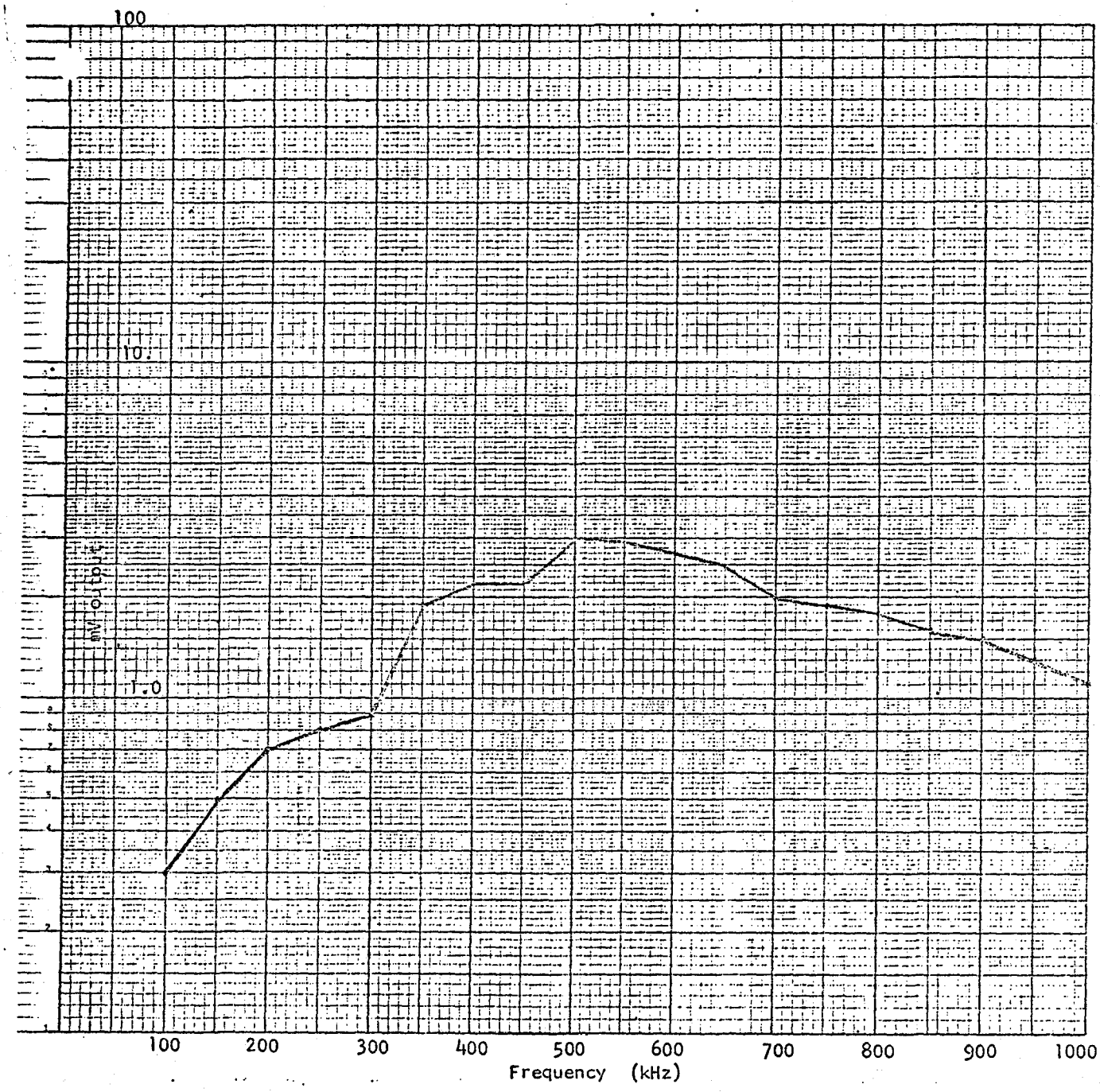

Figure 15- Spark Impulse Response of D9202 - AB34
(Compression Wave) Output recorded
through D/E 801P Preamplifier

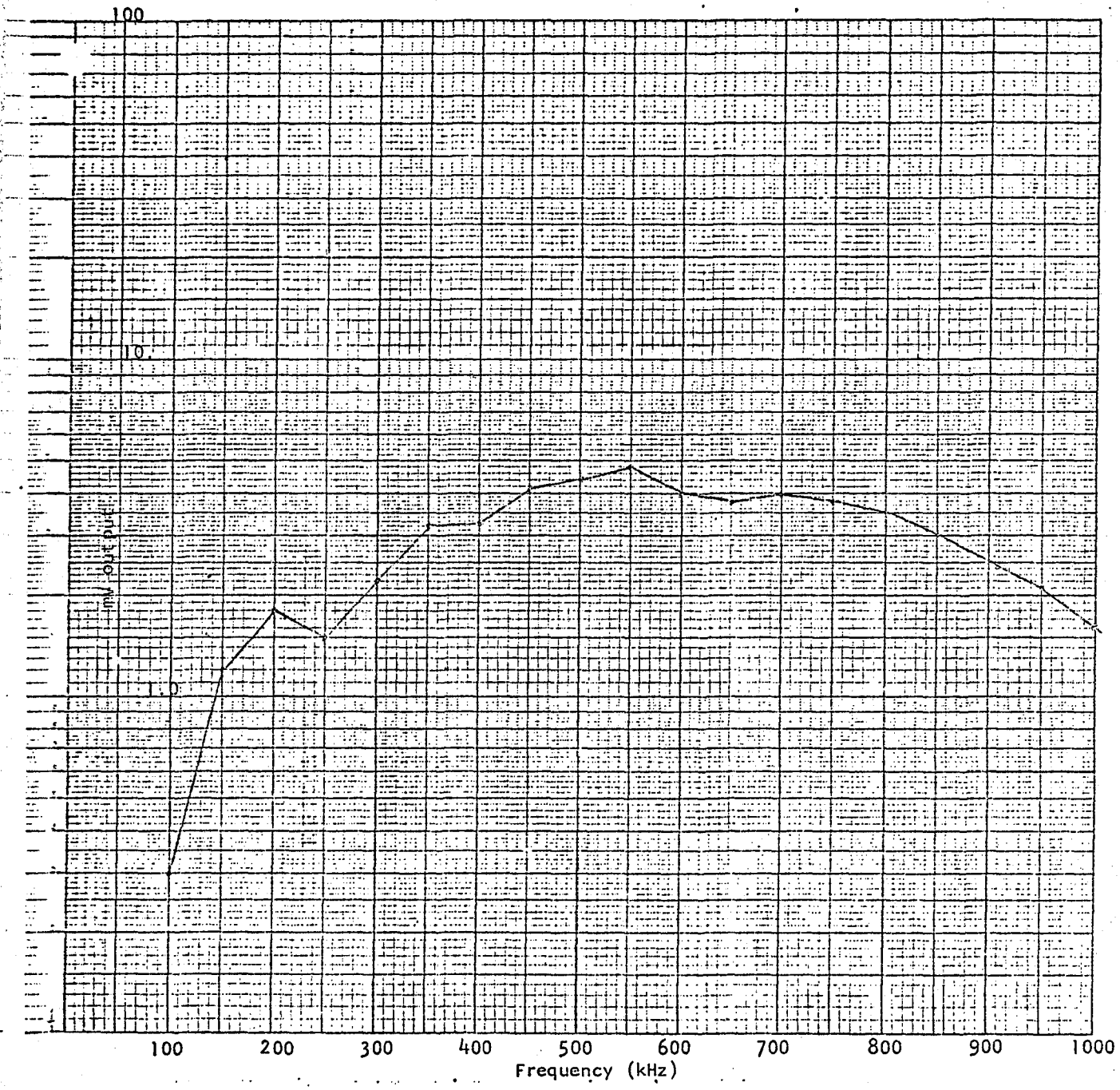

Figure 16 - Spark Impulse Response of D9202 - AB34 (Surface Wave) Output recorded through D/E 801 Preamplifier

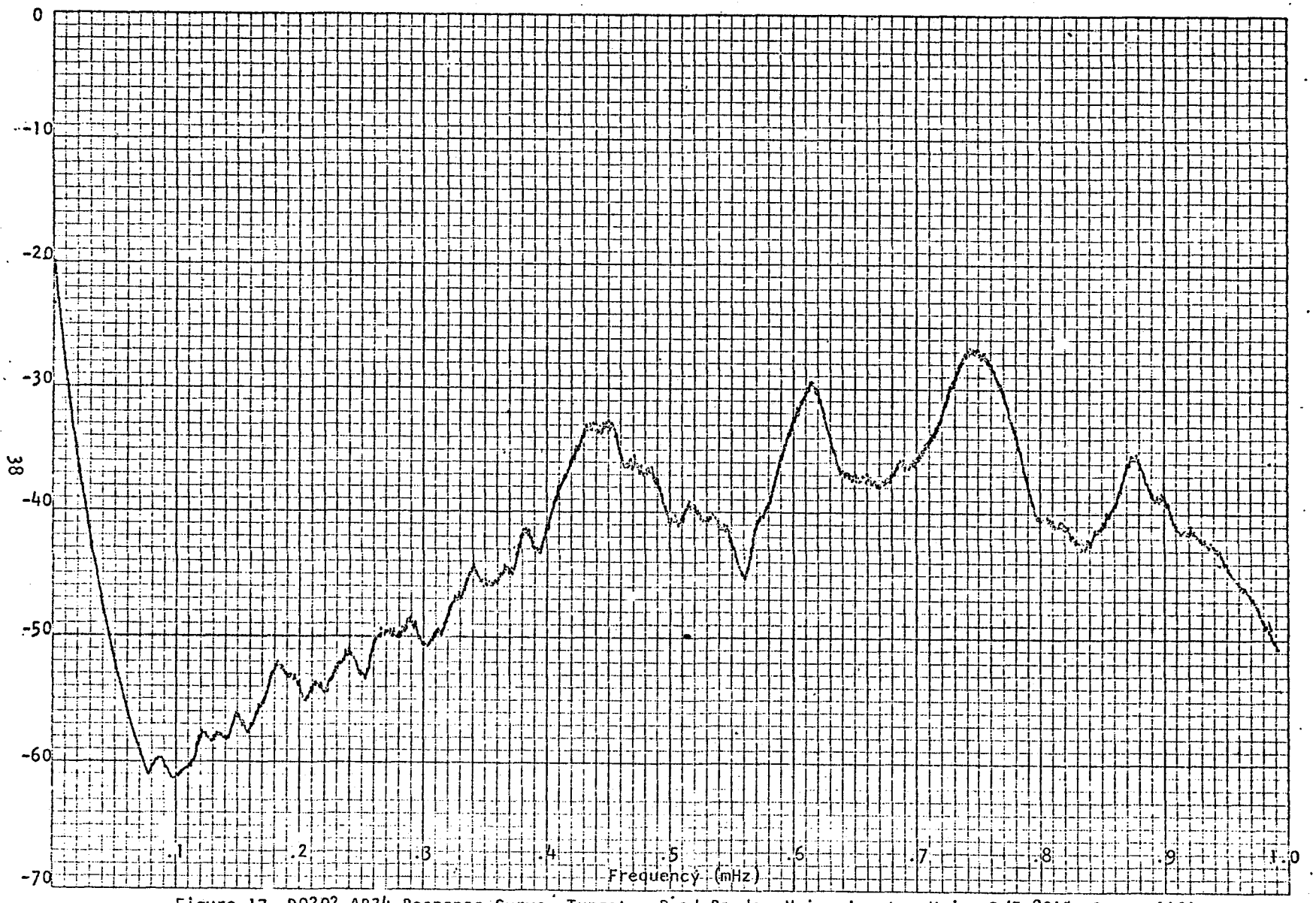

Figure 17- D9202-A834 Response Curve, Tungsten Bead Random Noise Input - Using D/E 801P Preamplifier

a series of spikes in an otherwise flat line at time intervals corresponding to the ball pass frequencies when a faulted bearing was used.

The sensors were mounted on a surface of the housing which had been machined flat. The 2236 and the 6230M8 were bolt mounted. The D9202 was bonded with Eastman 910 type quick set cement. For the fatigue tests the Model D9202 was attached with Sperry ultrasonic couplant between the base of the sensor and the housing flat section and then held in place with teflon tape. The quick set cement had been used for the short term series of tests. However, after prolonged exposure to the temperature of the housing during the fatigue test, a bond was not maintained between the alumina seating surface of the sensor and the steel bearing housing when using the quick set cement.

D. Instrumentation

Two different instrumentation setups were used to condition the signals from the sensors, to provide recordings, and to process and analyse the data. One system was used for all data below 200 kHz. This was for use with the 2236 and 6230M8 sensors and is shown in a block diagram in Figure 18. The other system was for use above 100 kHz and is shown in a block diagram in Figure 19. Data was taken with this using the D9202 sensor. Figure 20 is a photograph of the instrumentation assembled for the bearing tests.

The signal conditioners used for the low frequency system were standard 2730 and 2740 single ended charge amplifiers.

No internal filters were used in these amplifiers so that the conditioned response represented that of the sensor for the 2236 up to

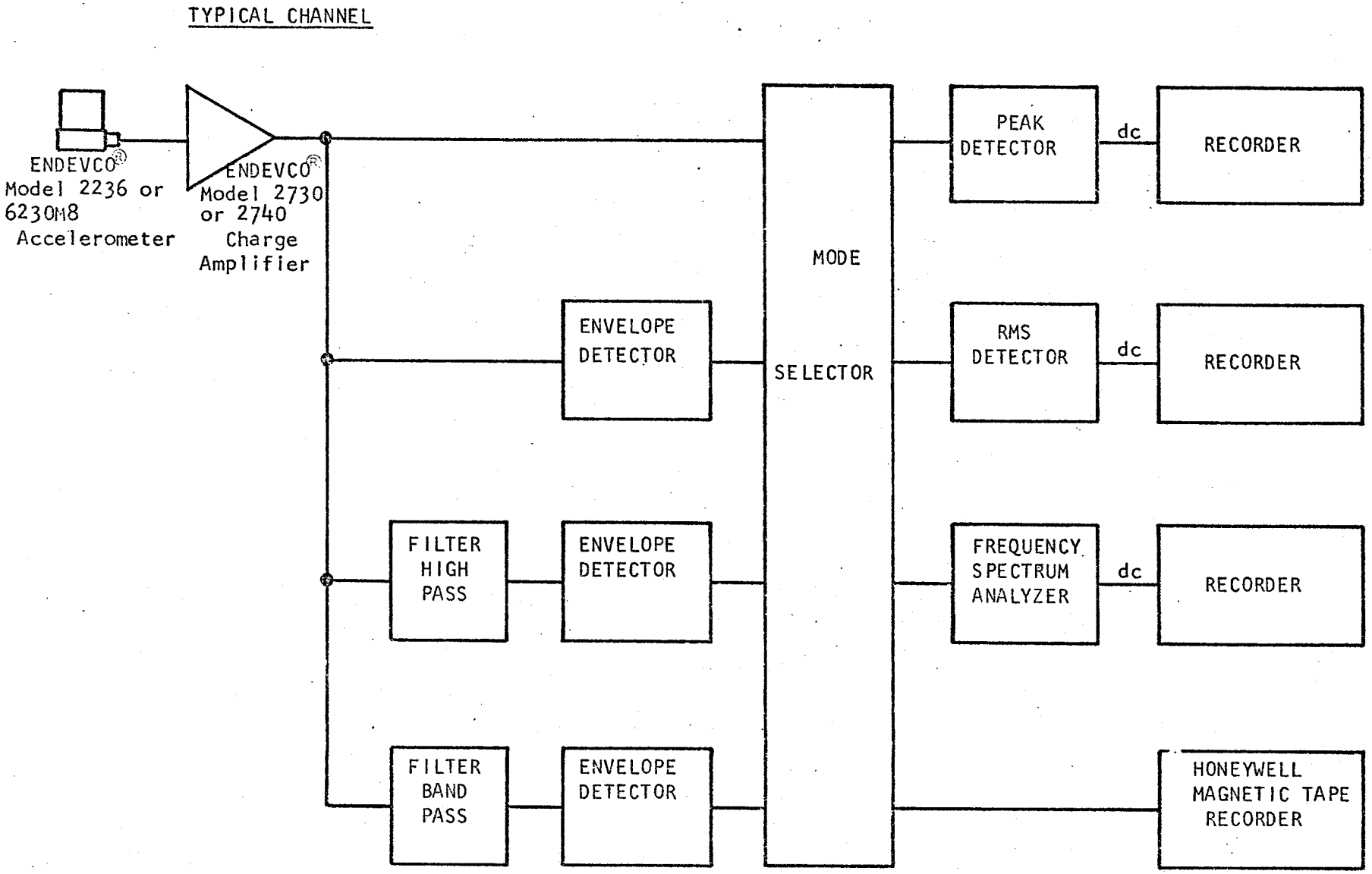

Figure 18 - Block diagram of test equipment with sensors operating in frequency range of 200 kHz and below.

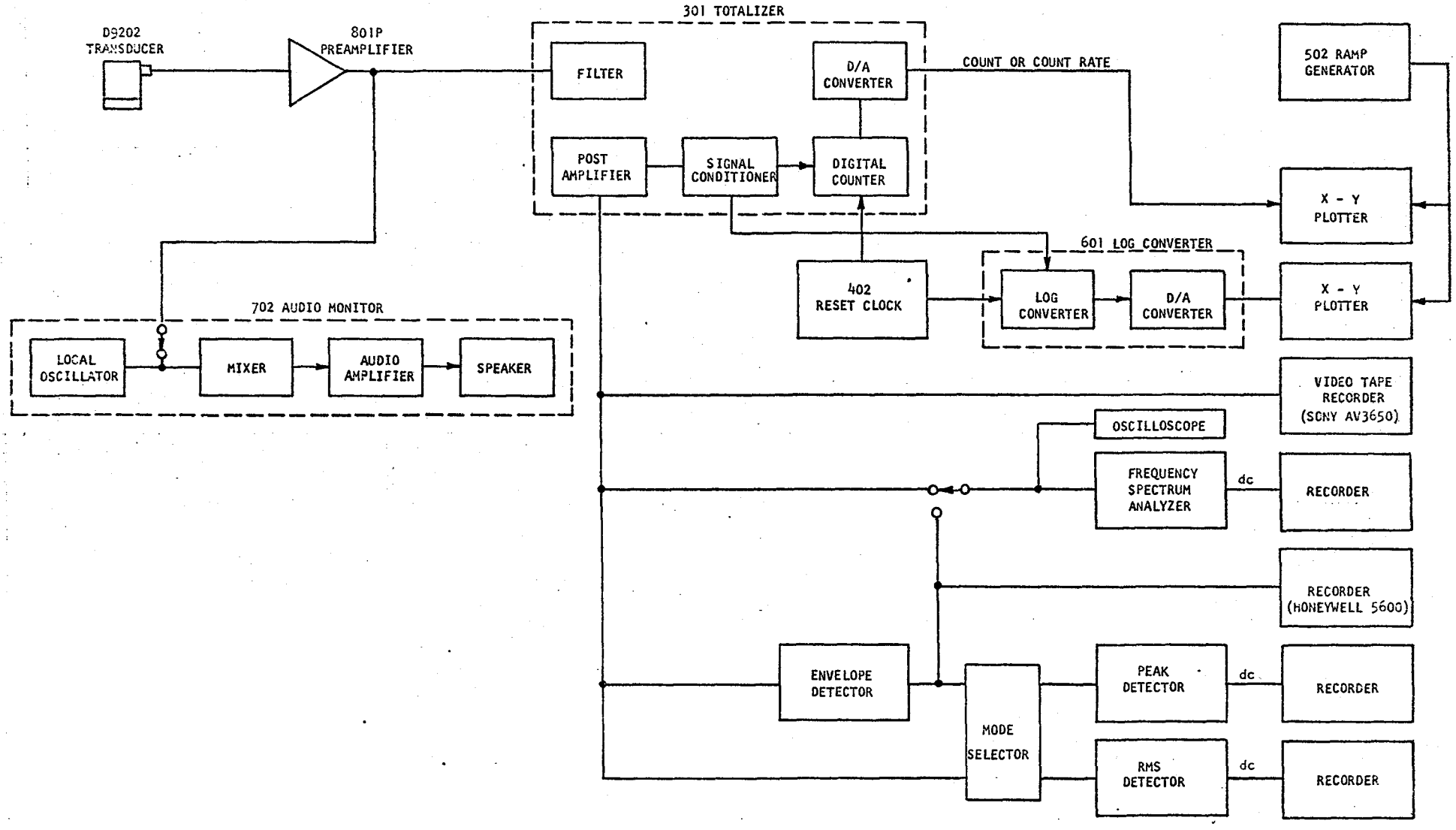

Figure 19 - Block Diagram of Test Equipment for sensors operating above 100 kHz

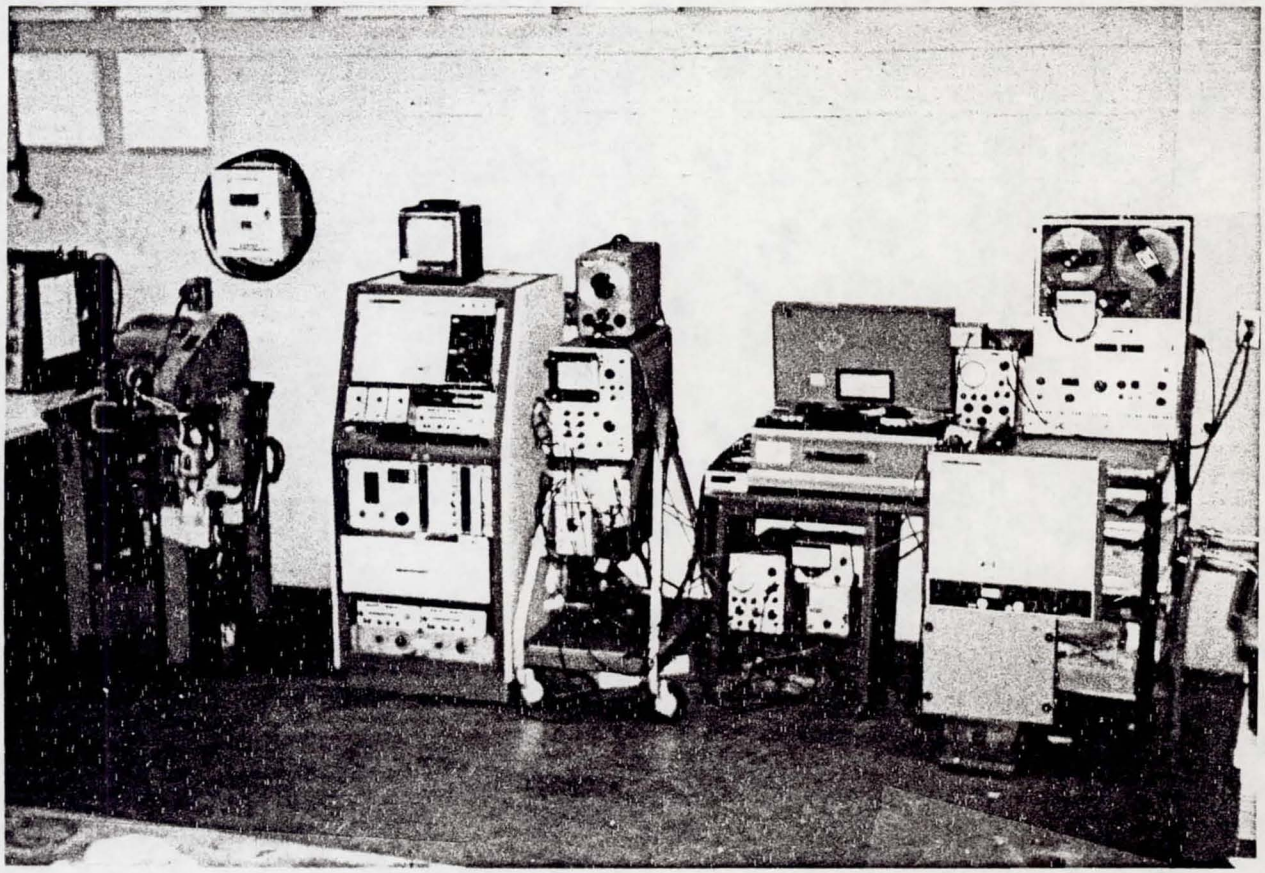

Figure 20 - Bearing test machine with equipment used to record and process the data from the bearing tests.

50 kHz and for the 6230M8 up to 200 kHz. All low frequency data below 200 Hz was taken with the 2236 sensor using an FM recording channel on the Honeywell 5600 Magnetic Tape Recorder. The remaining data was recorded in direct mode at 60 ips tape speed using high quality instrument tape to allow measurement up to 200 kHz. Amplifier gains were set for a standard 1V rms full scale.

During the continuous monitoring test phase additional processing equipment was added for the 2236 and 6230M8 so to provide a continuous recording of certain qualities of the signal. This consisted of adding certain filters to study the relative value of different frequency ranges and the addition of envelope detectors so to examine the modulation characteristics of the high frequency vibrations. A peak and an RMS detector circuit was added to permit plotting of data onto strip chart recorders during the continuous monitoring.

The high frequency data from the D9202 was examined using a Dunegan-Endevco Acoustic Emission Instrumentation Setup. This setup is described by Figure 19 and is shown in the photograph in Figure 21. The D/E Model 801P Pre Amplifier is a voltage sensing device with 40 dB gain and frequency response band passed for -3 dB at 100 kHz and 2 mHz. The totalizer provides an additional adjustable gain of up to 60 dB for proper setting of recording levels, and circuitry for totalizing the number of times a signal exceeds a preset level. A threshold of 1 volt is preset in the Model 301 so that a "count" can be made every time when a signal crosses that threshold. This count information can be plotted directly from the output of an internal D/A converter. The "count rate" is provided by using the 402 Reset Clock on the count information in the totalizer. This count rate and the count

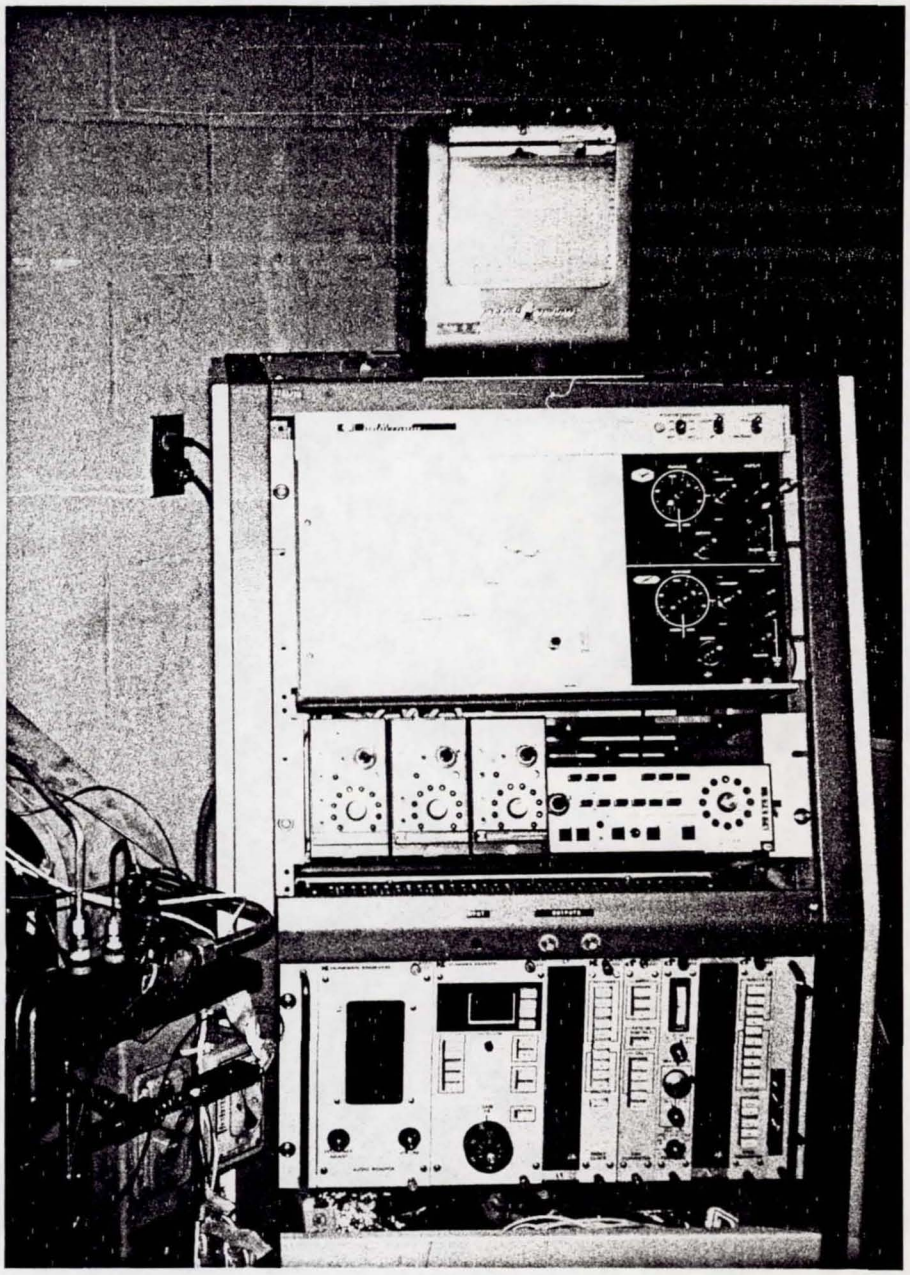

Figure 21 - Signal conditioning electronics with typical recorders used for the bearing tests.

can be plotted in log scale by using the 601 log converter. The adjustable 10 Volt ramp voltage for the X-axis of the plotter is supplied by the 502 Ramp Generator to provide a ramp of duration from 1 minute to 48 hours. The 702 Audio Monitor enables an operator to hear high frequency signals.

To record the pre-analysed signal from the D9202 at high frequency, a video tape recorder, Sony-Matic with Realistic Card, Model AV3650 was used. This recorded signal levels for analysis up to 1 mHz.

A Honeywell Real Time Spectrum Analyzer, Model SA1-52B was used for frequency analysis of all signals. The analysis and tape recorders are shown in the photograph in Figure 22. Data was obtained for "on line" measurements while the tests were running of the various vibration outputs. Analysis of ranges up to 1 kHz, 2 kHz, 10 kHz, 50 kHz, and 1 megahertz were conducted as appropriate for the data channel. The tape recorded information was also analyzed for further comparisons as well as after additional processing as discussed later. The analyzer included an averaging feature which provides signal to noise improvement for the data display. The frequency spectrum analyses were plotted on an X-Y recorder for a permanent record when desired.

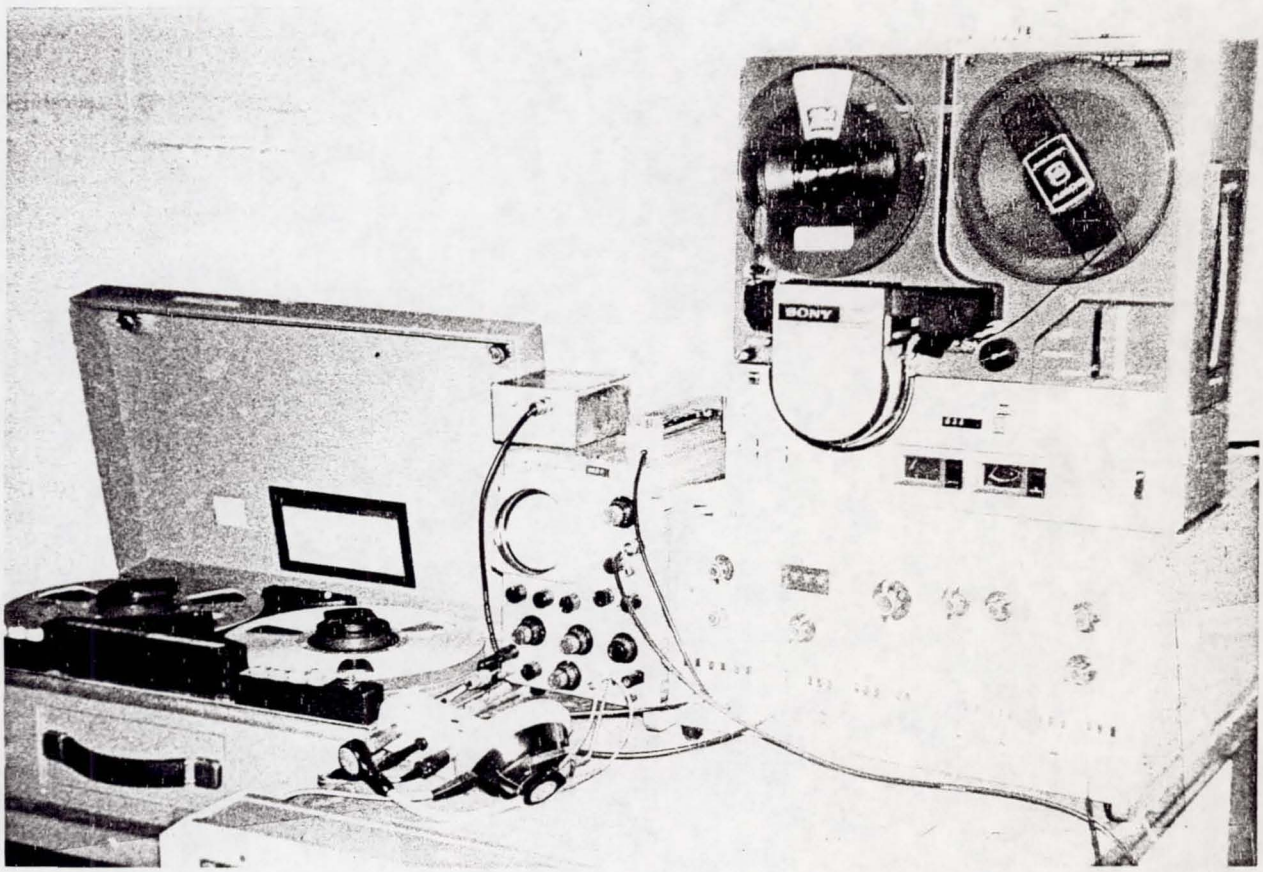

Figure 22 - Magnetic Tape Recorder and Frequency Spectrum Analyzer used for the bearing tests.

IV TEST BEARING PREPARATION

A total of twenty-four bearings were used in the program. Thirteen bearings were disassembled by Bearing Inspection Corporation, Santa Fe Springs, California. Nine of the thirteen bearings were selected to have faults eloxed across the race in the ball travel area. Different size slots were made on the inner race of some and on the outer race of others. In order to provide a smaller fault than practical with the elox, two bearings were marked with a sharp alumina scribe, one on an outer race, and the other on an inner race. One ball of another bearing was scribed along two equators, 90° apart from each other. The remaining bearing was reassembled without any applied fault.

A profilometer recording was made on each race of the unfaulted bearing, one each race that had a fault applied, and on the ball with the fault. Typical examples from these measurements are displayed in Appendix 3.

The results are summarized in Table III showing the overall dimensions of the faults.

Other bearings were tested as purchased with no faults employed. Several of those were used for the fatigue study and others used as side bearings in the rig.

TABLE III

BEARING FAULTS

S/N	FAULTED MEMBER	LEADING EDGE ELEVATION μ - INCH	WIDTH INCH	DEPTH INCH	TRAILING EDGE ELEVATION μ' - INCH
1	Ball*	100 nominal	0.007 nominal	0.0001	50 nominal
2	Outer Race	0	0.0448	0.0127	0
3	Outer Race	160	0.0115	0.0052	200
4	Inner Race	80	0.0078	0.0048	140
5	Outer Race	30	0.0096	0.0054	120
6	Outer Race	0	0.0133	0.0102	0
7	Outer Race	480	0.0087	0.0065	360
	Outer Race at 180°	340	0.0086	0.0054	160
8	Outer Race	180	0.0069	0.0028	180
9	Inner Race	0	0.0090	0.0064	40
10	No Fault	-	-	-	-
11	Inner Race	80	0.012	0.010	60
12	Outer Race*	5	0.0014	0.00013	2
13	Inner Race*	0	0.0018	0.00024	2

*Scribed with alumina

V. FAULT CHARACTERIZATION TESTS

A. Procedures

For this first series of fault characterization tests, the data was obtained with a minimum operating time on each bearing tested to establish the level of detection for the induced fault before it progressed into a larger failure, possibly then causing other failure modes. These short duration tests were conducted at two different loads at each of the two speeds. These tests correspond to an L_{10} life expectance of from about 800 hours to 11,500 hours for the center bearing. The life for the bearing under various loads at the two speeds selected for the tests is shown in figure 23 and was computed from the standard equation (13):

$$L_{10} = \frac{50,000}{N} \left(\frac{C}{P}\right)^3$$

L_{10} is the life in hours for which ten percent of the bearings will fail. "C" is the basic load value for the bearing, "P" is the applied radial load used for the tests and "N" is the speed in rpm. Modifiers may be assigned to this equation based on quality of lubrication, different percentage of bearing failures, and for other factors of load, bearing design, etc. For the tests in this program, the lubrication system was to achieve the expected life in this equation for the two operation speeds.

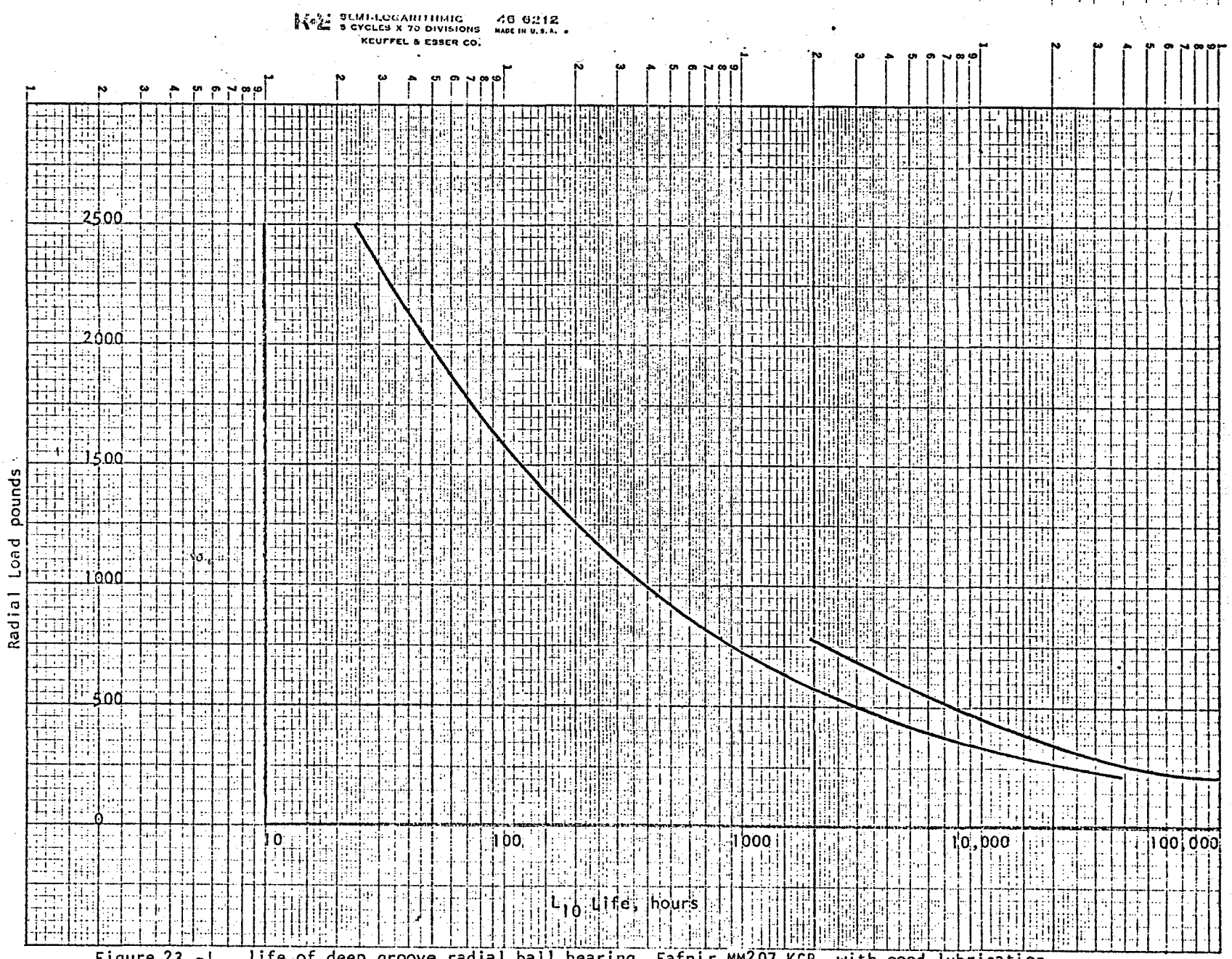

Figure 23 - L_{10} life of deep groove radial ball bearing, Fafnir MM207 KCR, with good lubrication, versus applied radial load

Page intentionally left blank

The size of the bearing faults are shown in Table III. This is discussed in Section IV. Bearings which had a fault groove cut into the outer race were oriented to place the fault at the top where it would be under maximum load. One exception to this was for bearing number 7 which had two faults diametrically opposed to each other. This bearing was used for run number 6 with one of the faults on top and the other at the bottom where it would experience minimum loading. For run number 7, the faults were positioned horizontally across the housing and hence each had similar loading at something less than when positioned at the top of the housing. The other faults were on rotating members of the bearing and therefore were installed without specific orientation.

B. Results and Discussion

Frequency spectrum measurements were made at the various conditions of load and speed for the test run discussed above. The results of these analyses are summarized in Tables V, VI, VII and VIII. The discussions in the earlier sections of this report on bearing failure characteristics and sensor characteristics are reflected in these tables. For example, the significant data recorded from Model D9202 Sensors occurred in the 0.5 megahertz region near the sensor peak response. Similarly, significant data were obtained in the 120 kHz region for Model 6230M8 and in the 30 kHz region for the Model 2236 outputs; typical frequency spectrum plots have been selected to further elaborate on this and these are displayed in Appendix 4.

Additional data was obtained by frequency spectrum analysis in the regions of 5 kHz, 13 kHz, 20 kHz, and 30 kHz for both the 2236 and 6230M8 sensors as shown in the tables VI and VII and Appendix 4. These frequencies

TABLE V - Analyzed Output (g) in the Outer Race Fault Ball Pass and the Once Per Revolution Frequency Regions for the Center Bearing

TYPE	SENSOR	RUN* CONDITION	FREQUENCY	RUN NUMBER 1	2	3	4	5	6	7	8	9	10	11
ONCE PER REVOLUTION FREQUENCY	Model 2236	a	215	-	.69	.28	.79	.98	.69	.64	.78	.32	.47	-
		b	215	.22	.62	1.77	.77	.56	.64	.64	.64	.97	.37	.37
		c	89	-	.07	-	-	.12	.12	-	-	.05	.08	-
		d	89	-	-	.13	.08	.11	-	-	-	.08	.02	-
	Model 6230M8	a	215	-	-	-	.21	.6	.38	.46	-	.15	.25	.045
		b	215	.60	.57	-	.23	.46	.38	.25	0.3	.53	.14	low
		c	89	-	-	-	.1	.15	.29	-	-	.31	.15	.59
		d	89	-	-	-	.07	.17	.32	-	-	.30	.2	low
BALL PASS FREQUENCY	Model 2236	a	668	-	.7	1.63	.55	.42	.56	.45	3.8	.26	-	-
		b	668	.35	.22	1.99	.64	.1	.29	.51	1.27	.19	.35	-
		c	281	-	.32	.16	.19	.12	.15	-	-	.12	.09	.07
		d	281	-	-	.13	.12	.11	-	-	-	.11	.06	-
	Model 6230M8	a	668	-	-	-	.68	.97	.79	1.01	-	.25	.65	.54
		b	668	.45	.48	.85	.63	-	.62	.48	.6	.35	.59	.21
		c	281	-	-	-	.58	.59	.61	-	-	.26	.56	.22
		d	281	-	.52	-	.32	.16	.48	-	-	.20	.26	low

* a - 12900 RPM, 781 lb. load
b - 12900 RPM, 430 lb. load
c - 5400 RPM, 780 lb. load
d - 5400 RPM, 430 lb. load

TABLE VI - Analyzed Output (g) in the Regions of the Bearing Race Resonant Frequencies from Model 2236 Accelerometer on the Center Bearing

FREQUENCY (kHz)	RUN* CONDITION	RUN NUMBER 1	2	3	4	5	6	7	8	9	10	11
5	a	-	6.5	2.8	.23	1.6	2.0	.91	58.	.17	-	-
	b	-	3.9	1.3	.13	-	1.9	1.0	24.4	.13	.23	.34
	c	-	3.0	1.1	.24	1.2	3.3	-	-	.05	.04	.05
	d	.08	1.0	1.38	.1	3.1	-	-	-	.05	.05	.04
13.5	a	-	5.71	3.46	-	1.5	2.1	-	22.7	.15	.15	-
	b	.5	5.1	2.2	.16	-	2.56	-	-	.22	.18	-
	c	-	1.26	.36	.06	.8	1.07	-	-	.05	.03	-
	d	.35	.4	.58	.06	-	-	-	-	.04	.04	-
20	a	-	9.0	6.7	.87	14.6	8.3	9.7	23	.42	-	-
	b	2.0	6.0	2.3	1.0	10.6	12.8	15.8	9.8	.42	1.1	.74
	c	-	.88	.75	.21	1.9	.97	-	-	.003	.1	.13
	d	.38	-	.27	.15	.9	-	-	-	.06	.13	.08
30	a	-	15.8	11.0	.52	18.4	10.6	-	67.3	.56	-	-
	b	1.8	48.0	19.3	.9	21.7	35.2	3.3	60.6	.56	1.0	-
	c	-	1.94	1.32	.26	1.85	.95	-	-	.02	.1	-
	d	-	2.3	4.07	.22	1.9	-	-	-	.09	.15	.15

* a - 12900 RPM, 780 lb. load
b - 12900 RPM, 430 lb. load
c - 5400 RPM, 780 lb. load
d - 5400 RPM, 430 lb. load

TABLE VII - Analyzed Output (g) in the Regions of the Bearing Race Resonant Frequencies from Model 6230M8 Accelerometer on the Center Bearing

FREQUENCY (kHz)	RUN* CONDITION	RUN NUMBER 1	2	3	4	5	6	7	8	9	10	11
5	a	-	5.6	2.54	.23	1.18	1.6	.93	32.5	.41	.42	.57
	b	.60	4.3	1.23	.1	.88	-	.87	23.7	.43	.43	.50
	c	-	1.5	1.46	.11	1.32	2.95	-	-	.09	.072	.02
	d	-	-	1.19	.09	.7	1.78	-	-	.10	.075	.03
13.5	a	-	4.3	2.17	.14	1.0	4.0	.50	13.8	.17	.20	.15
	b	-	3.5	1.47	-	2.47	-	.60	11.8	.18	.10	.13
	c	-	.27	.23	.02	.57	.75	-	-	.02	.03	.03
	d	-	-	.37	.03	.74	.63	-	-	.03	.03	.03
20	a	-	1.92	1.46	.18	2.69	1.6	4.07	3.3	.13	.17	.20
	b	-	.9	.55	.17	3.12	-	3.41	6.30	.17	.21	.19
	c	-	.075	.17	.032	.54	.31	-	-	.02	.03	.037
	d	-	-	.06	.31	.53	.84	-	-	.02	.03	.026
30	a	-	3.4	2.19	.20	5.72	2.15	1.59	35.9	.13	.24	.18
	b	-	8.21	4.05	.17	4.15	-	1.58	22.9	.18	.23	.23
	c	-	.18	.43	.032	.54	.30	-	-	.015	.037	.053
	d	-	-	.73	.032	.34	.85	-	-	.029	.034	.059

* a - 12900 RPM, 780 lb. load
b - 12900 RPM, 430 lb. load
c - 5400 RPM, 780 lb. load
d - 5400 RPM, 430 lb. load

TABLE VIII - Analyzed Output (mV) Near 450 kHz for Model D9202 on the Center Bearing, Using a 40 dB Gain Preamplifier

RUN * CONDITION	RUN NUMBER 1	2	3	4	5	6	7	8	9	10	11
a	-	74.6	-	8.46	29.4	29.8	14.1	31.8	8.2	10.9	8.91
b	17.9	52.4	21.9	9.9	21.3	19.7	14.1	30.4	6.5	10.3	7.78
c	-	5.57	3.26	2.09	7.83	5.7	-	-	1.56	1.46	2.24
d	2.1	-	2.39	-	4.63	7.83	-	-	2.06	1.23	1.79

* a - 12900 RPM, 780 lb. load
b - 12900 RPM, 430 lb. load
c - 5400 RPM, 780 lb. load
d - 5400 RPM, 430 lb. load

correspond to the various radial and flexural modes of the outer race of the bearing as discussed in Table II of Section II. Data near 50 kHz and 70 kHz, corresponding to higher orders of flexual resonances, was also obtained on the spectrum analyses of Model 6230M8 outputs.

The g levels indicated by the 6230M8 and the 2236 are nearly the same for the frequencies below about 5 kHz. However, the frequency analyses do indicate there is a gain effect from the resonance frequency of Model 2236 near 20 kHz and 30 kHz. The data is about 10 dB to 15 dB higher in this region for Model 2236 than for Model 6230M8.

One significant point shown in the data tables V, VI, and VII is that the high frequency energy content of the signal is larger when faulted bearings are tested whereas the energy in the ball pass frequency range is not significantly different from new condition bearings.

Table V shows that the one cycle per revolution signal level is nearly the same for all tests with the same speed and load. For example, Model 2236 data in the "a" line, corresponding to 12,900 rpm and 780 pound load, is 0.79 g in run 4, (a nonfaulted bearing). The other runs with faulted bearings range from 0.32 g to 0.98 g. The same nearly consistent values are shown in the "b" line for 12,900 rpm and 430 pound load.

Similarly, the signal levels corresponding to the ball pass frequency for a discrete fault on the outer race also shows nearly the same level for all runs with a few exceptions as for Model 2236 in run 8 and in run 3. In general, however, this data must be closely observed and the tests carefully controlled in order to relate bearing damage to ball pass frequency spectrum analysis of raw data.

The faulted inner race test in run 5 was barely detectable from the analyzed data at the inner race ball pass frequency. It is possible that this may have been a result of the pure radial loading. As the inner race of the bearing rotates, the fault in the inner race is unloaded at the bottom half of the cycle. Hence, large outputs occur only near the maximum load which occurs at one cycle per revolution. If thrust load were also used in the tests, a load would have been more constant on the faulted area of the inner race.

The bearing with a ball defect in run 10 was again barely detectable in the ball pass frequency region. The fault applied to the ball was very small, designed to determine the minimum level of detection. However, it was expected that the nature of the fault, described previously as a scribe around the two equators of the ball, would result in two or four times the normal single fault ball pass frequency.

Observe again the 2236 data for the nonfaulted bearing of run 4 at one cycle per revolution, at the outer race ball pass frequency, and at the high frequencies. The output is on the order of 0.5 g for all these frequencies. Comparing all of this data to that from run numbers 2, 3, 5, 6, 7, and 8 shows a significant change in signal level for faulted bearings at high frequencies only. For example the data table VI shows levels of 10 g to 67 g near 30 kHz. Similar high g levels are shown for 5 kHz, 13 kHz, and 20 kHz for the 6230M8 data for the faulted bearing test runs.

The high frequency results are consistent with information reported in the references (11, 12). Envelope detection of these high frequency signals has been used to enhance the ball pass frequency data. The output waveform from the Model D9202 was observed on an oscilloscope

to be very short duration ringing bursts on the otherwise flat portion of data almost as if it were envelope detected. When a sweep speed of 1 millisecond per centimeter is used to observe the 215 Hz or 668 Hz data, these ringing bursts appear almost as spikes at a very distinct frequency in this ball pass frequency range. Comparable data from low frequency sensors appears as almost random data unless the fault is very large. Even then, the ringing continues from one peak to the next since this data includes the modulated high frequency ringing as well as other low frequency sources from the structure.

Data table VIII shows the relative output at 450 kHz from the Model D9202 Sensor for the various test runs. Again as with the two lower frequency sensors, the signal is higher for runs 2, 3, 5, 6, 7, and 8 where elox faulted bearings were tested than for run 4 with a nonfaulted bearing. Note however that the difference between run 4 and the others is not as great as for the two lower frequency sensors.

The effects of load and speed are also indicated in the tables for this phase of the program. High speed always produces much larger output than the lower speed. The increase in load has a more random effect, sometimes increasing and sometimes decreasing the output. These effects show the importance of using changes in a signal level from a base line established during normal operating conditions (rather than absolute levels).

The resolution of the detection systems used in this phase may be examined by comparison of signals to the size of the faults. For the eloxed fault 0.0028 inch deep by 0.0069 inch wide in run 3, there is an obvious indication in the data table that this is a faulted bearing when

referenced to the nonfaulted bearing in run 4. However, for bearings scribed with a fault about 0.0002 inch deep by about 0.001 wide in runs 9, 10, and 11, the data does not indicate a significant change from the nonfaulted bearing in run 4. Appearently the depth of this scratch is not sufficient to produce a high frequency impulse of adequate magnitude to excite the resonances of the sensor and/or races to produce decernable changes in level of output. It is probably that the signal level from these 3 bearings would differ one from another in a new, non-scribed condition of test. Therefore, it is possible that detection of fault propagation of this size would be feasible if a lower base line had been established.

VI BEARING FAILURE PROPAGATION TESTS

A. Procedure

The objective for the second phase of this test program was to study the changes in signal levels from bearings during accelerated life tests. Both good and faulted bearings were used. The side support bearings were good (nonfaulted) bearings for all the tests. To accelerate the failures, the load was increased and the highest speed of 12,900 RPM was used for all tests.

Tape recordings were made at the start of the test and at some intervals during the test. Continuous X-Y and strip chart records were made of several outputs. Frequency spectrum analyses were made of real time data, envelope and/or filtered data.

The high frequency AE measurement system was used for continuous monitoring while the bearings were operating. The use of count rate was observed to be most useful in the detection of changes in vibration or stress wave activity and was therefore employed.

An automatic shut down circuit was provided by ENDEVCO® Model 6634 Signal Conditioner with a Model 2236 Accelerometer. Some tests were terminated prior to automatic shut down to assess bearing condition by disassembly and inspection. This was done in part to correlate damage with the output signal prior to incurring the substantial level of damage that would normally precipitate the 6634 signal conditioner to identify that the conditions for shutdown existed. For those runs where the data remained relatively constant, visual inspection of the bearings was used as a verification of fault detection sensitivity.

The fatigue test program schedule is shown in Table IX.

TABLE IX - FATIGUE TEST SCHEDULE

RUN NO.	OPERATING TIME/HRS	CENTER BEARING NO.	CENTER BEARING FAULT LOCATION	SUPPORT BEARINGS NO.	SUPPORT BEARINGS NO.
I	66.5	13	Inner Race	18	19
II	0.7	3	Outer Race	15	16
III	20.3	6	Outer Race	15	16
IV	46.75	10	None	15	16
V*	0.5	14	None	*	*
VI	82.3	17	None	20	21
VII	22.5	12	Outer Race	20	21

*Test was aborted. Side bearings of another manufacturer and supposedly equivalent bearings, but actually were designed for operation with some thrust loads.

The first test run used bearing number 13 in the center position. The load was increased to 2150 pounds which corresponds to an L_{10} life of about 40 hours for an undamaged bearing. Recordings were made of the vibration outputs at the start of the test with this increased load. During the test, recordings were also made of the count rate and envelope detected output of the Model D9202 Sensor, the envelope detected broadband output of the Model 6230M8, the envelope detected filtered output from 25 kHz to 30 kHz of the Model 2236, and the broadband peak detected output of the Model 2236 Sensor.

After 27 hours, no change in performance was indicated and hence the load was increased to 2500 pounds which corresponds to an L_{10} life of about 25 hours. After 20 additional hours of operation (47 hours total),

there was a strong indication of probable failure development from the Model D9202 recordings. Some change was also measured on Model 2236 output recordings as will be discussed in Section VI B. Since this test was continuing over a weekend, unattended, the test was not stopped at this time. However, after an additional 20 hours, the broadband vibration level increased above the shut down level (which was set on the Model 6634 Signal Conditioner at 50% above the operation level at the beginning of the test). The test was automatically shut down.

Test run number 2 was conducted with bearing number 3 which had a much larger fault than bearing number 13. Additionally, the fault was in the outer race and since the fault was always placed at the maximum load position at the top of the housing failure was expected earlier. Unfortunately, the failure and rig shut down occured after only 0.7 hours with the 2150 pound load. Recordings were made of the sensor outputs at the start of the test. The rig was started up again and ran long enough to record final value data after the failure.

Number 6 bearing, with a fault on the outer race was installed for test number 3 to establish a longer fatigue progression test with this type fault. The load was set at 430 pounds in view of the very quick failure in the previous test. After 16.7 hours, no change in output was observed and the load was increased to 860 pounds. After 3.6 more hours, a total of 20.3 operating hours, the test was terminated. There still had been no indication of any change in the condition of the bearing, but the test was discontinued to examine the physical appearance of the fault area.

Test number four was run with a good, nonfaulted bearing operating with 2500 pound load over the entire test, corresponding to a L_{10} life of about 25 hours. The test was terminated manually after 46 hours when significant indication of change in Model D9202 sensor outputs was observed.

Test number five was designed for a repeat of a good, nonfaulted bearing running until fatigue failure occurred. However, the test was aborted after 0.5 hours due to increased vibration outputs. The cause was later determined to be from incorrect side bearings used for this test run.

Test number six was conducted with 2500 pound load on good, new bearings. The test was shut down automatically by broadband acceleration output with the Model 6634 Signal Conditioner during a weekend unattended operating time.

Test number seven was conducted with a lower load of 1650 pounds since the bearing number 12 used had a small fault scribed into the outer race. This test was discontinued after 22.5 hours because it was estimated that the outer race of the bearing was rotating within the housing at one revolution per 2.2 minutes. If this continued, excessive housing wear would result.

B. Results and Discussion

Since the most optimum detection was shown to be in the higher frequency region in the fault characterization tests, this was used as a basis for priority of continuous recording of data. Data in the filtered range of 20 KHZ to 35 KHZ as well as high pass above 20 KHZ and 100 KHZ were used for the most of the recording, although some broadband data were also obtained.

For frequencies above 100 KHZ, the "count" and "count rate" from the Model D9202 sensor with Model 301 totalizer were used. Additionally, peak detection of the data output and of the envelope detected output from the Model D9202 sensor was recorded.

The test results show that the most sensitive indicator of change is count rate recording of the Model D9202 Sensor with Model 301 Totalizer. In fact, before faults were developed to near the size of the eloxed slots previously tested, the D9202 showed large changes in level, whereas the lower frequency sensors showed minimal change if any. As our example, data shown in figures 24, 26, and 27 for test number one, four and six show these large changes in count rate. Specifically, the count rate changes from about 100 counts per second to 900 counts per second at the first large indication of probable failure development near 47 hours in test number one, Fig. 24. While this change of a factor of nine times was recorded from the rate data, the envelope detected data on Fig. 25 indicated a change of about 1.6 times from 1000 mV to 1600 mV. These results for test number one were for a bearing which may have been considered to have been "failed" before the test began, since it had a scribed line 0.00024 inch deep across the inner race.

The count rate data had changed gradually during the first 24 hours of test one by a factor of about ten and an additional factor of ten over the next 23 hours prior to the large indication discussed above. It is not known if the gradual increase in count rate is indicative of crack propogation, stress waves, or impacts increasing in magnitude as the

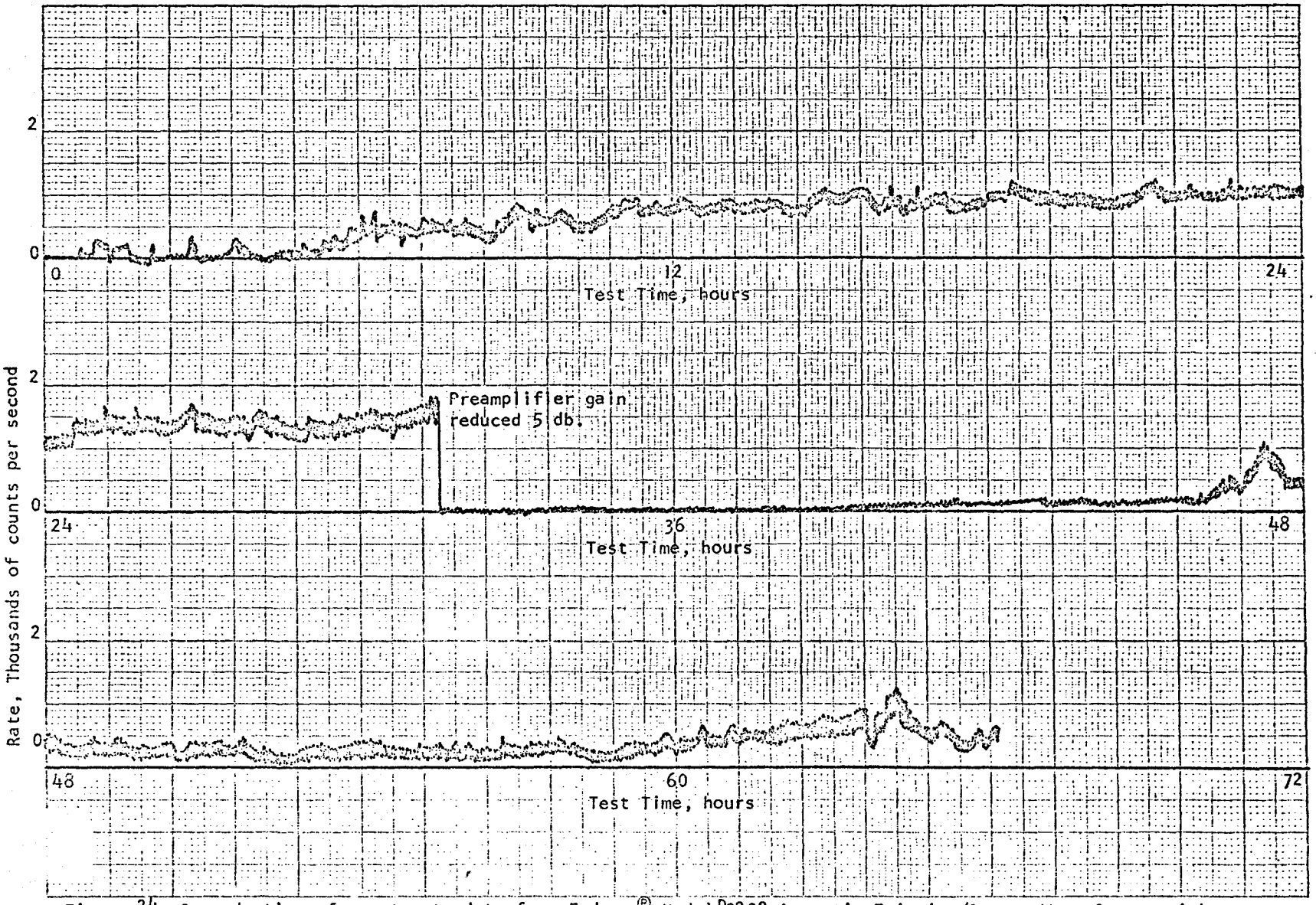

Figure 24- Reproduction of count rate data from Endevco® Model 9202 Acoustic Emission/Stress Wave Sensor with Model 301 Totalizer on fatigue test run number one, bearing number 13.

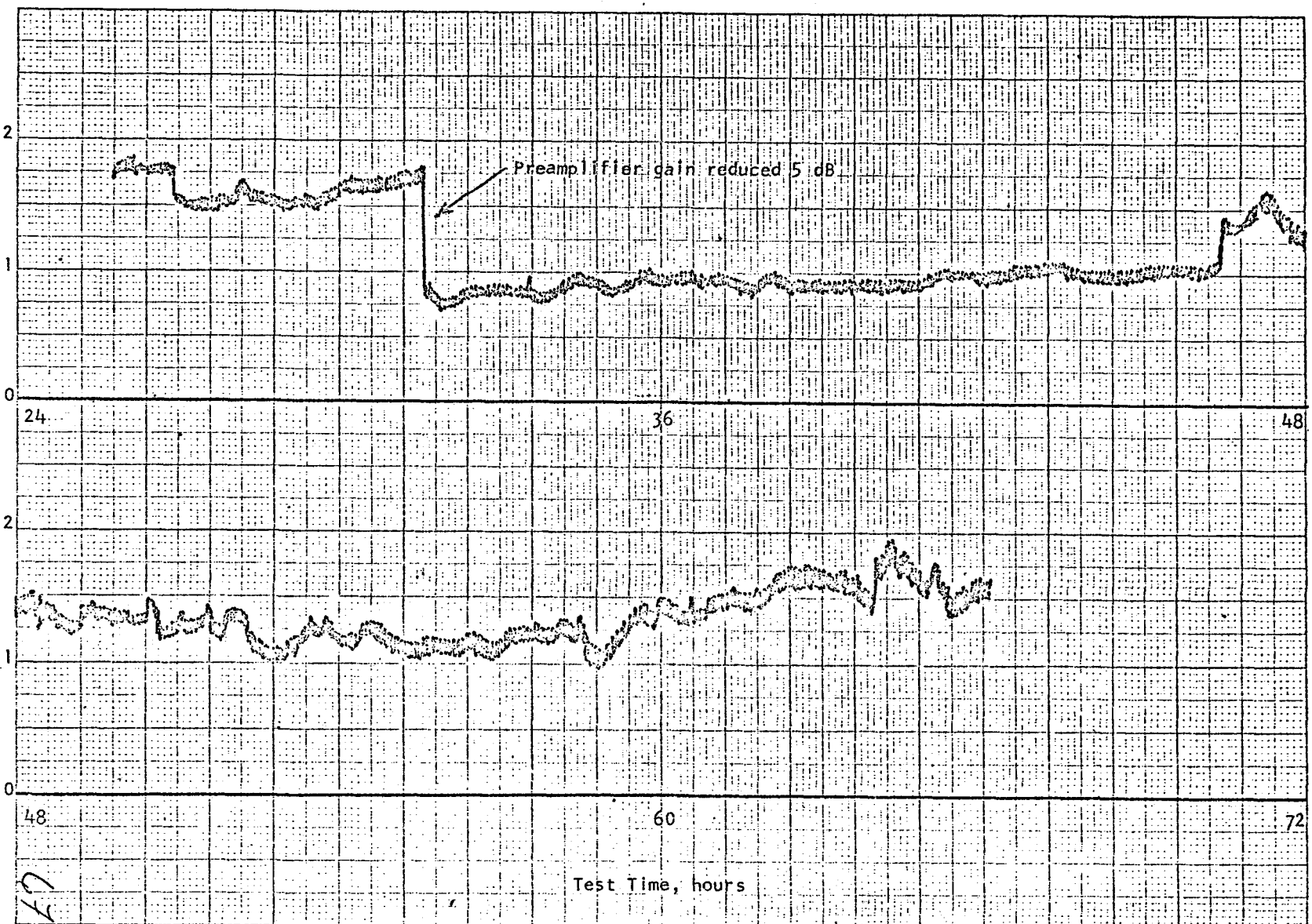

Figure 25 - Reproduction of peak envelope detected data from Endevco® Model D9202 Acoustic Emission/Stress Wave Sensor on fatigue test run number one, bearing number 13.

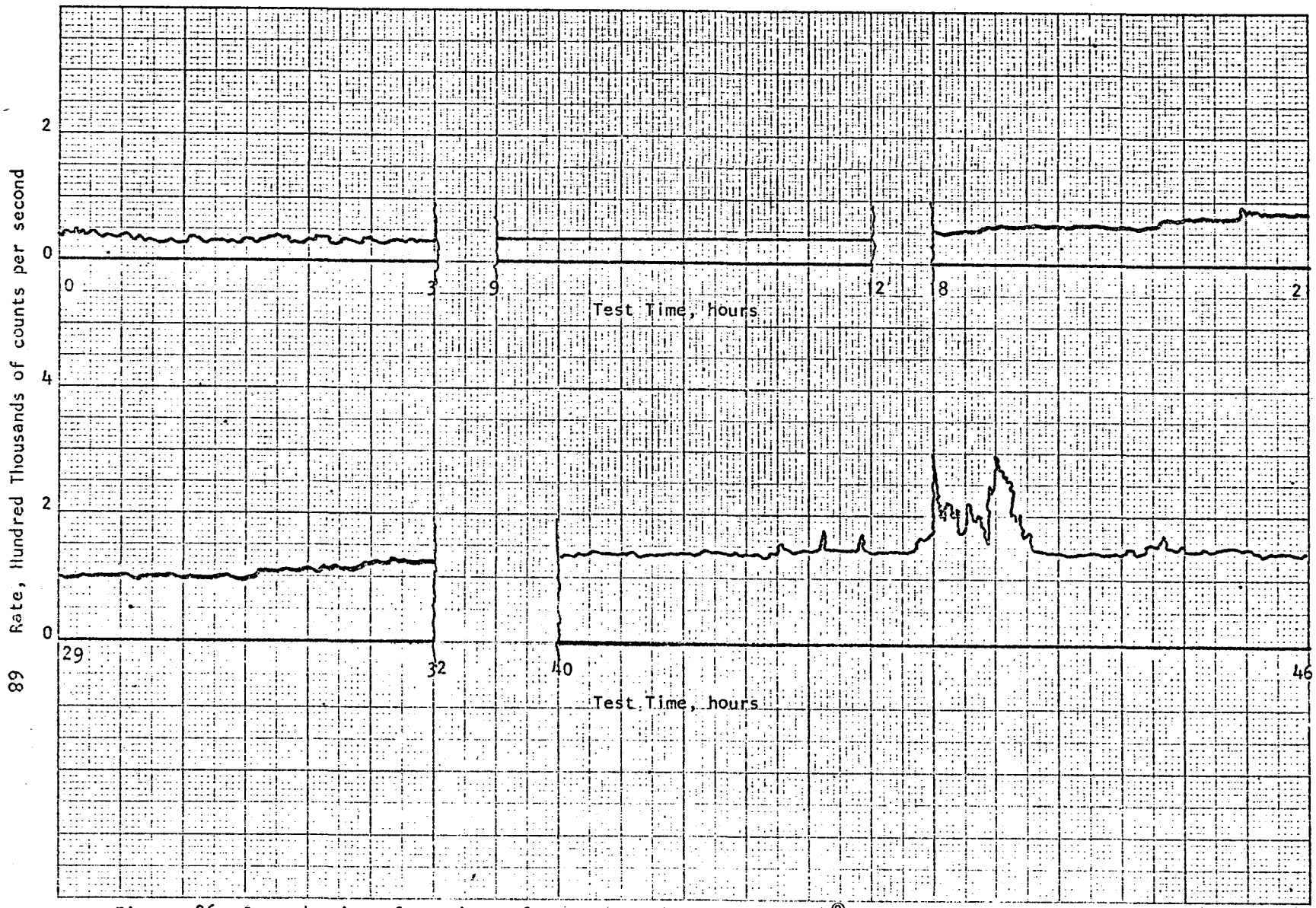

Figure 26 - Reproduction of sections of count rate data from Endevco® Model D9202 Acoustic Emission/Stress Wave Sensor with Model 301 Totalizer on fatigue test run number four, bearing number 10.

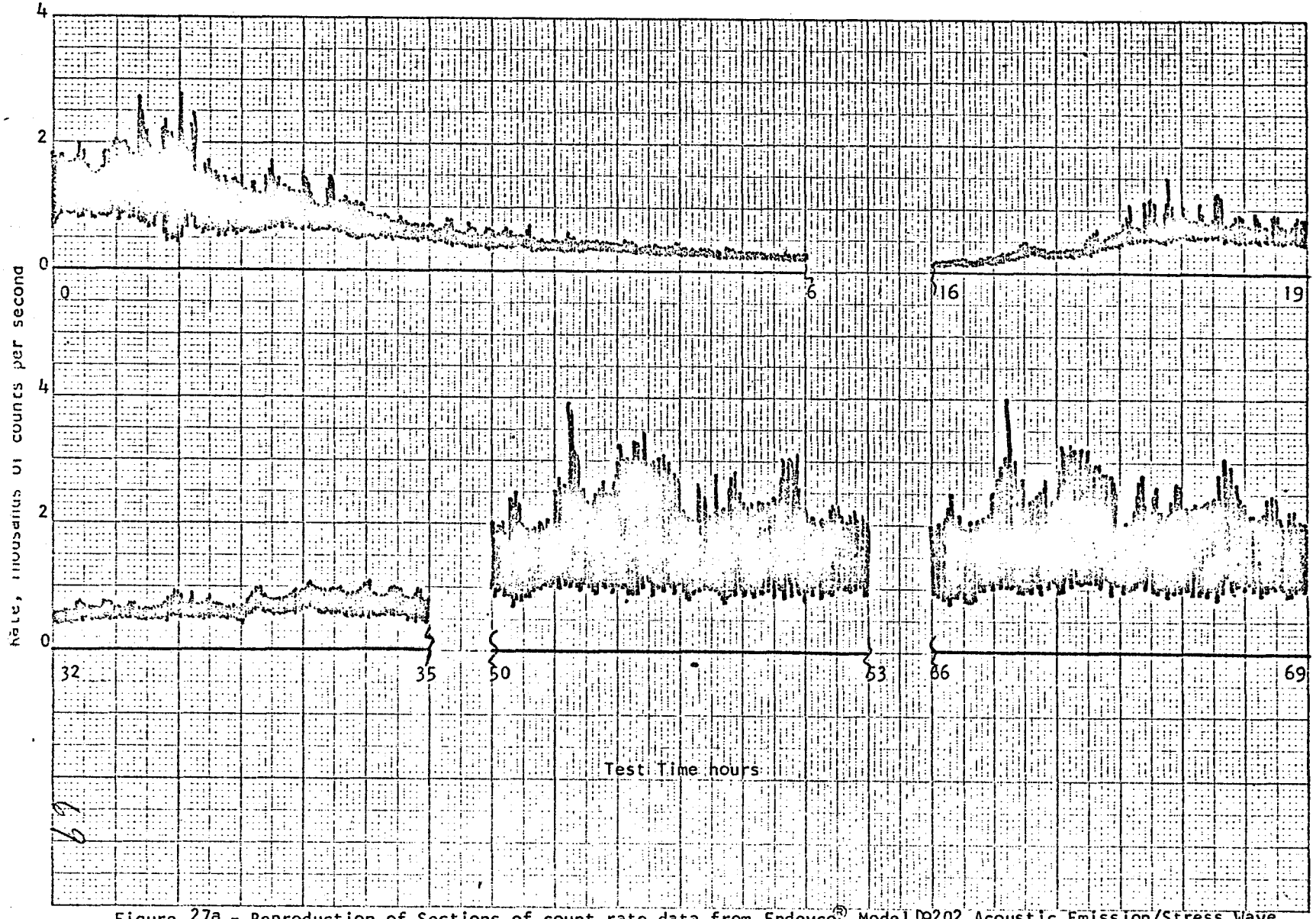

Figure 27a - Reproduction of Sections of count rate data from Endevco® Model D9202 Acoustic Emission/Stress Wave Sensor with Model 301 Totalizer on fatigue test run number six, bearing number 17. (See Figure 27b for conclusion of test)

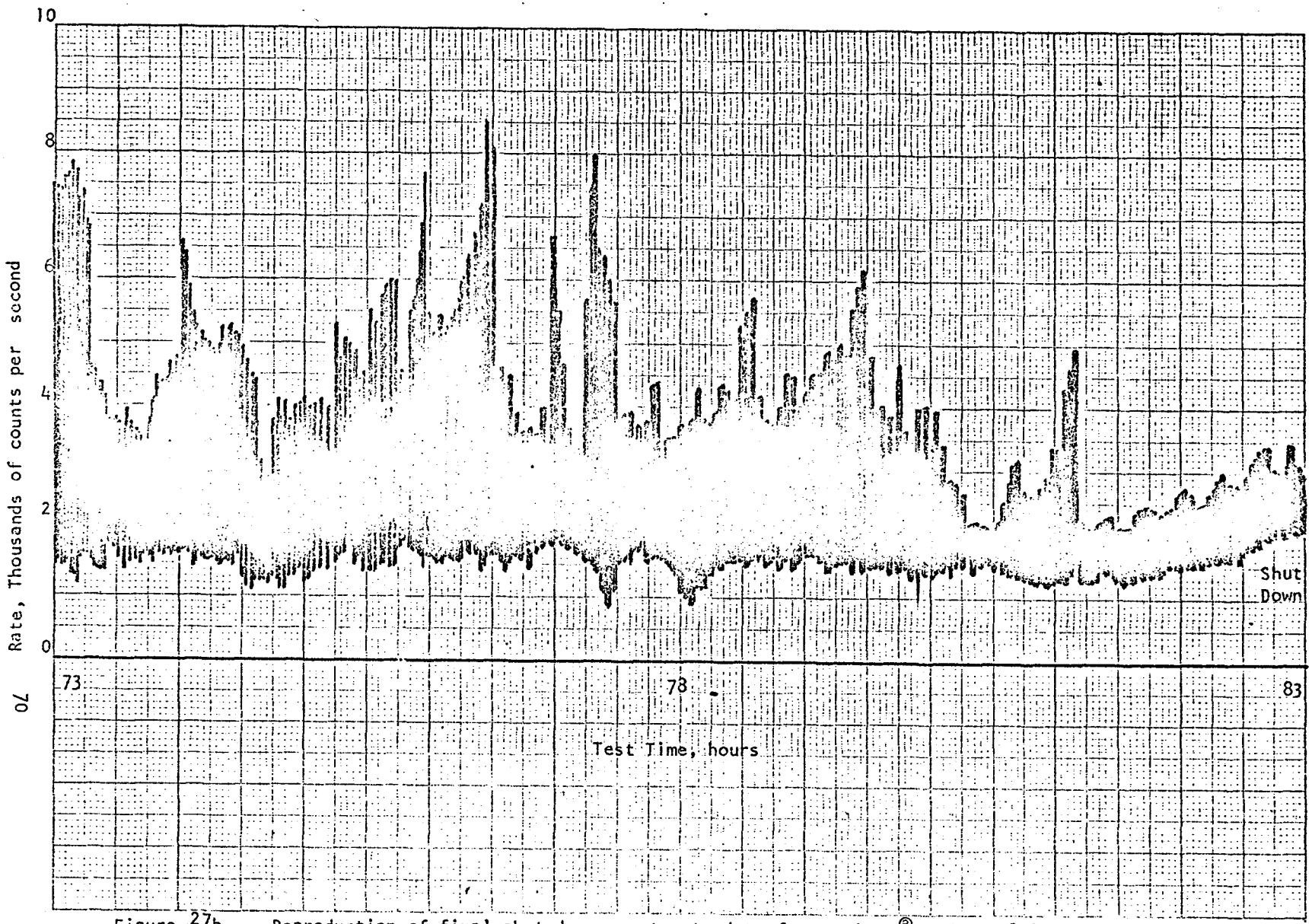

Figure 27b - Reproduction of final shut down count rate data from Endevco® Model D9202 Acoustic Emission/Stress Wave Sensor with Model 301 Totalizer on fatigue test run number six, bearing number 17.

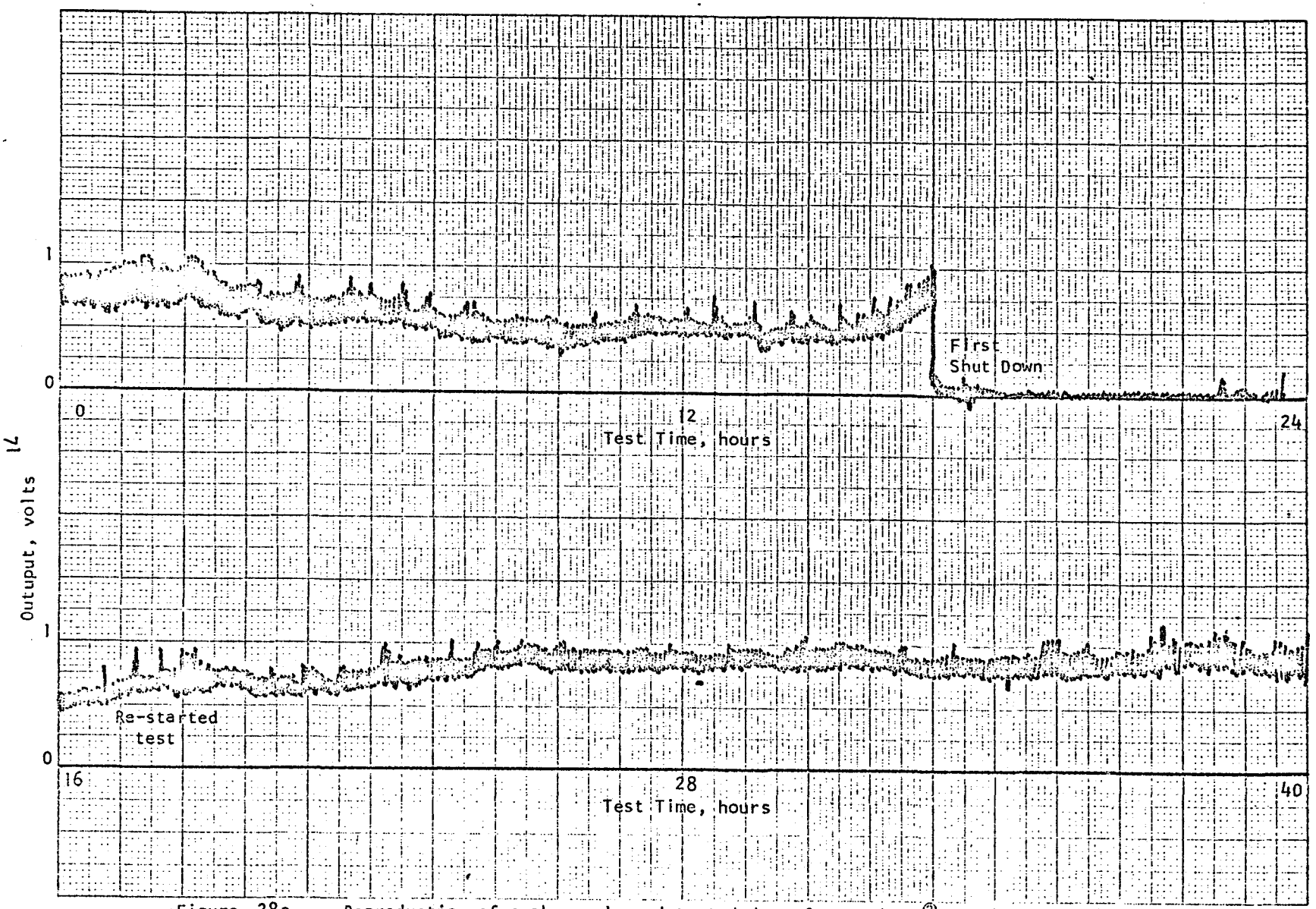

Figure 28a. - Reproduction of peak envelope detected data from Endevco® Model D9202 Acoustic Emission/ Stress Wave Sensor on fatigue test run number six, bearing number 17. See Figure 28 b for conclusion of tests.

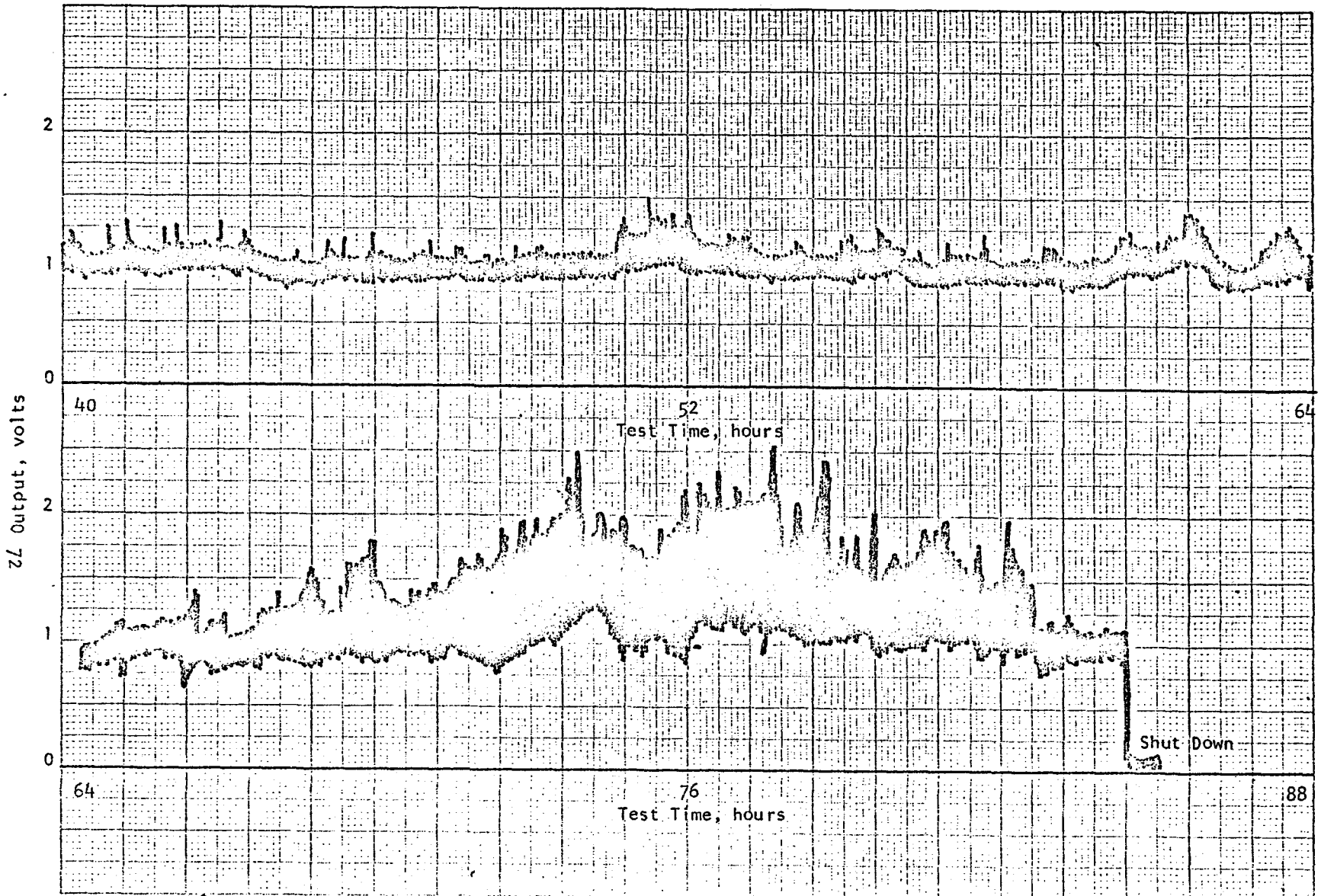

Figure 28b. Conclusion of tests. Reproduction peak envelope detected data from Endevco® Model D9202 Acoustic Emission/ Stress Wave Sensor on fatigue test run number six, bearing number 17.

bearing operates under this high load. It may also be that this gradual change is related to the gradual deterioration of the surface finish of the bearing.

The output from Model 2236 and 6230M8 sensors was also larger at the conclusion of the test run. A change of 15% was recorded for the band passed (25 K to 35KHz) envelope detected peak and 40% for the broadband peak from the Model 2236 output. No discernible change was noted for the broadband envelope detected peak from 6230M8 output.

The fairly large difference in resolution capability between the Model 9202 count rate and the outputs of Model 2236 sensors may be caused by the frequency characteristics of the mechanical phenomenon during failure propagation. Broadband frequency or very high frequency stress waves may be generated by metal removal during spalling action. In addition, when metal particles (previously welded to the race by ball pressure) are again torn away by similar action, these broadband stress waves may be produced. The intensity of these stress waves still is greater when the maximum load is applied at the fault development area, and are therefore expected to have a ball pass frequency envelope. If the race is not excited by these high frequency disturbances the signal may not be of sufficient magnitude to be detected and measured above the already present "noise" (random excitations of the race resonance present even in a new bearing).

Bearing number 13 was photographed after disassembly to show the extent and character of the damage to the faulted members. The results are in evidence in Figures 29 to 36. As discussed before, the test ran longer than desired since the automatic shut down was referenced to the broadband

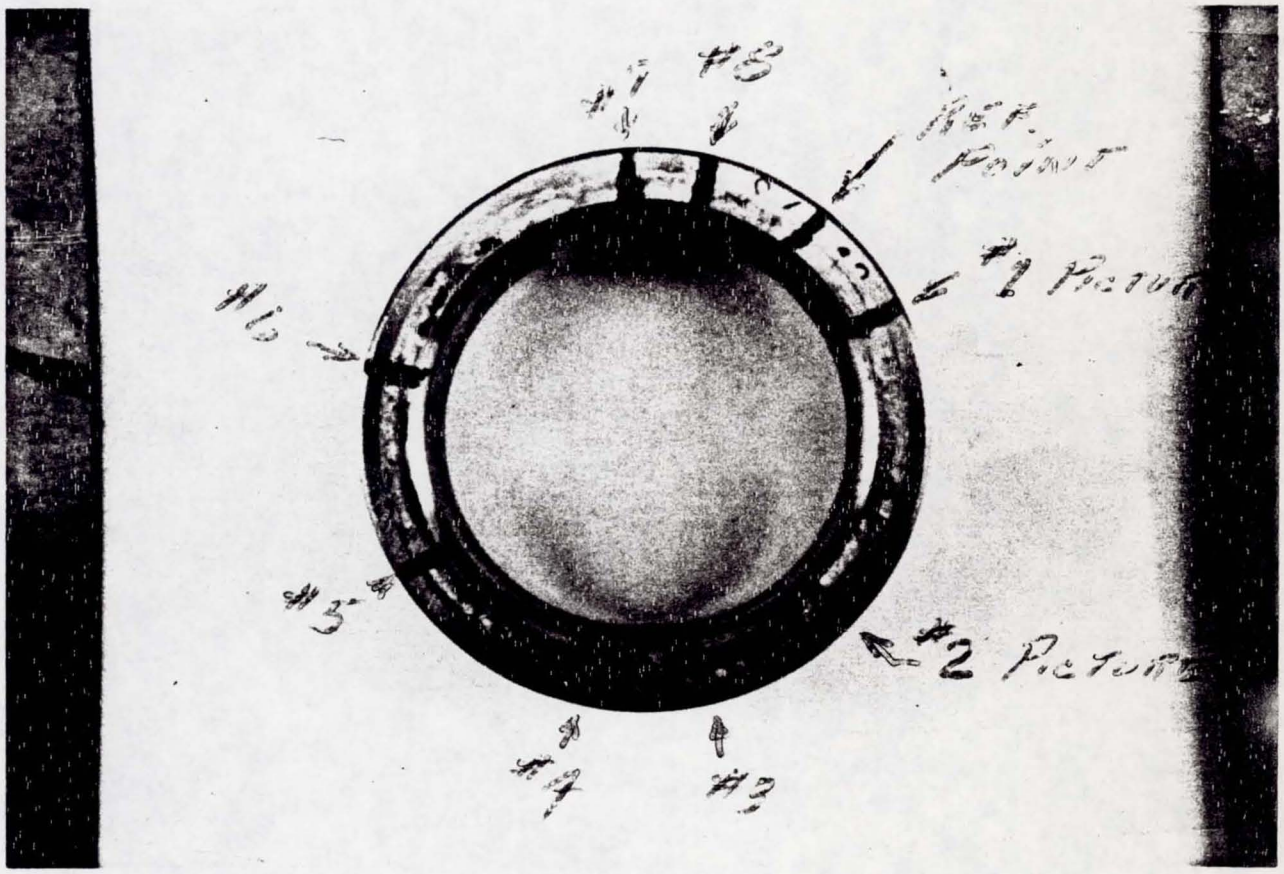

Figure 29 - Inner race from bearing number 13 after completion of fatigue test number one showing the positions of major area of damage. (approx. 1.5X)

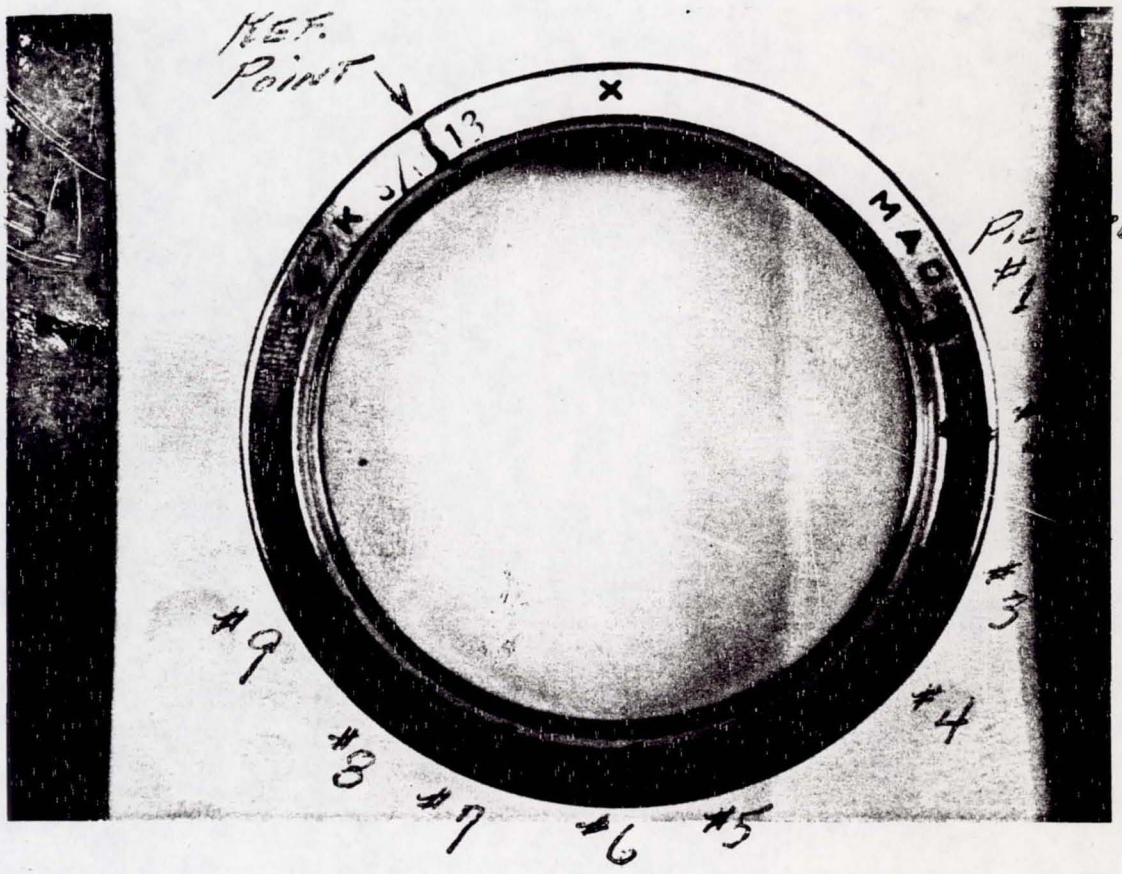

Figure 30 - Outer race from bearing number 13 after completion of fatigue test number one showing the positions of major areas of damage. (approx. 1.3X)

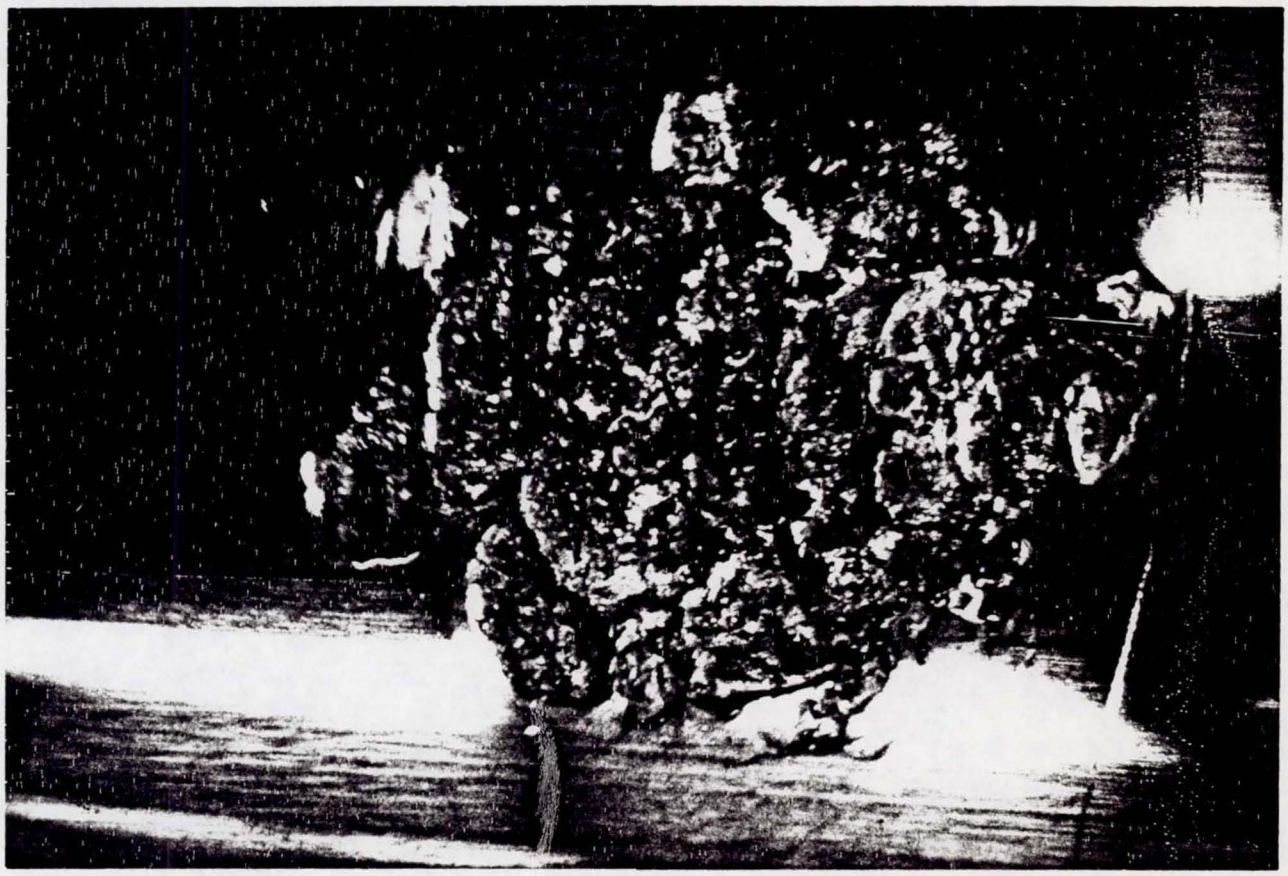

Figure 31 - Spalled area of inner race of bearing number 13, near the scribed fault line after completion of fatigue test. (approx. 20X)

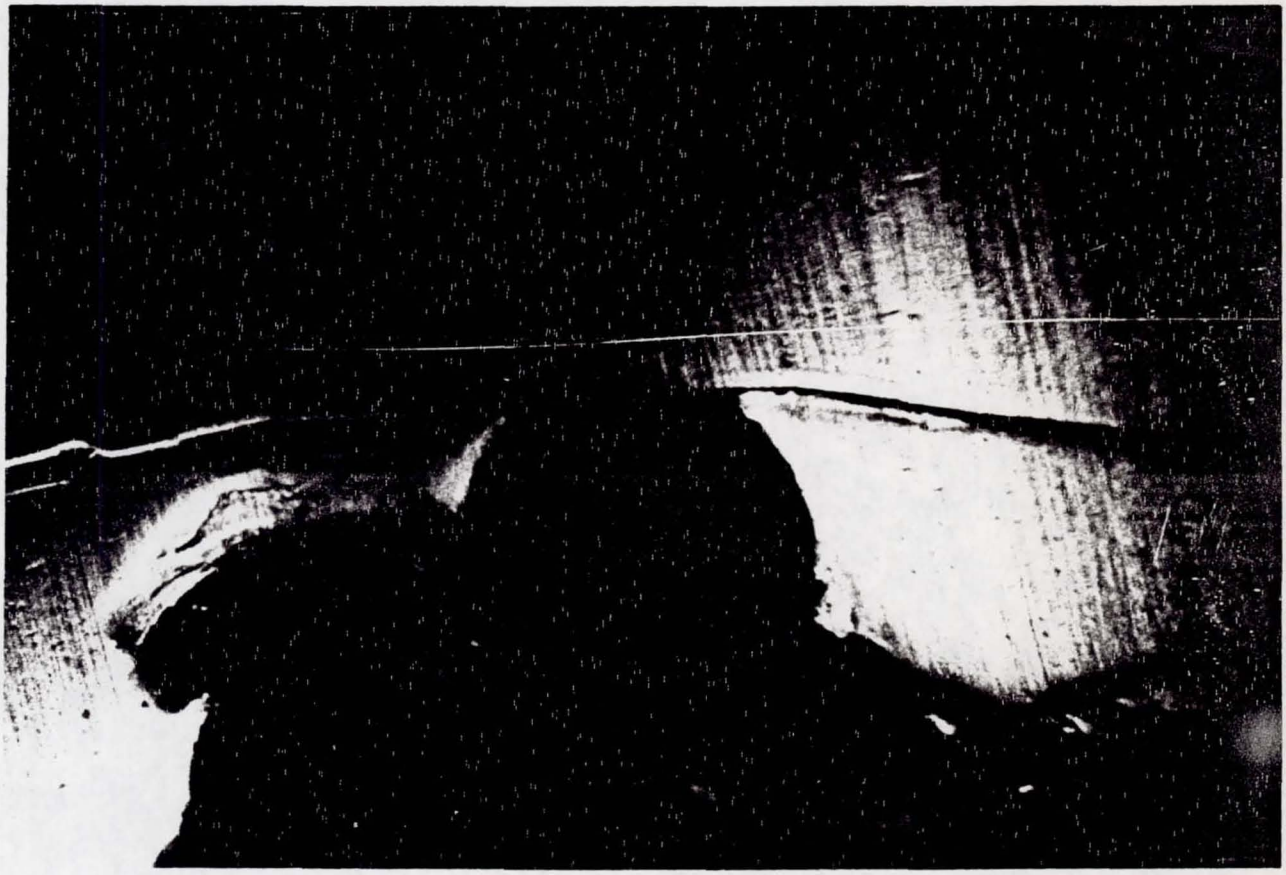

Figure 32 - Spalled area of inner race of bearing number 13, near the scribed fault line after completion of fatigue test. (approx. 60X)

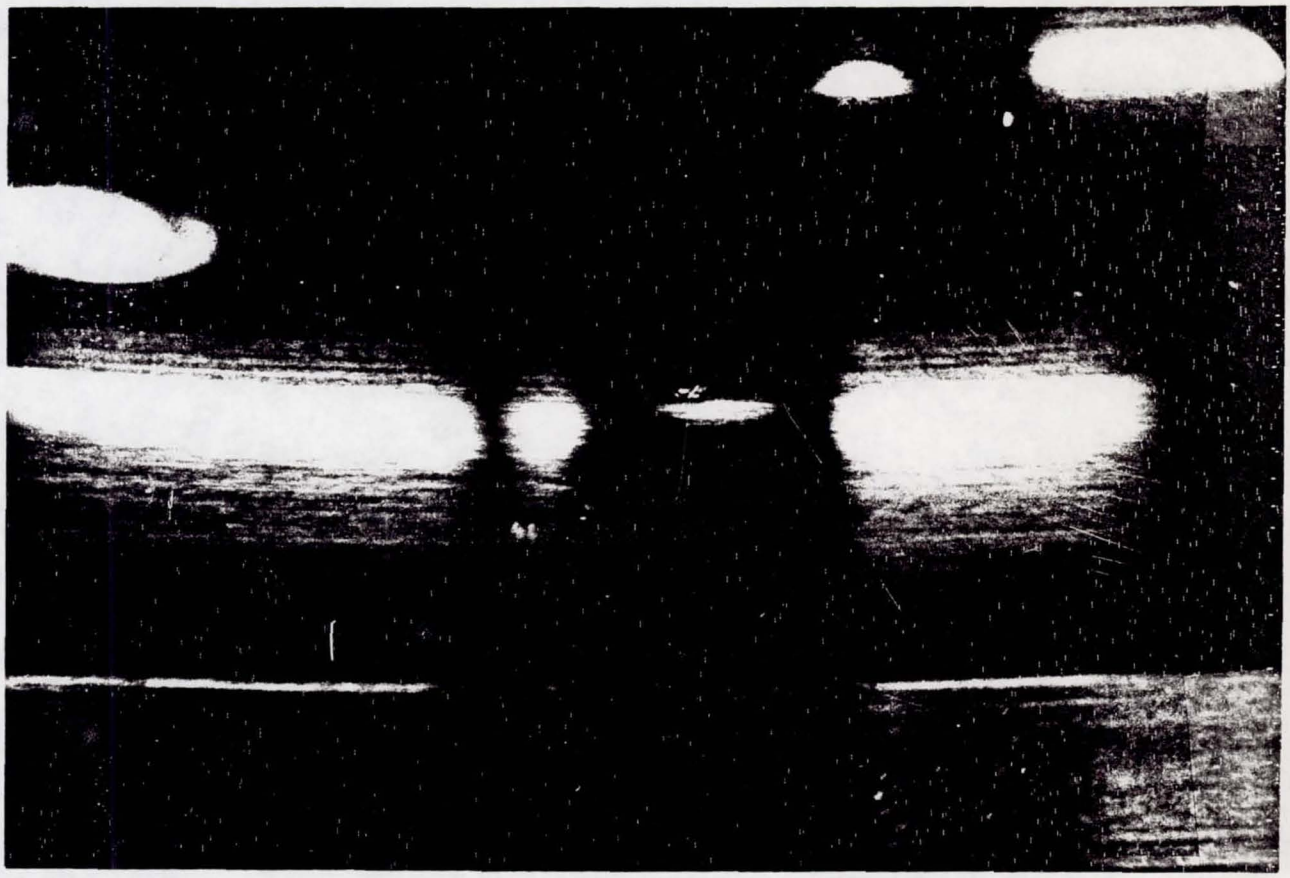

Figure 33 - Metal deposits and pits on outer race of bearing number 13 after completion of fatigue test number one. (approx. 10X)

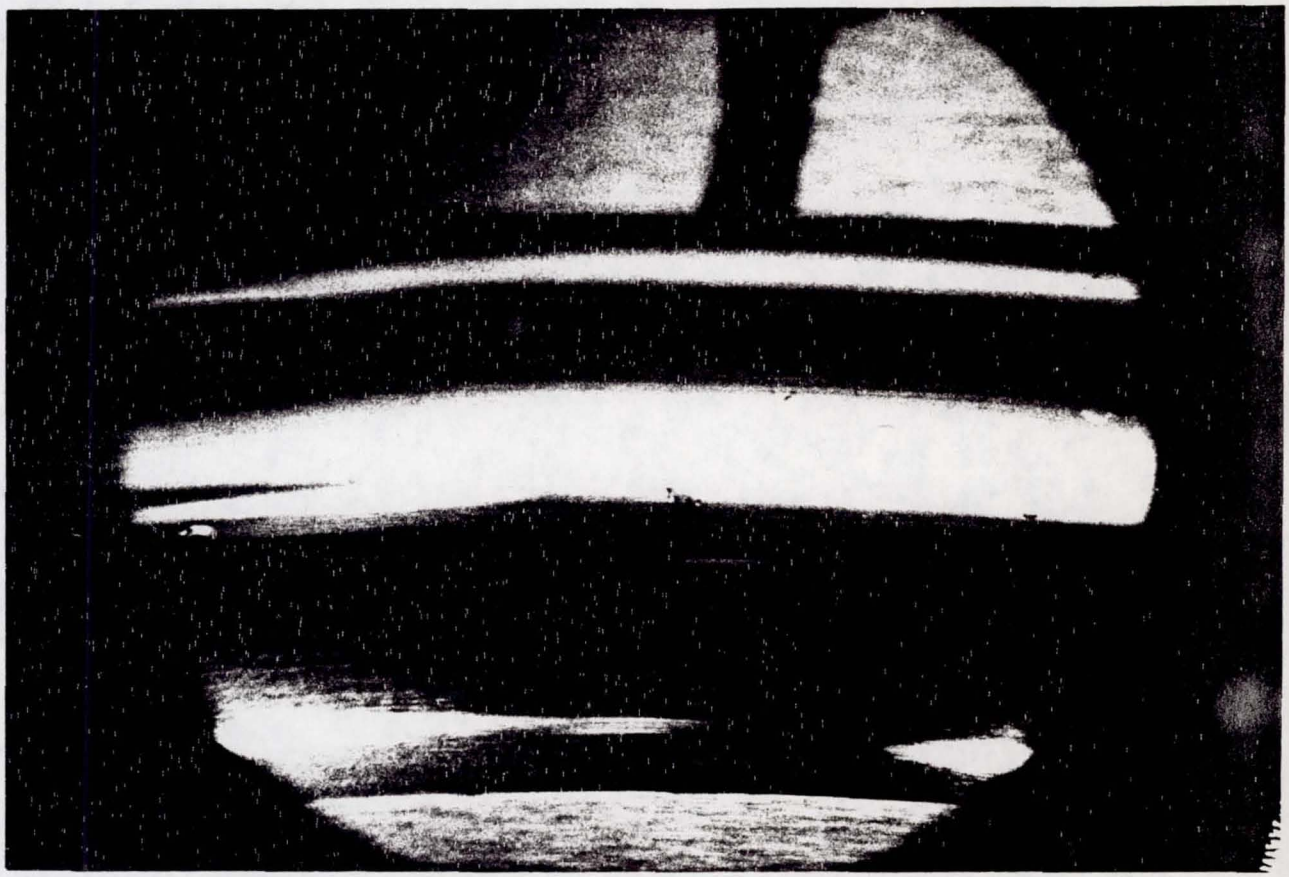

Figure 34 - Metal deposits and pits on outer race of bearing number 13 after completion of fatigue test number one. (approx. 10X)

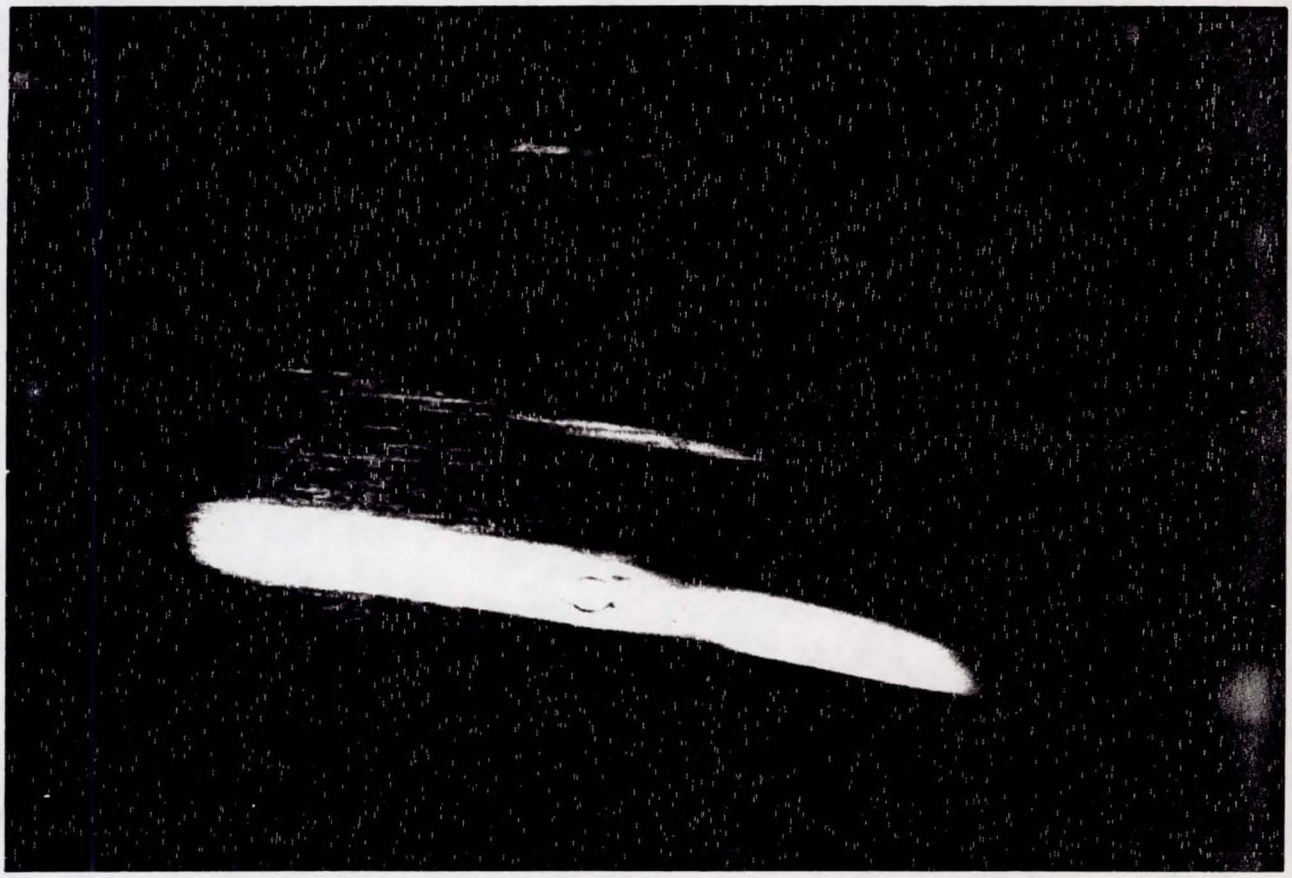

Figure 35 - Indentations in inner race of bearing number 13 after completion of fatigue tests number one. (approx. 10X)

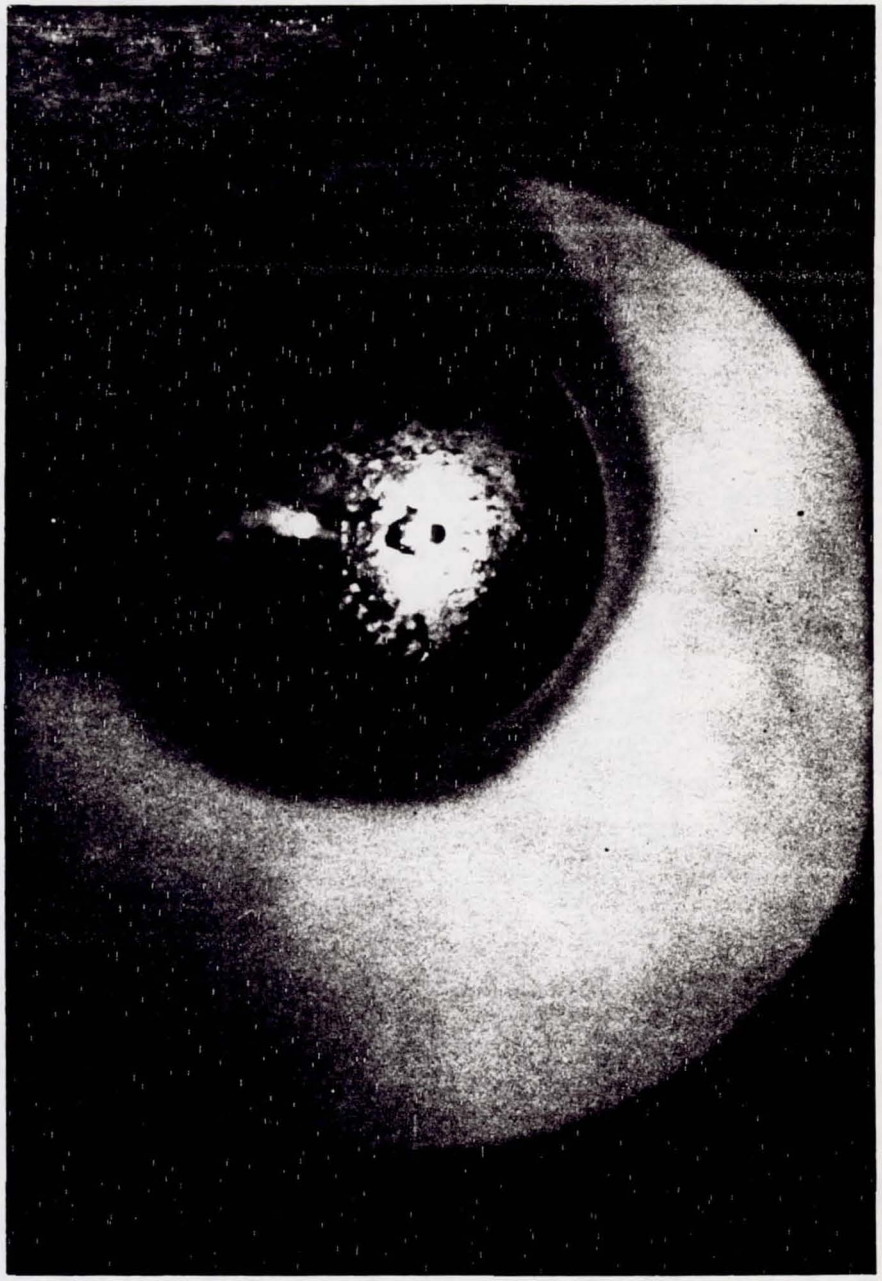

Figure 36 - Ball fault from bearing number 13 after completion of fatigue test number one. (approx. 5X)

data below 50 kHz which did not increase sufficently to terminate the test before major spalling occurred. The large spalling on the inner race emanates from the scribed line shown in Figures 31 and 32 and extends over a large area in the direction of rotation of the bearing. The size of this spall can be approximated at 0.25 inch across by 0.15 inch long by .033 inch deep. Additional smaller pitting occurred around the races as shown in the overview of the races marked to indicate the faulted areas, see Figures 29 and 30. Much of the area on the outer race had small deposits of chips attached to the race or spalls as shown in Figures 33 and 34. Some depressions were probably caused by balls rolling over chips or spall particles followed by being torn free and leaving the resulting imprint as in Figure 35. Three of the balls were pitted (the largest pit is shown in Figure 36).

Even though this bearing lasted longer than the predicted L_{10} life for new condition bearing the scribe mark was definitely of adequate size to propogate failure as shown by the major spalling area.

The data from the second fatigue test is less useful since the failure occurred much more rapidly than anticipated. A preset level of 50% above the level at the beginning of the test was established for the shut down criteria. Recorded data for the rms output of Model 2236 began to change about 0.1 hour before shut down occurred, increasing by 15 percent. The peak detected D9202 signal also increased about the same time but had increased by a factor of about 3 before shut down.

The bearing was disassembled and a spall area was again in evidence adjacent to the fault groove in the outer race. This spall area was smaller than that in the previous test but still adequate to cause pitting in the races as the small particles of metal from the spall were rolled between the balls and the races.

The next run, number three, was approached with more respect for the large groove fault effects on fatigue life. This run resulted in no significant change in output level from any of the sensors for 16.7 hours with 430 pound load followed by 3.6 hours with 860 pound load. This test was discontinued in order to obtain verification that the actual bearing condition had not yet changed significantly. When disassembled, there was found to be minimal change in the groove in the outer race. The edge was rounded or peened over by a few thousandths of an inch. There was no evidence of large metal removal or pitting on any part of the bearing and only some very small pits in the order of one thousandth of an inch in diameter, 15 to 70 μ inch deep, were found.

Test run number four produced results using a bearing in new-unfaulted condition. After 43 hours, the Model D9202 count rate showed a large increase for about one hour and then returned to a relatively normal level, see Figure 26. The peak detected signal and the envelope detected Model D9202 signal also showed an increase in this time period. The peak signal level of the Model D9202 Sensor output increased over the

first 24 hours by about 25 percent. However, at the 43 hour time period, the peak signal increased by about 80 percent and the envelope detected peak and the count rate both increased by a factor of about 2. No discernable increase was recorded for the rms broadband 2236 output.

Because the D9202 level increase was observed at 46 hours, it was decided to shut the test down and attempt to study whatever small beginning faults were in evidence.

The bearings was disassembled and examination showed many very small pits about 20 μ inches deep by about .001 to .005 inch diameter in the races of the bearing. One pit in the outer race was found to be about 0.0002 inch deep by 0.005 inch diameter. The rotational orientation of the fault relative to the maximum load could not be established. It is possible that the outer race rotated and possible changed the effect of the fault which may account for the decrease in output level after the 43 hour period. It was estimated by one observer that at least the larger pit could have been an electrical pit.

Test number five was discontinued after 0.5 hours with inconclusive results. Large increases in vibration outputs from all sensors indicated a malfunction of the bearing test machine. The cause of the vibration was the use of improper substitute bearings in the side support positions. The bearings in question had been replaced immediately prior to the test. These side support bearings, purchased as equivalent to the proven bearings used throughout the program were designed to be used with a thrust load.

Both side support bearings were positioned in the same direction to produce a thrust force on the center bearing when the radial load was applied. The difficulty was resolved by replacing the side support bearings with the type previously used.

In test number six, an increase in outputs from the D9202 Sensors were obtained similar to test number four. This time, however, the test was automatically terminated by a 20 percent increase in level as detected by the Model 6234 Signal Conditioner. More than 8 hours prior to this time, the count rate for the high frequency D9202 Sensor indicated large increases as shown in the Figure 27b. No significant change in output was indicated with envelope detection of 20 kHz to 35 kHz data from the Model 2236 Sensor or from Model 6230M8 envelope detected data above 20 kHz. Closer examination of the count rate data shows that the number of counts per second on the graph scale in Figure 26 for test number four is 100 times that of test six in Figure 27. This explain the larger excursions present on test six graph due to the scale change. Also of some interest is the apparent "run in" or start up level of test six. Test number six used a new bearing not previously tested which may account for the somewhat larger count early in the test which then decreased to a nearly constant lower level for many hours of the fatigue test. In contrast, bearing number 10 in test run four had been used in the earlier series of test for several hours. With the resolution used for the fatigue test run number four, there appeared to be a more nearly constant count rate from the start. For the purposes of this report, some additional transient outputs were assumed to be electrical noise and would normally be eliminated by an averaging circuit. It is not certain that these transients are in fact noise but

possibly may relate to stress waves or impacts that occur at rare occasions in the life of the bearing.

A careful examination of bearing number 17 on fatigue test number 6 showed a small pit in the outer race about 0.0002 inch deep by 0.002 inch diameter. This was similar to that found in bearing number 10. In addition, there were many very small imperfections, perhaps one tenth this depth around the path of the ball on the races. On the inner race, a streak appeared as if ball skidding had occurred. The depth of the skid marks were very small but extended for 0.5 inch at a slight angle to the travel of the ball on the race. The depth of the marks are extremely shallow, about 20 μ inch and may not be of much significance at this time. It is possible that test continuation would cause a large fault to be generated under these circumstances as occurred with the small scribe line on bearing number 13.

The detection of the very early indications of failure in the fatigue tests is best illustrated by a display of data over the period of the tests. In the case of test number four, the output increased for about one hour and then returned to near the normal level. Again in test number six, the level decreased after an extended period of hours of high level signals. It is possible that this was caused by rotation of the outer race which would change the load on a particular area where a fault may be developing. The outer race was forced to rotate to some degree in the fatigue tests where the applied load was chosen to be very large in order to accelerate the failure. This rotation may have been caused by a number of reasons relating to the higher load effects on the friction in the bearing itself, slight distortion of the bearing races and/or the housing, and

flexing or bending the shaft.

Fatigue test run number 7 was scheduled for improving the correlation of damage development after a fairly small scribe had been fabricated on an otherwise good new condition bearing. The test was stopped after twenty two hours with a load of 1650 pounds corresponding to an L_{10} life of a non-faulted bearing of 90 hours. The data from the Model 2236 which was bandpass filtered 20 kHz to 35 kHz and peak detected, as well as the Model D9202 Sensor showed that the output level was increasing and decreasing at a rate of 2.2 minutes per cycle. It is suggested that this was caused by rotation of the outer race within the housing which would cause increased signal when the fault was at the top of the housing and maximum load was applied. The test was terminated to prevent damage to the housing of the bearing test machine. It appears likely that the established clearance at the start of the test may have been slightly excesssive, possibly due to less relative thermal expansion of the race than assumed in the design. Possibly some wear developed in the housing due to some outer race rotation during the previous fatigue tests. Rotation was noted in these fatigue tests since the outer race was never in the same position after the tests when disassembled. This rotation had not occurred in the earlier bearing fault characterization tests which were run at much lower loads.

Frequency spectrum analysis was performed on the envelope detected signals at the start of the fatigue tests and at various times during the tests. Examples of these analyses are shown in Appendix 5. There were indications of increase in the one cycle per revolution and ball pass

frequency data after the fault became very large as in fatigue tests to number one. However, much more data is required with more fatigue tests to be able to correlate envelope detection analysis with bearing faults.

The oil temperature and the bearing outer race temperature were monitored during the tests.

The oil temperatures and bearing temperatures increased as the speed and load were increased. After several minutes of operation, the temperature remained constant within a few degrees of the values shown in Table X.

TABLE X

OIL TEMPERATURES

Speed RPM	Load Pounds	Oil In °F	Oil Out °F	Bearing Outer Race °F
5400	430	90	100	105
5400	780	95	105	110
12,900	430	95	130	140
12,900	780	105	135	150
12,900	860	110	140	160
12,900	1650	120	145	185
12,900	2150	130	155	195
12,900	2500	140	165	205

C. Implications of Fatigue Test Results

We should consider the causes of the large change in the D9202 count rate for very small physical evidence. As previously described in fatigue test number four, the count rate increased for about one hour to a signaificant level over normal. This occurred after a time period exceeding

the L_{10} computed life when damage could be expected to be developing. The damaged areas were smaller than those detectable as discrete faults in the first series of bearing characterization tests. The outputs levels from the lower frequency sensors showed very low, if any, detection. The primarily mechanical phenomenon is therefore judged to be of high energy and concentrated in the high frequency spectrum which is on the edge or beyond the detection range of the other sensors.

It may be possible for further study of fatigue tests to determine by x-ray or sectioning what changes occur in the subsurface metal of the bearing races.

The information obtained using the high frequency D9202 Sensor relative to early failure development in bearings indicates the need for a more detailed and related study. Longer continued testing should be done on bearings at lower loads corresponding to actual applications. The tests should be stopped at various intervals of time to inspect the bearing components in order to correlate damage and signal output.

Many complete channels of instrumentation are needed for these types of studies in order to provide simultaneous comparisons of data processing and acquisition techniques. These tests would verify the resolution of detection of fault progression with normal loads. Other types, sizes, and installations of bearings should be studied to establish more general guidelines for incipient failure detection and life prediction. The effects of other equipment operating near the monitored bearing may cause the

C.2

practical application to be more difficult than laboratory experience suggests. More measurements with high frequency sensors of various types, should be performed on various locations on the bearing housing. The study of effective detection levels for various sensors located on the exterior of the bearing housing is an important prerequisite of application oriented results.

VII. CONCLUSIONS

Because of the broad investigative nature of this program the data provides a valuable comparison of vibration and stress wave techniques as applied to the detection, characterization, and monitoring of the progress of faults artifically and naturally induced in rolling element bearings. The experimental results lead the authors to strongly conclude that stress wave sensing provides a technique that permits early warning of impending bearing failure.

The D9202 Acoustic Emission Transducer has a frequency response centered at about 550 kHz and a bandwidth of about 900 kHz. This instrument provided the greatest sensitivity to the phenomena investigated. Signal levels from the D9202 were sufficiently high and noise free to accommodate analysis even though the mechanical information had to be transmitted through the bearing and into the supporting housing.

The following observations are offered in support of our conclusions:

1. Count rate of signals above 100 kHz was the strongest indication of failure propagation with larger changes in this quantity than those of other methods.

2. The sensors operating below 100 kHz showed minimal change of envelope detected signal during the early stages of the failure propagation tests.

3. Discrete faults as small as about .003 inch machined into new bearings were discernible by all the sensors used. The induced faults of about .001 inch size were not obviously discernable.

4. The sensor with its resonance frequency in the range of the lower resonance modes of the bearing races did have higher sensitivity

to the ringing of those races with new condition bearings as well as with faulted bearings.

Because the D9202 was capable of sensing the occurance of surface faults a few thousandths of an inch in size, while the lower frequency sensors were not, we conclude that the energy content at high frequencies was significant in comparison to the background noise. This may also indicate that as faults are created, (even though quite small) the signals may be generated more through an acoustic emission process than through stress waves created by the elastic impacts.

Since the vibration and stress wave results in the ultrasonic frequency range containing the information of primary value, the selection of a suitable sensor can be seen to be critical to the utility of the system. System design requires understanding of how the sensor will be excited, if the stress wave or vibration signal will be transmitted to it, and how the sensor will respond. The effect of the sensor frequency response can be seen by comparing the impulse calibration data to the frequency spectrums of the bearing data. For a detection system to be viable it must utilize a sensor which has a known responsive characteristic. The impulse calibration technique is probably the most useful for providing that.

Without question, there are yet areas of exploration not covered by this study. The results of this investigation do not provide an immediate solution in the form of an incipient failure detection system, but they do provide a significant clarification of alternative approaches most likely to lead to a result oriented system.

REFERENCES

1. Olof G. Gustafsson and Tibor Tallian, "Detection of Damage in Assembled Rolling Element Bearings", ASLE Transactions 5, 197-209 (1962)

2. T. J. Rosinski, "Can You Identify the Cause of a Service Connected Bearing Failure?", Product Engineering Magazine, 35-39 (May, 1974)

3. A. S. Tetelman and R. Chow, "Acoustic Emission Testing and Micro-Cracking Processes", Acoustic Emission, 30-40 (1972)

4. T. F. Drouillard, "Acoustic Emission - A Bibliography for 1970-1972", Special Technical Publication 571, ASTM, 241-284 (1975)

5. L. Balderston, "The Detection of Incipient Failure in Bearings", Materials Evaluation, 121-128 (June, 1969)

6. A. Palmgren, Ball and Roller Bearing Engineering, S. H. Burbank and Company, Philidelphia, Pa. (1959)

7. W. F. Stokey, "Vibration of Systems Having Distributed Mass and Elasticity", Shock and Vibration Handbook, Volume 1, McGraw-Hill, New York (1961)

8. W. P. Mason, Physical Acoustics and the Properties of Solids, D. Van Nostrant, Princton, New Jersey (1958)

9. D. O. Harris & R. L. Bell, The Measurement and Significance of Energy in Acoustic Emission Testing, Dunegan/Endevco (January, 1974)

10. C. C. Feng, "Spark Impulse Calibration Method", Engineering Report 74-7-C, Endevco (1974)

11. "Dynamic Analysis for Rolling Element Bearing", Mechanical Technology, Inc., Latham, New York (March 20, 1973)

12. K. A. Smith, "Mechanical Signature Analysis of Rotating Machinery", General Electric Company

13. "Fafnir Extra-Precision Ball Bearings", The Fafnir Bearing Company, New Britain, Conn., Catalog 449

APPENDIX 1

Contractual Statement of Work

Reference: NASA Contract NAS8-29916

Perform tests of rotating machinery using 20 - 30 test bearings with 3 - 5 different bearing defects both individually and simultaneaously induced. The tests and evaluation shall include, but not be limited to the following instrumentation/analysis techniques:

a. Spectrum analysis of audio frequency vibration in the range from 10 Hz to 20 kHz.

b. Analysis of the amplitude and modulation characteristics of selected bands of ultrasonic vibration in the range of 20 kHz to 100 kHz.

c. Count, count rate, and energy analysis of acoustic emissions in the range from 100 kHz to 3 MHz.

d. Using the above techniques test and analyze good bearings, defected bearings (inner race, outer race and rolling element) under rated loads and operation of good bearings under conditions which will accelerate bearing failure.

e. Prepare a final report of all tests (6 copies).

APPENDIX II

EQUIPMENT LIST

1.	HP 7035B X-Y Recorder	S/N 1049A04941
2.	Dunegan Power Supply 202	S/N 20285
3.	301 Totalizer	S/N 30208
4.	402 Reset Clock	S/N 40295
6.	601 Log Converter	S/N 60117
7.	502 Ramp Generator	S/N 50207
8.	702 Audio Monitor	S/N 70374
9.	801P Preamplifier	S/N 80077
10.	D9202 Sensor	S/N AB34
11.	Sony Video Tape Recorder "Sony Matic" With Realistic Card, Dynamic Microphone	S/N AV-3650
12.	Honeywell 5600 Tape Recorder P/N 16769681-002	S/N W02047-25889-J70
13.	Voice Actuate	S/N 16774540-001
14.	Honeywell SA1-52B Real Time Spectrum Analyzer/ Digital Integrator	S/N 802214
15.	HP 7005B X-Y Recorder	S/N E72003 (E)
16.	Heath Schlumberger Strip Chart Recorder, SR255B	S/N E75009 (E)
17.	Tektronix Type 564 Storage Oscilloscope Type 3A74 Plug In	S/N 002224 S/N 003667
18.	Tektronix Scope Mobile Type 201-2 Model C	S/N E 1228 (E)
19.	Tektronix Type 3A75 Amplifier	S/N 002125
20.	Tektronix Type 310A Oscilloscope	S/N 015844
21.	Tektronix Type 310A Oscilloscope	S/N 014516
22.	HP 400EL AC Voltmeter	S/N 536-04420
23.	HP AC Transistor Voltmeter 403A	S/N MA 8 (E)
24.	PI Model DG-1 Tape Degausser (Endevco Model SDF 002)	S/N 303

25.	Kepco Model ABC 40-0.5M, DC power supply	S/N E-4396
26.	HP Model 3400A RMS Voltmeter	
27.	Bently Model 3140-2388 Proimitor	S/N 42188
28.	Varian Strip Chart Recorder	R4A3
29.	Endevco Charge Amplifier 2730	S/N DE62
	" " " "	S/N DE90
	" " " "	S/N DE86
	" " " "	S/N DE83
30.	Endevco Charge Amplifier 2740	S/N BA14
	" " " "	S/N BA15
	" " " "	S/N AE06
31.	Krohm Hite Filter Model 3202R Console Rack	S/N E72011 (E)
32.	HP Oscillator	S/N 5055
33.	Eldorado Model 225 Frequency Meter	S/N 442164
34.	6230M8 Accelerometer	S/N G324
	" "	S/N G322
	" "	S/N G321
35.	2236 Accelerometer	S/N CH78
	" "	S/N CH88
	" "	S/N CH55
36.	Unit Gain Amplifier (Endevco Engineering Custom Built)	
37.	Envelope Detector (Endevco Engineering Custom Built)	
38.	Peak Detector (Endevco Engineering Custom Built)	

APPENDIX III

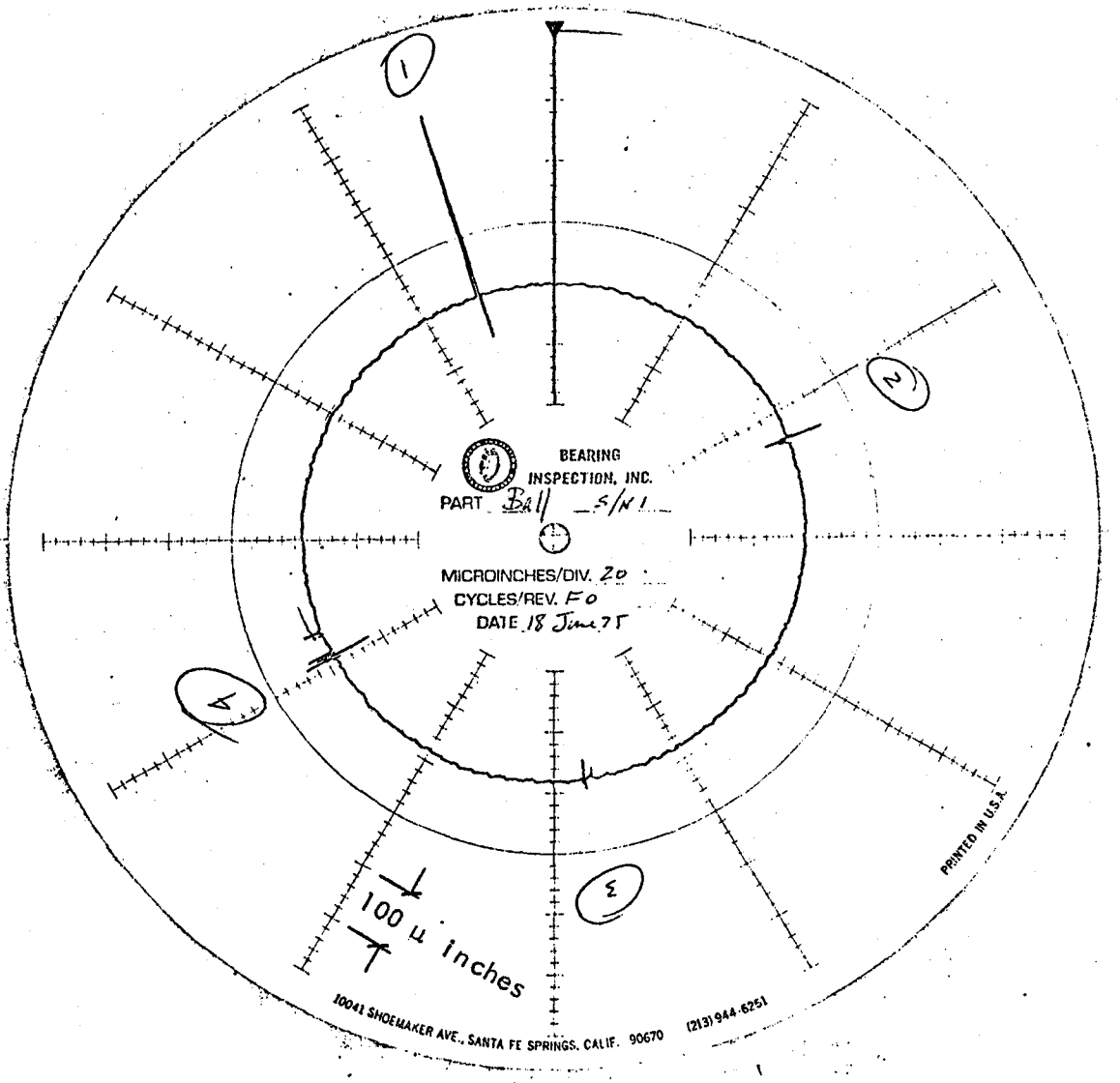

Figure 3-1a - Profilometer measurement of the fault locations scribed into one ball of bearing S/N 1.

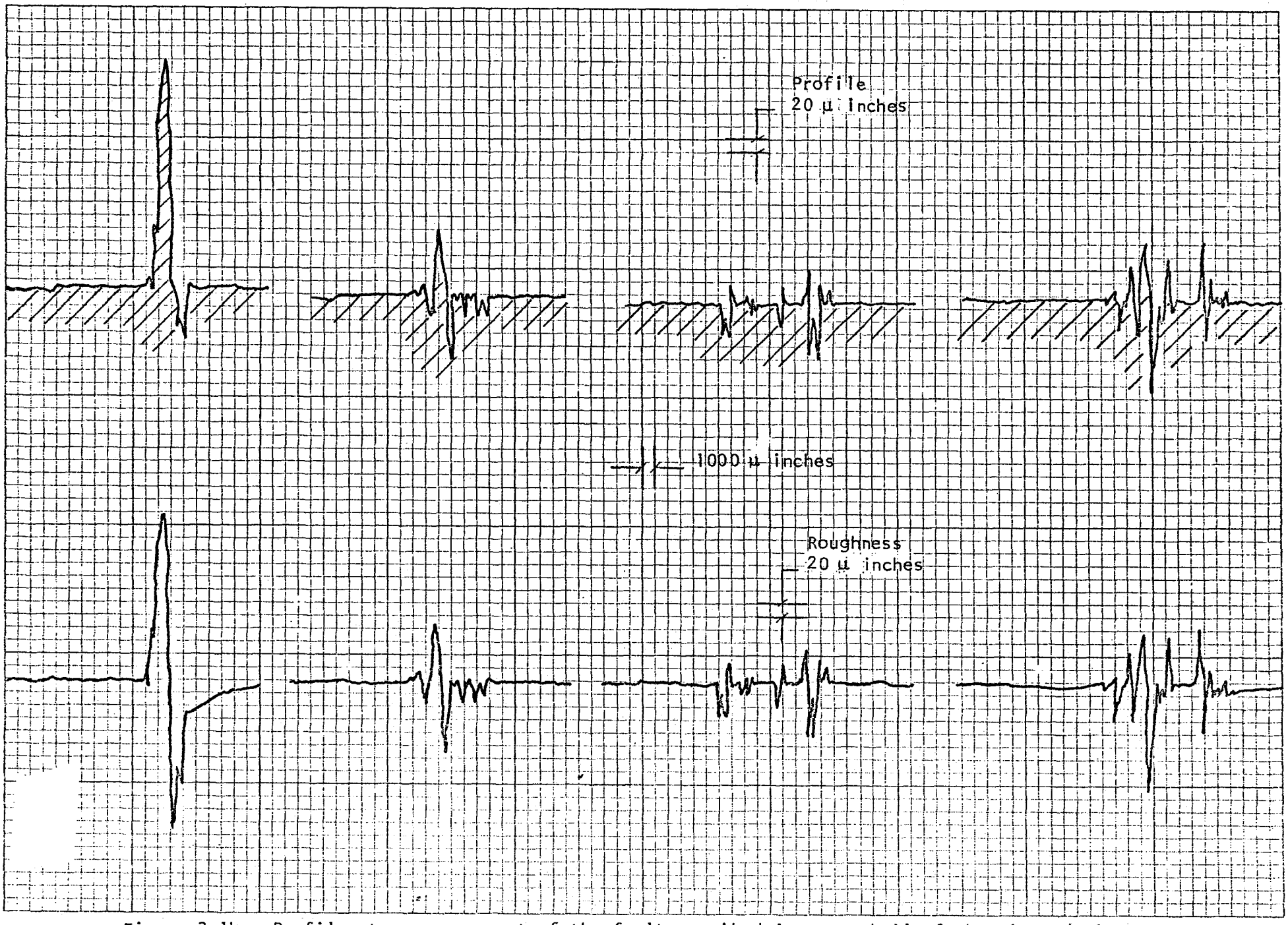

Figure 3-1b - Profilometer measurement of the faults scribed into one ball of bearing S/N 1.

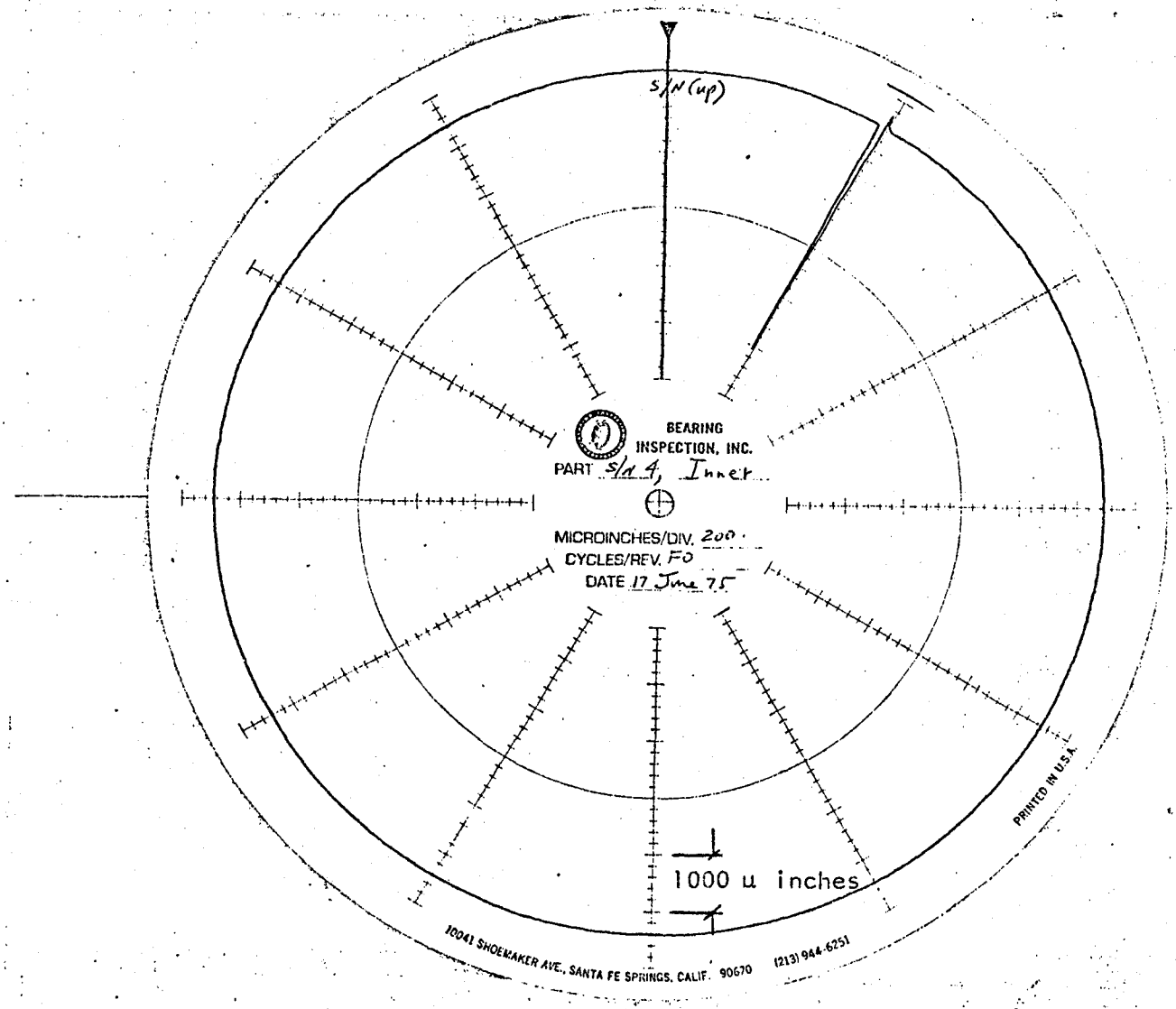

Figure 3-2a- Profilometer measurement of the fault location eloxed into the inner race of bearing S/N 4.

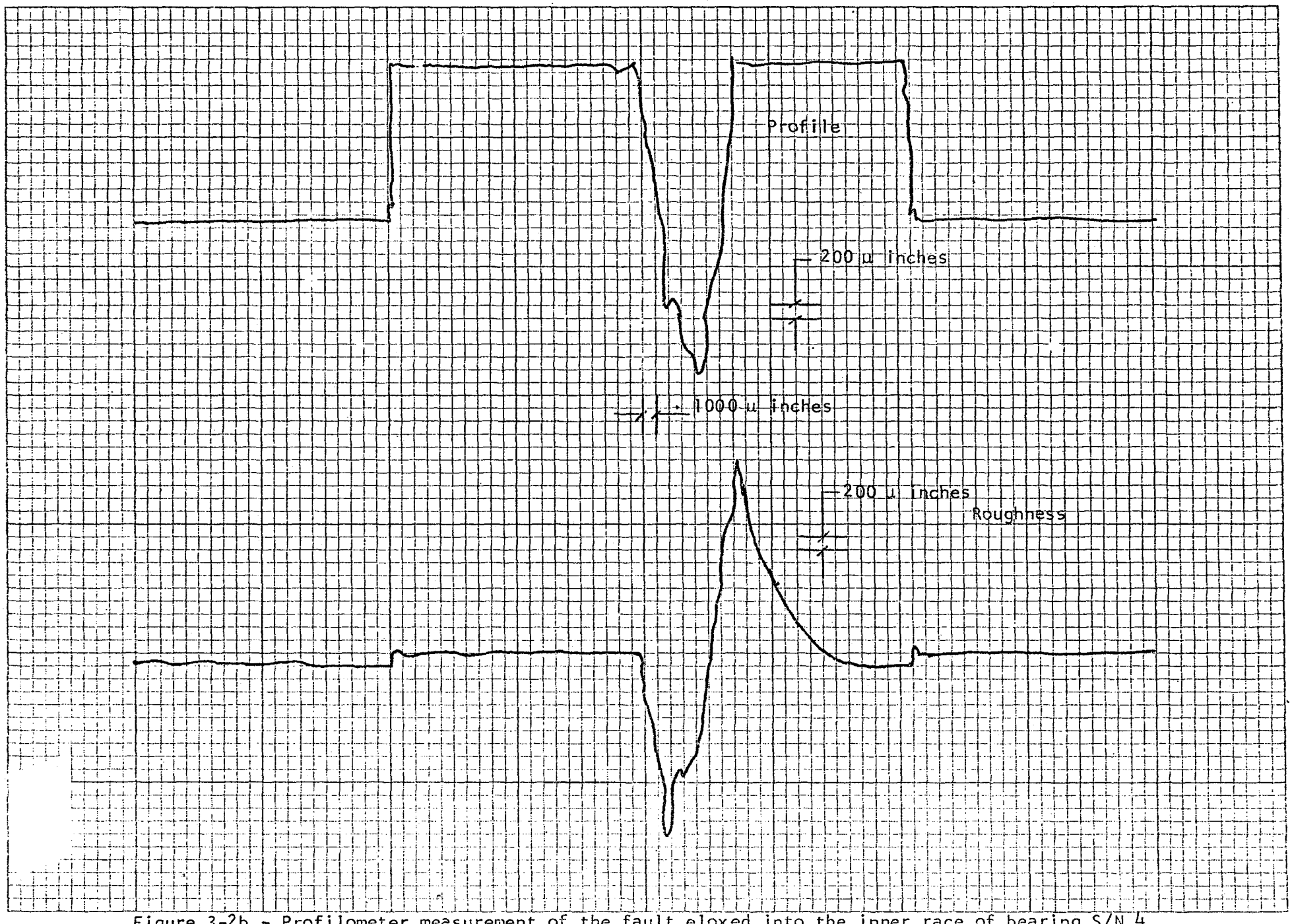

Figure 3-2b - Profilometer measurement of the fault eloxed into the inner race of bearing S/N 4.

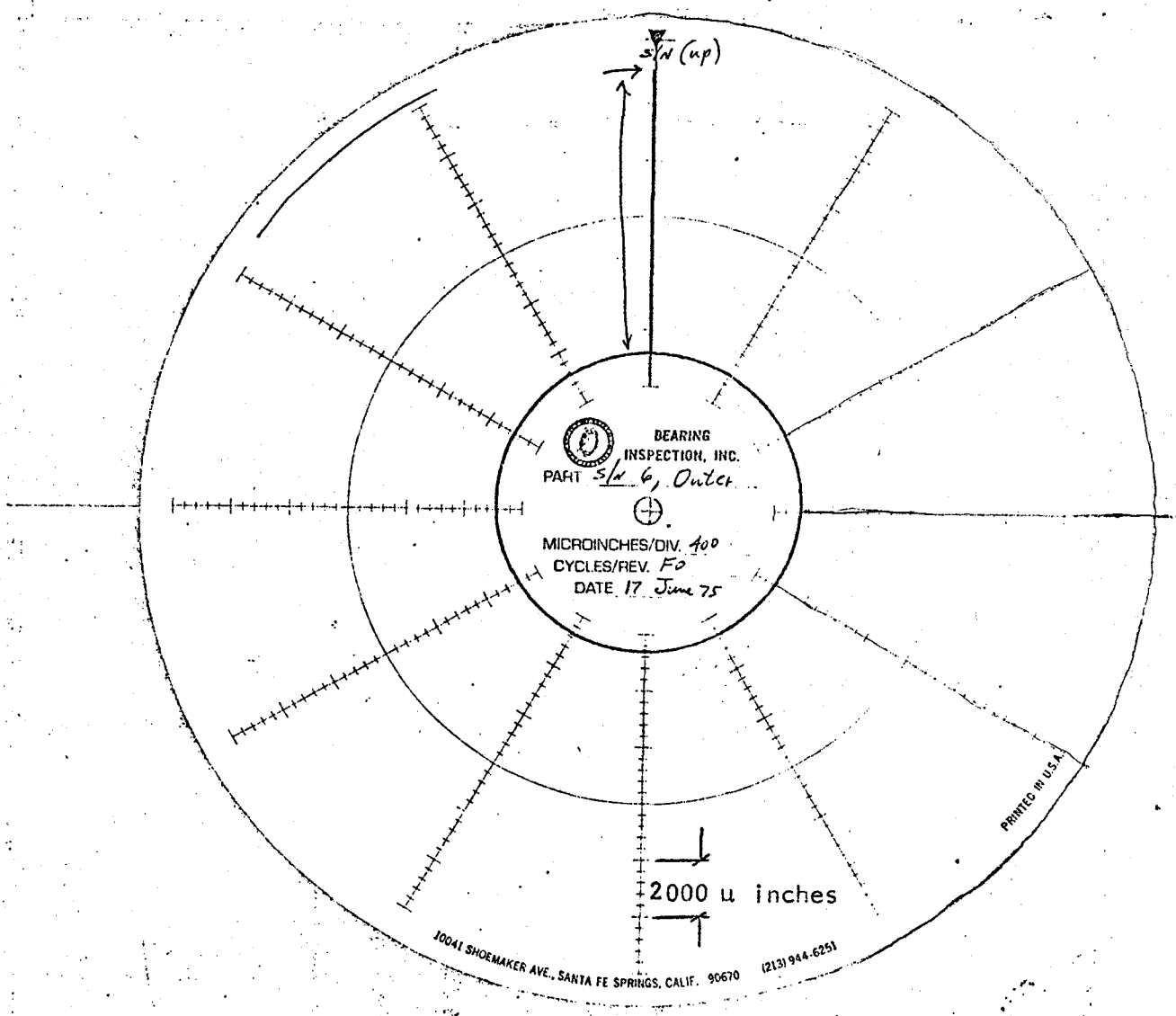

Figure 3-3a. - Profilometer measurements of the fault location eloxed into the outer race of bearing S/N 6.

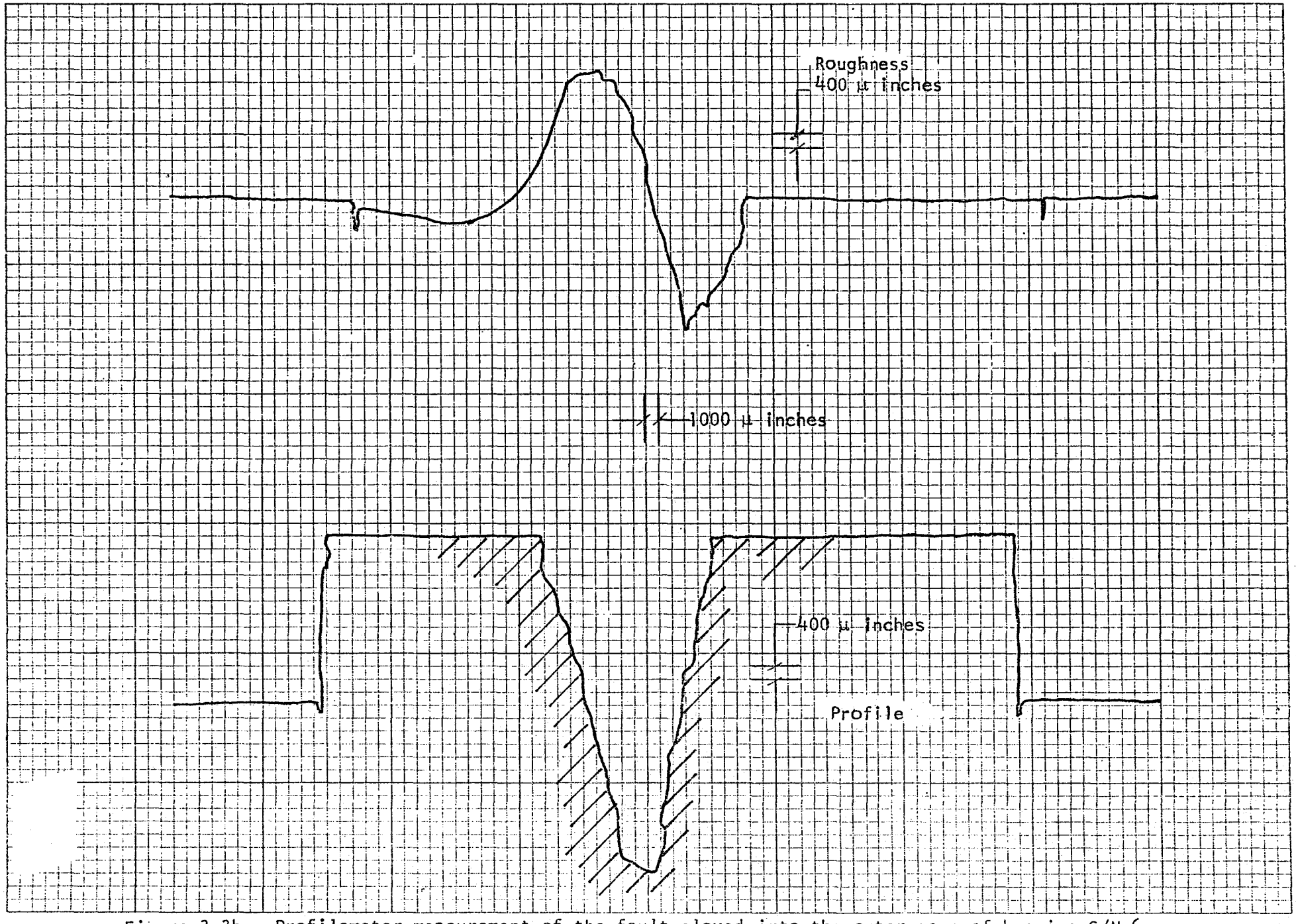

Figure 3-3b - Profilometer measurement of the fault eloxed into the outer race of bearing S/N 6.

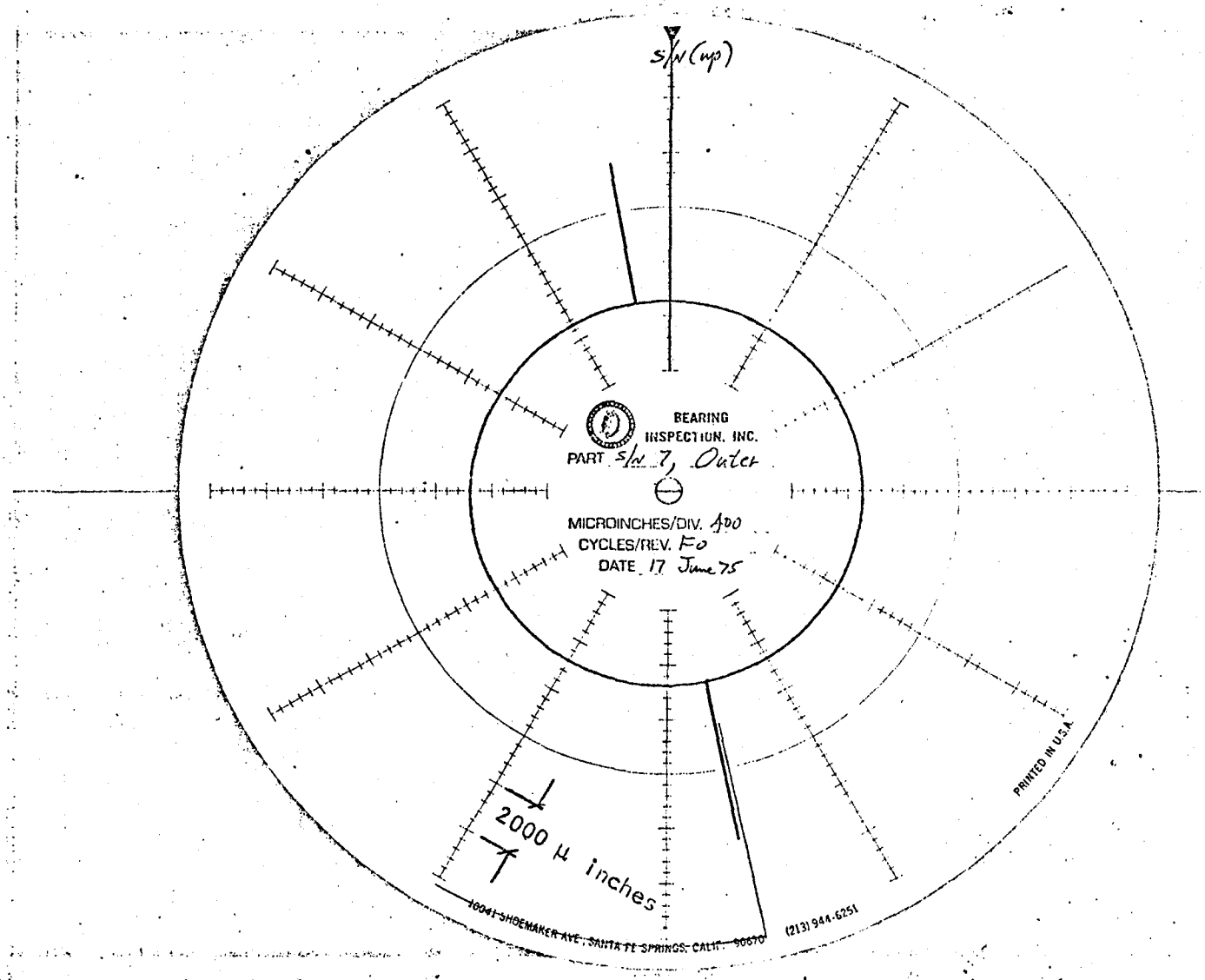

Figure 3-4a - Profilometer measurement of the fault locations eloxed into the outer race of bearing S/N 7.

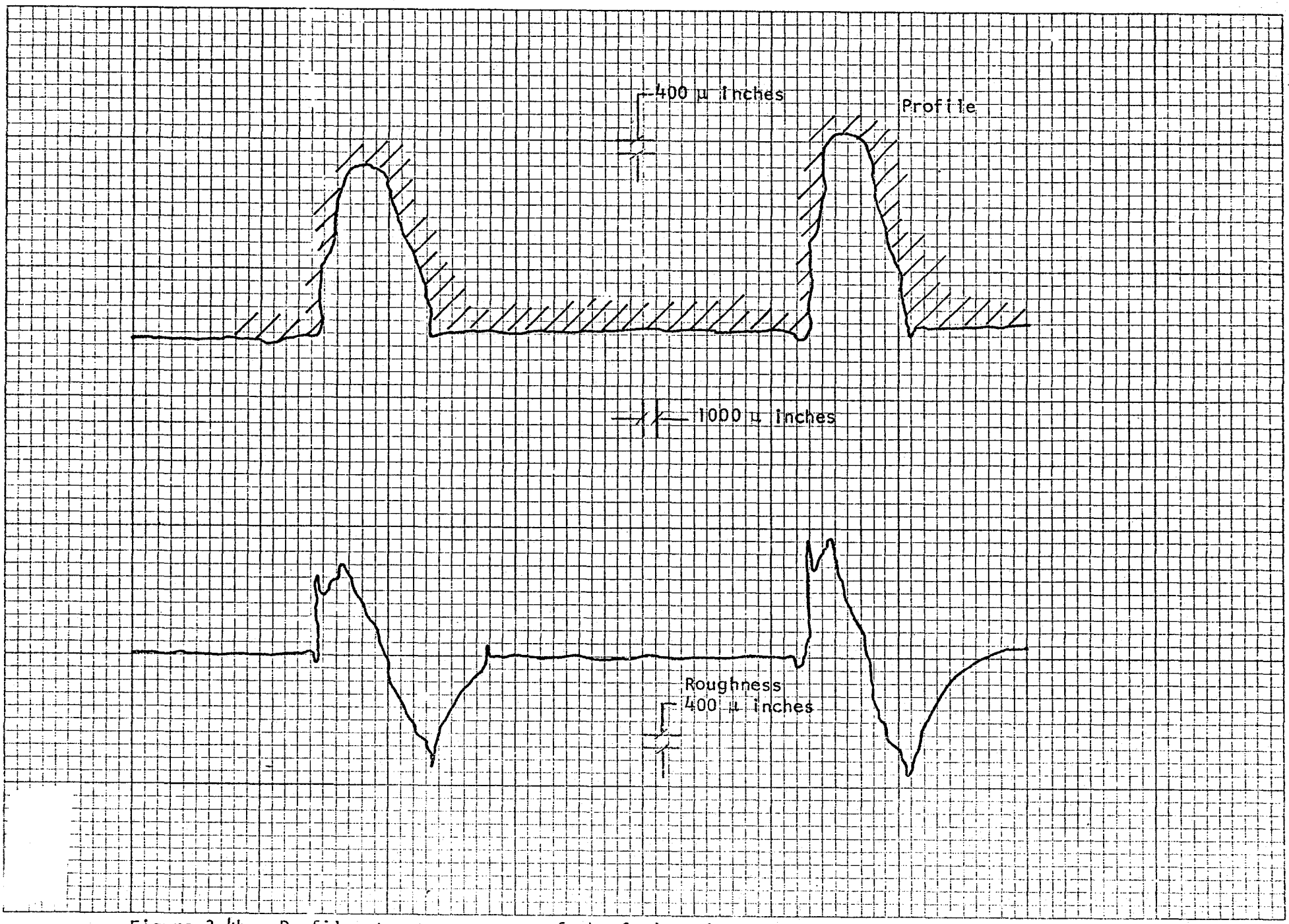

Figure 3-4b - Profilometer measurement of the faults eloxed into the outer race of bearing S/N 7.

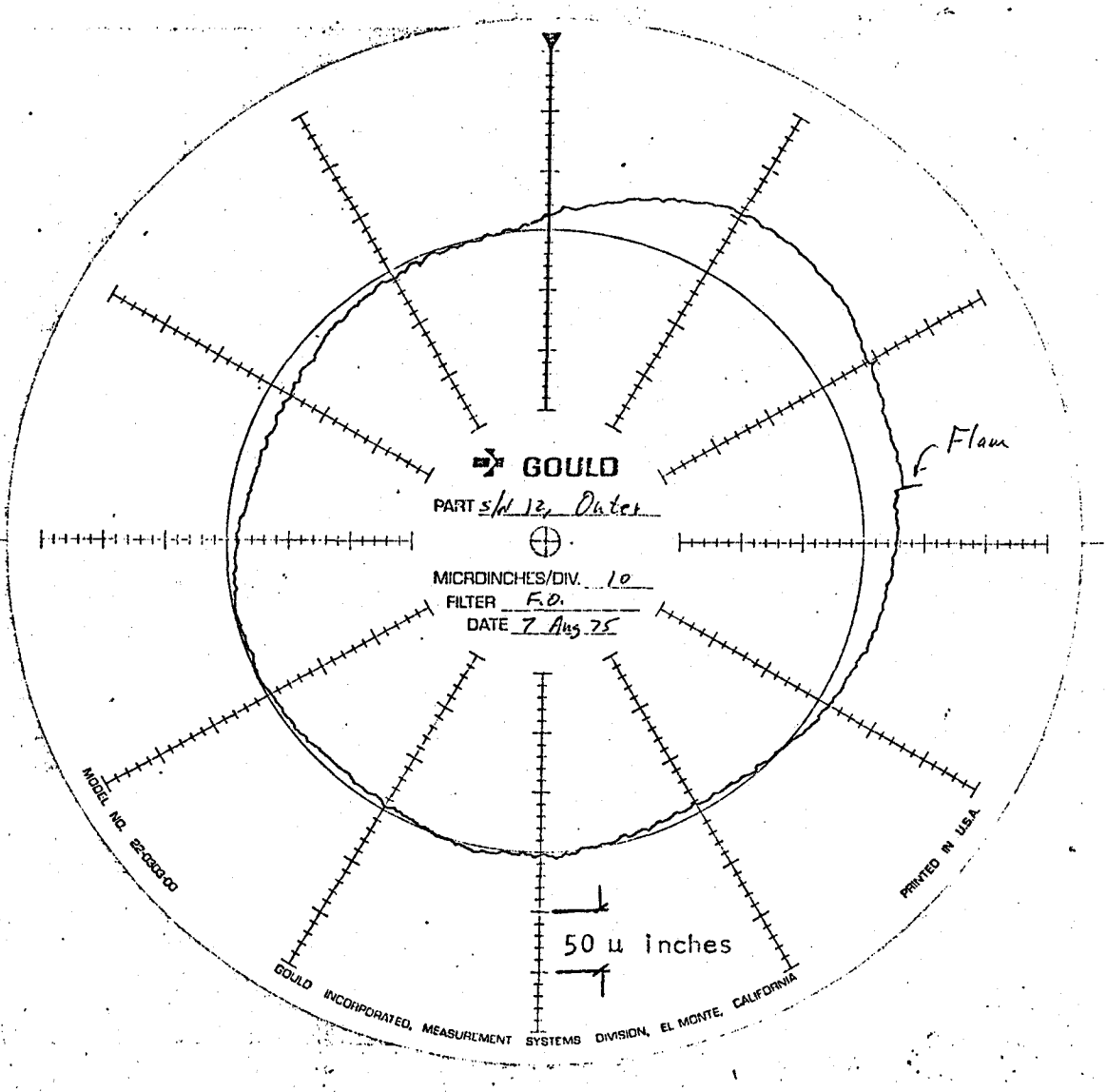

Figure 3-5a - Profilometer measurement of the fault location scribed into the outer race of bearing number 12.

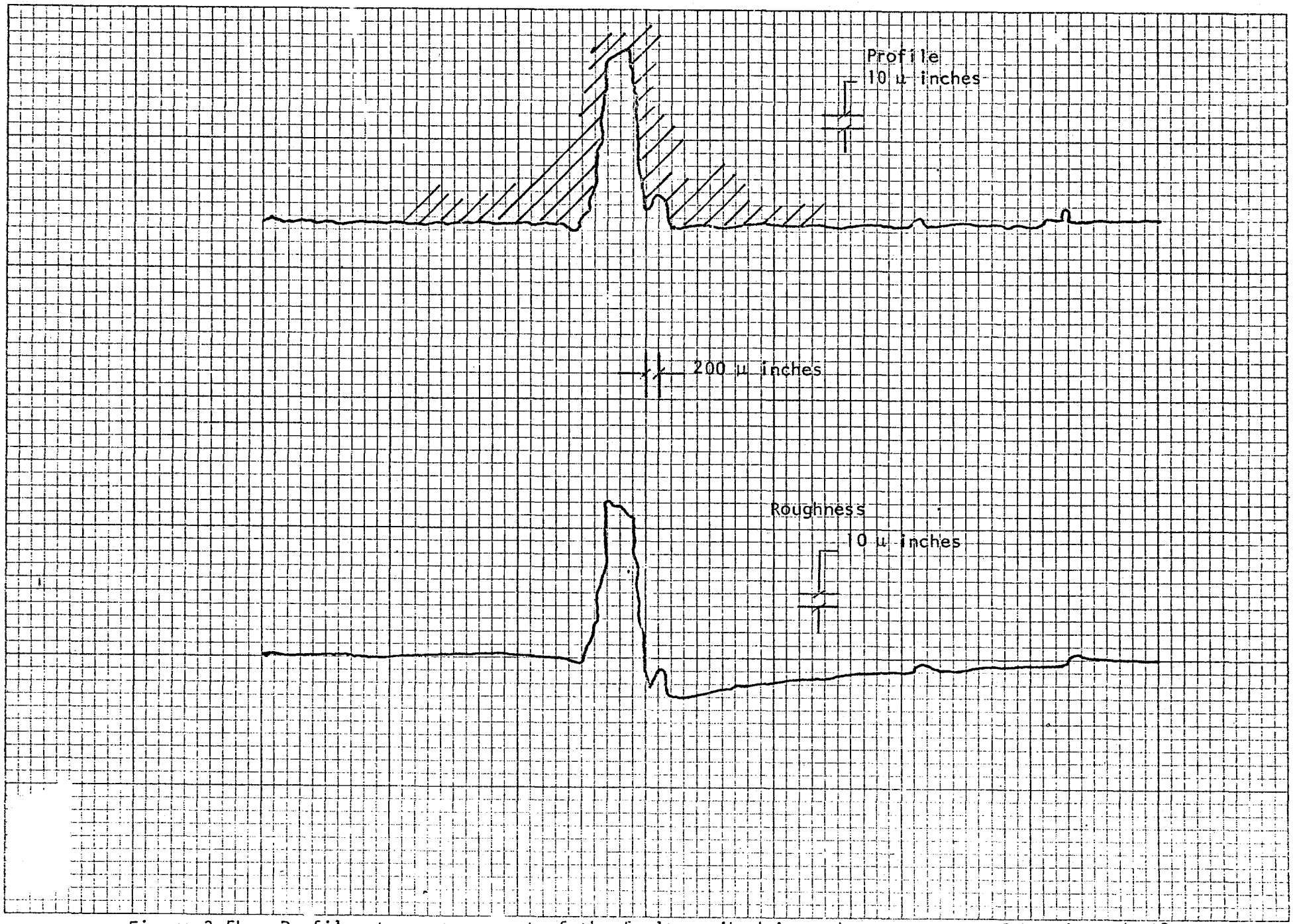

Figure 3-5b - Profilometer measurement of the fault scribed into the outer race of bearing S/N 12.

APPENDIX IV

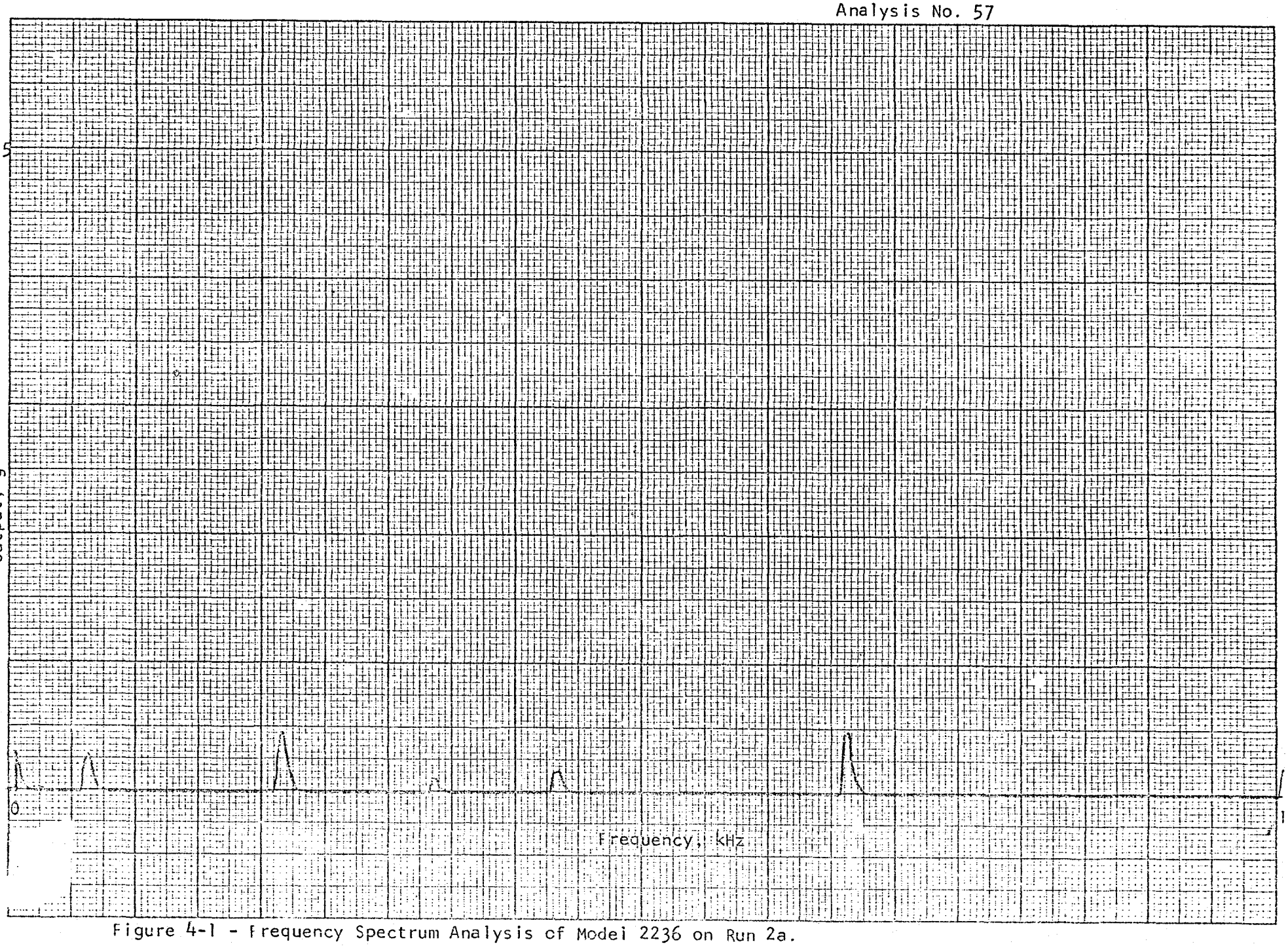

Figure 4-1 - Frequency Spectrum Analysis of Model 2236 on Run 2a.

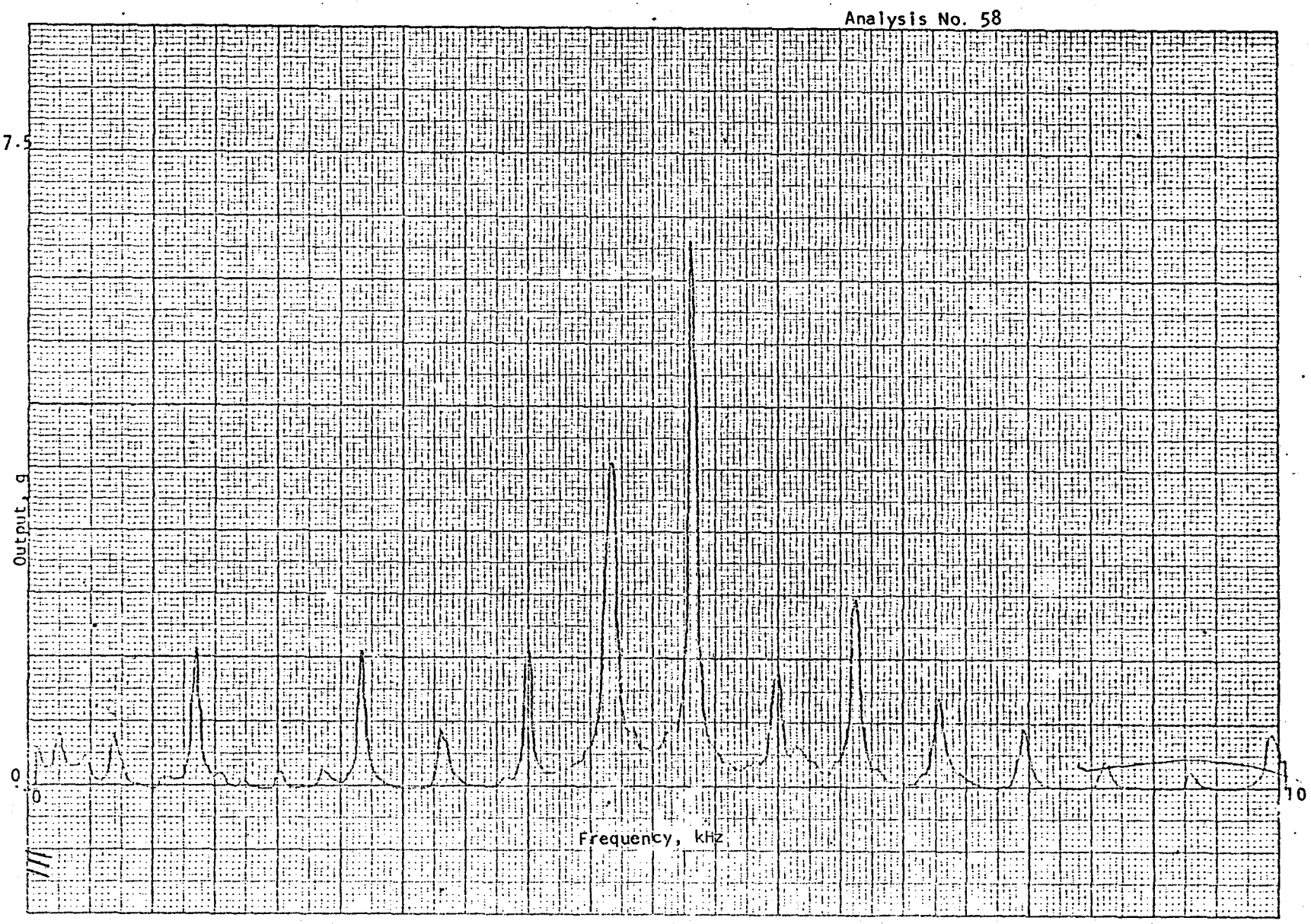

Figure 4-2 - Frequency Spectrum Analysis of Model 2236 on Run 2a.

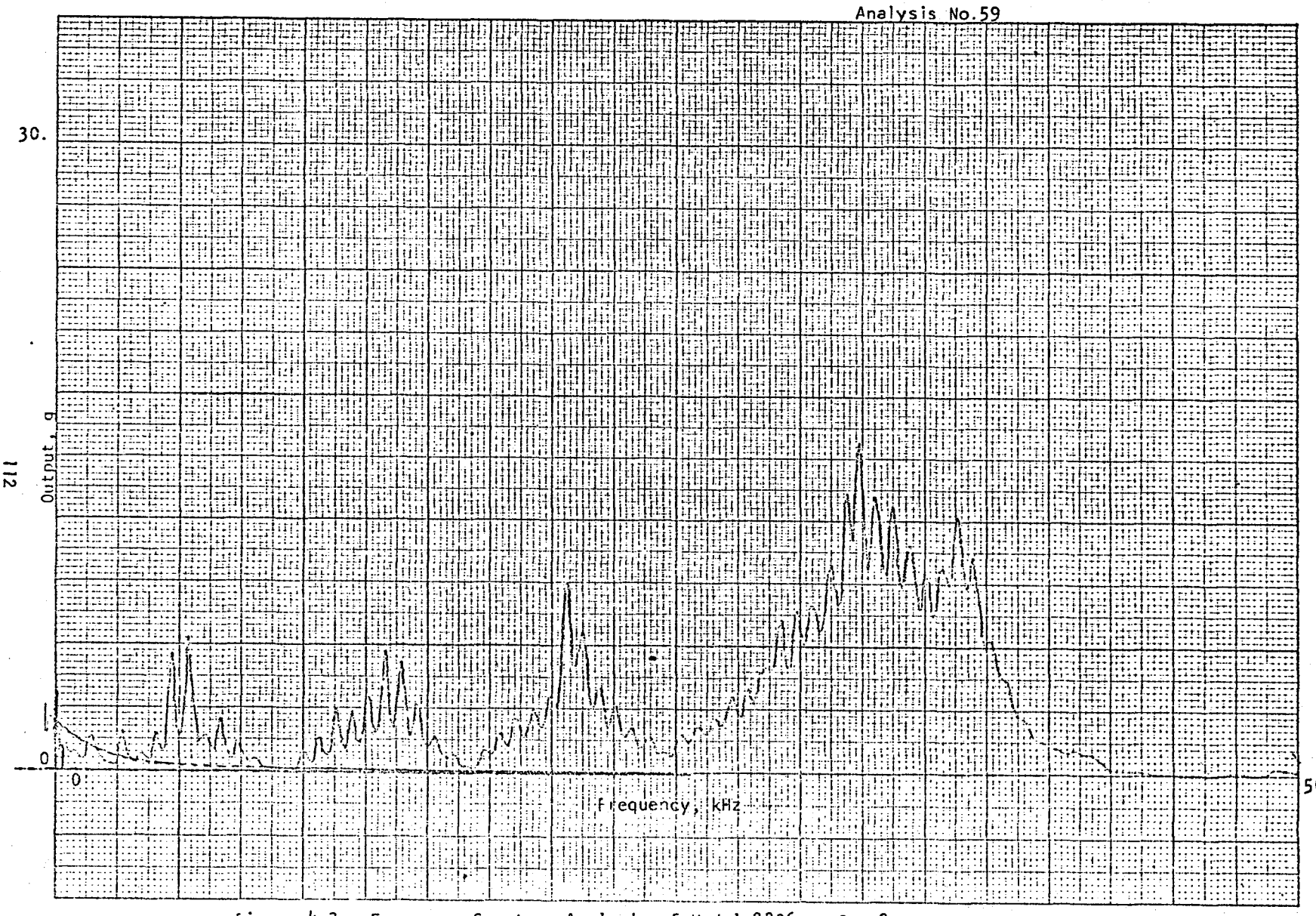

Figure 4-3 - Frequency Spectrum Analysis of Model 2236 on Run 2a.

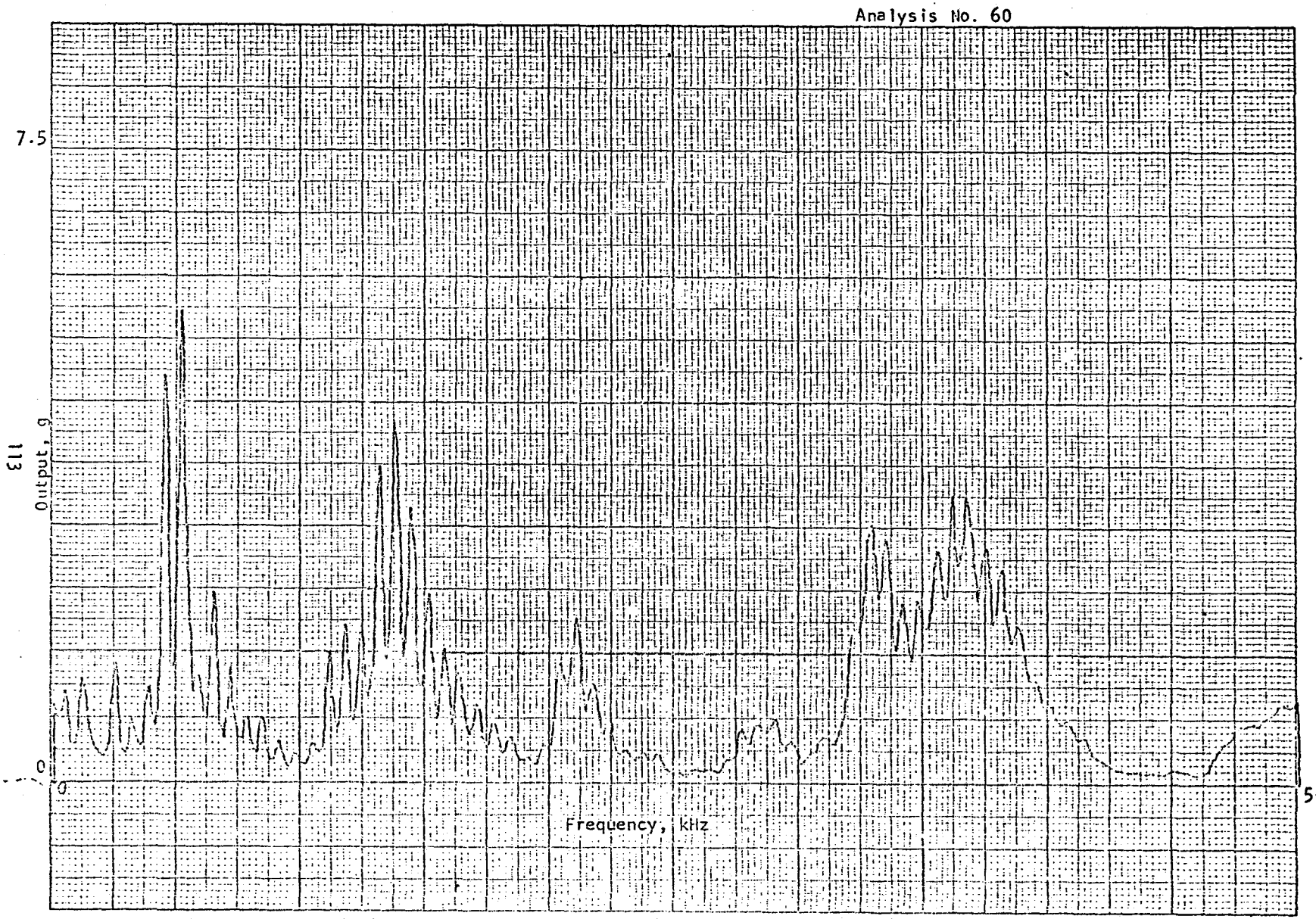

Figure 4 -4 - Frequency Spectrum Analysis of Model 6230M8 on Run 2.

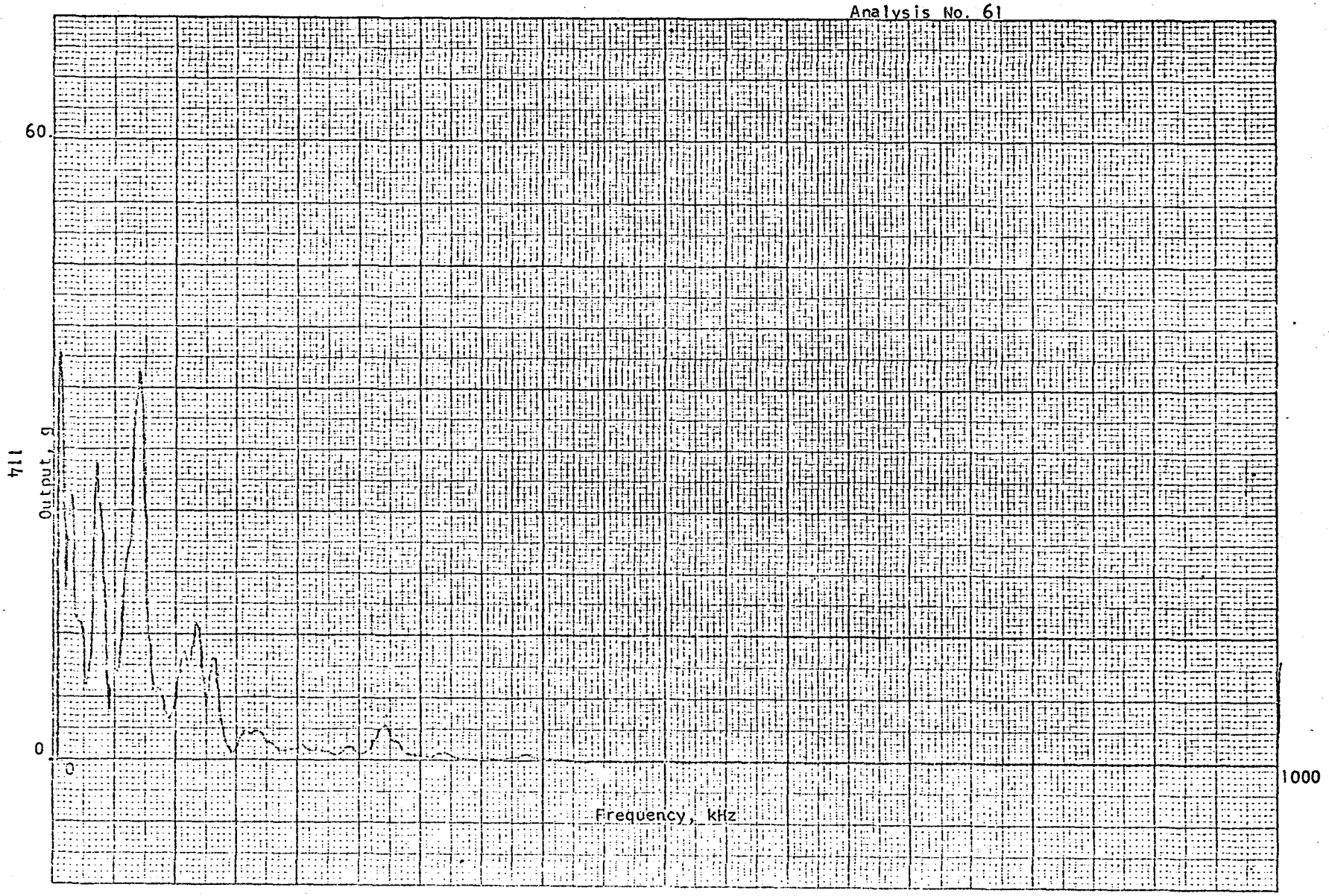

Figure 4-5 - Frequency Spectrum Analysis of Model 6230M8 on Run 2a.

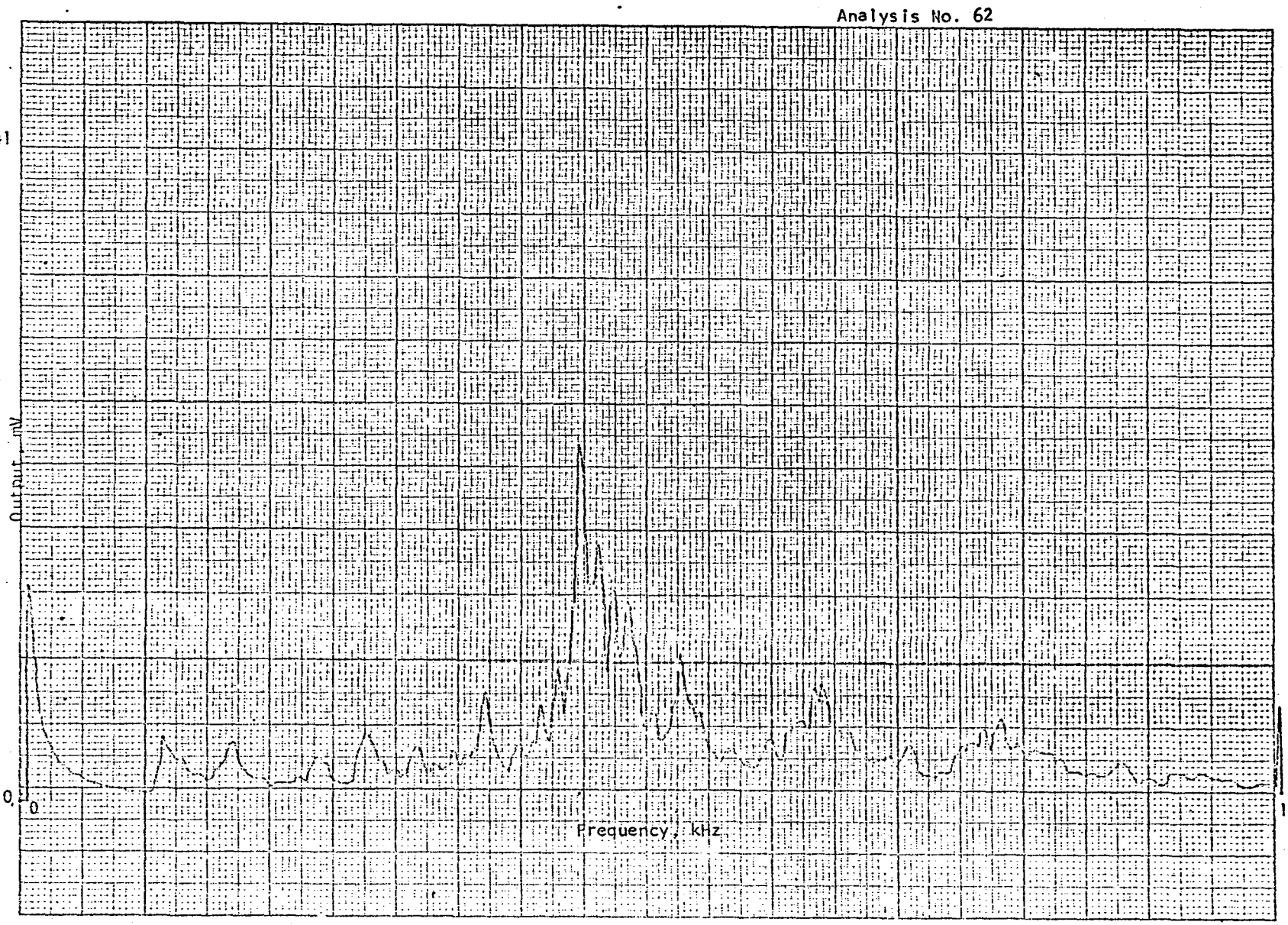

Figure 4-6 - Frequency Spectrum Analysis of Model D9202 with 40 db gain preamplifier on Run 2a.

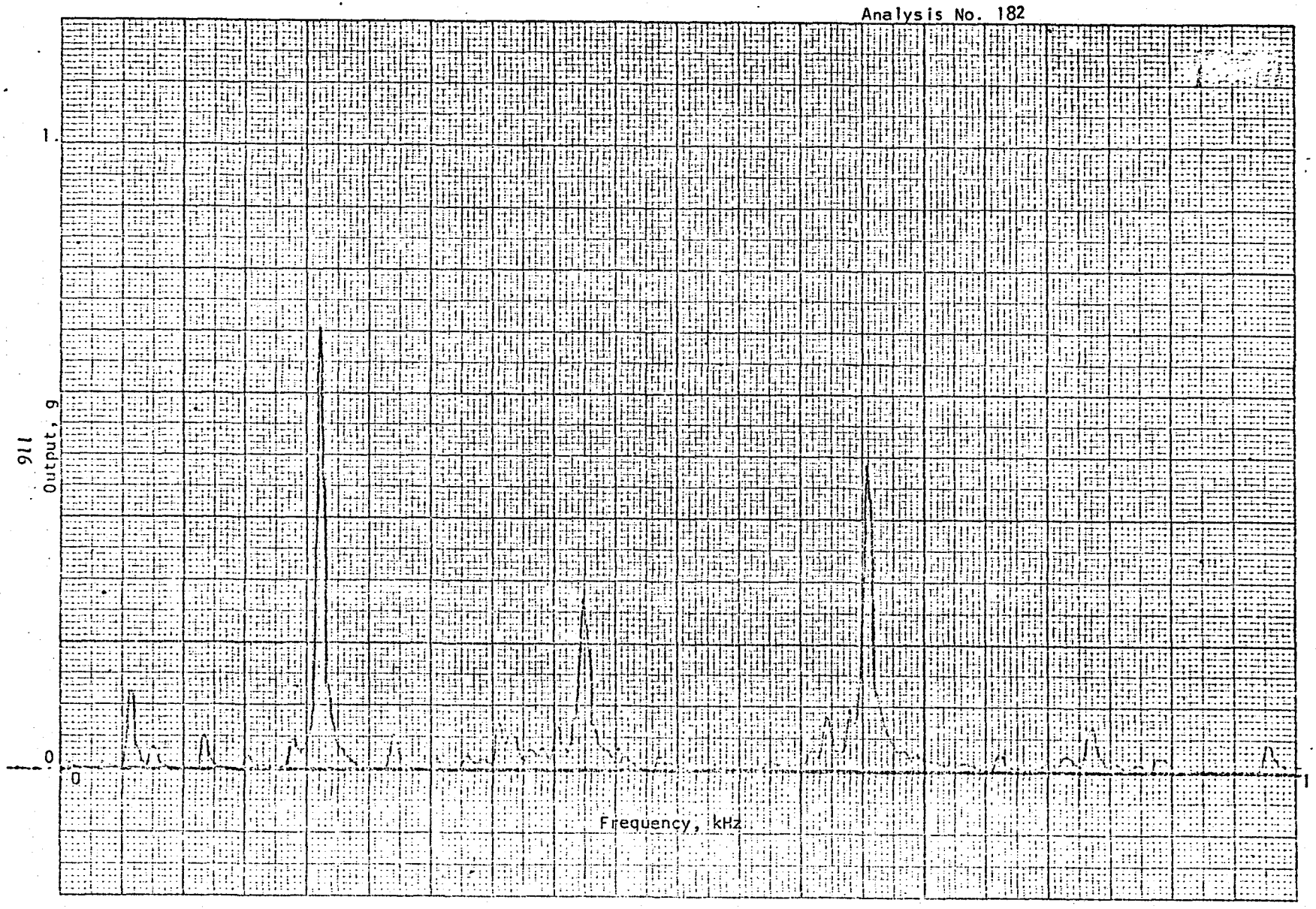

Figure 4-7 -- Frequency Spectrum Analysis of Model 2236 on Run 4a.

46 1242

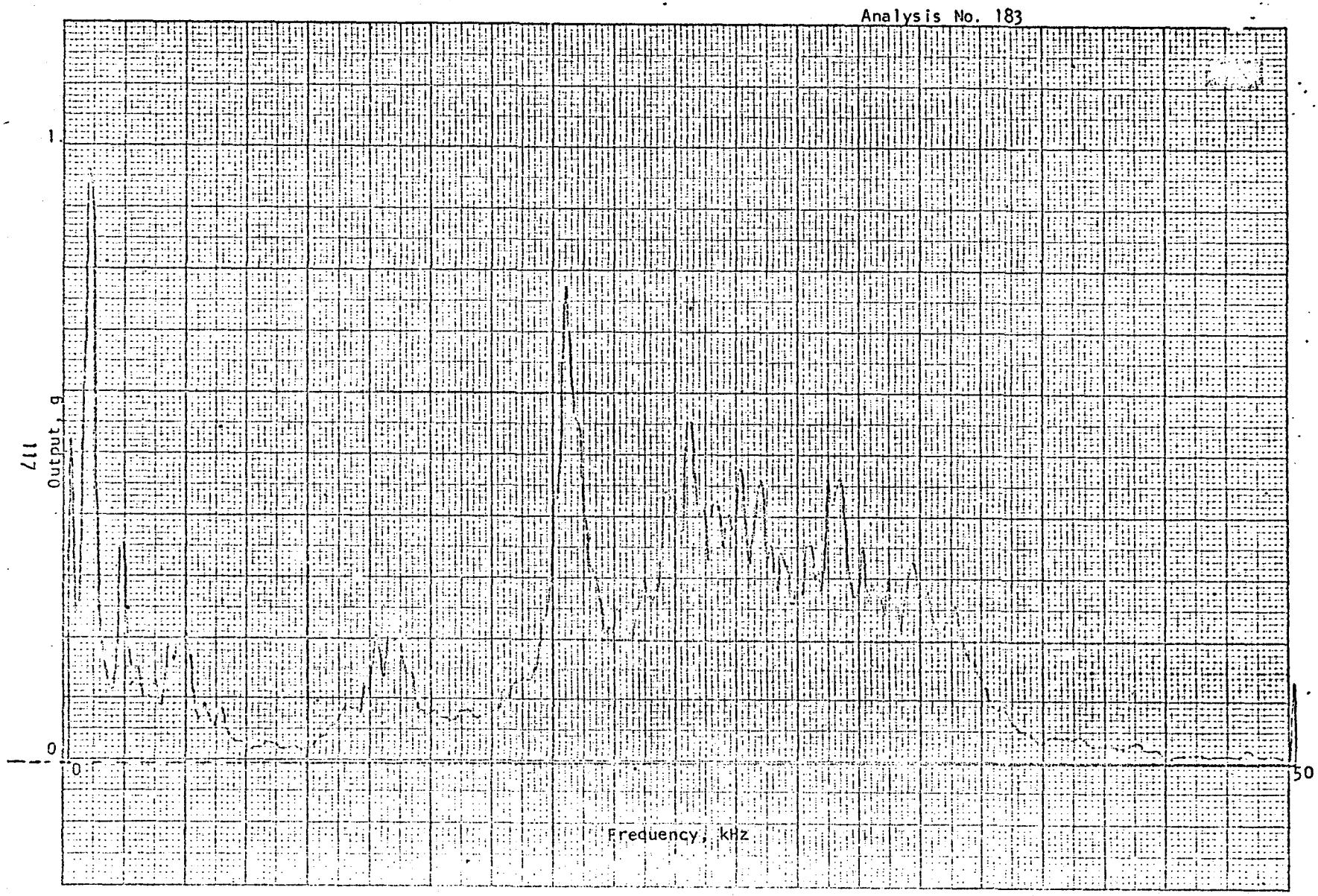

Figure 4-8 - Frequency Spectrum Analysis of Model 2236 on Run 4a.

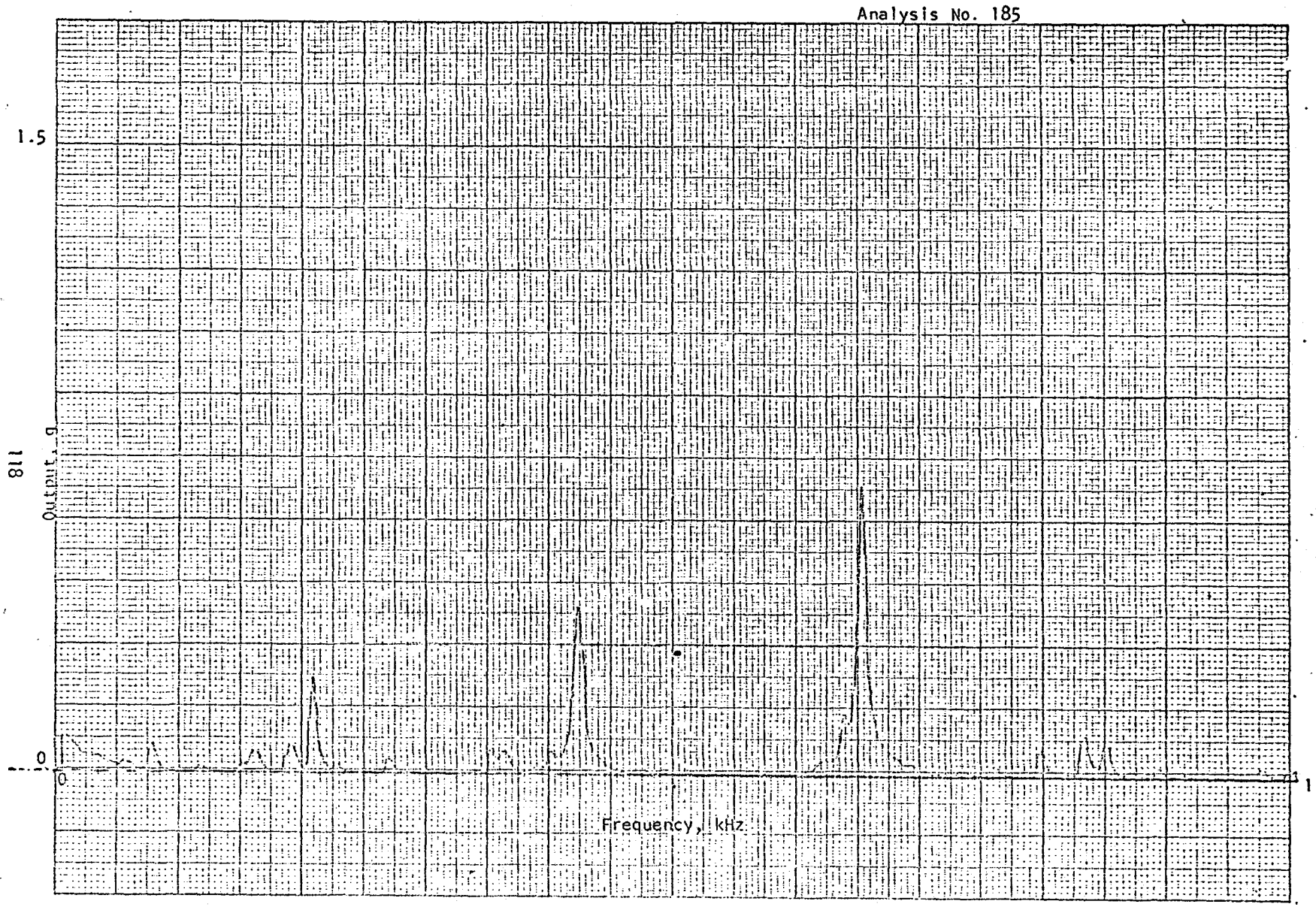

Figure 4-9 - Frequency Spectrum Analysis of Model 6230M8 on Run 4a.

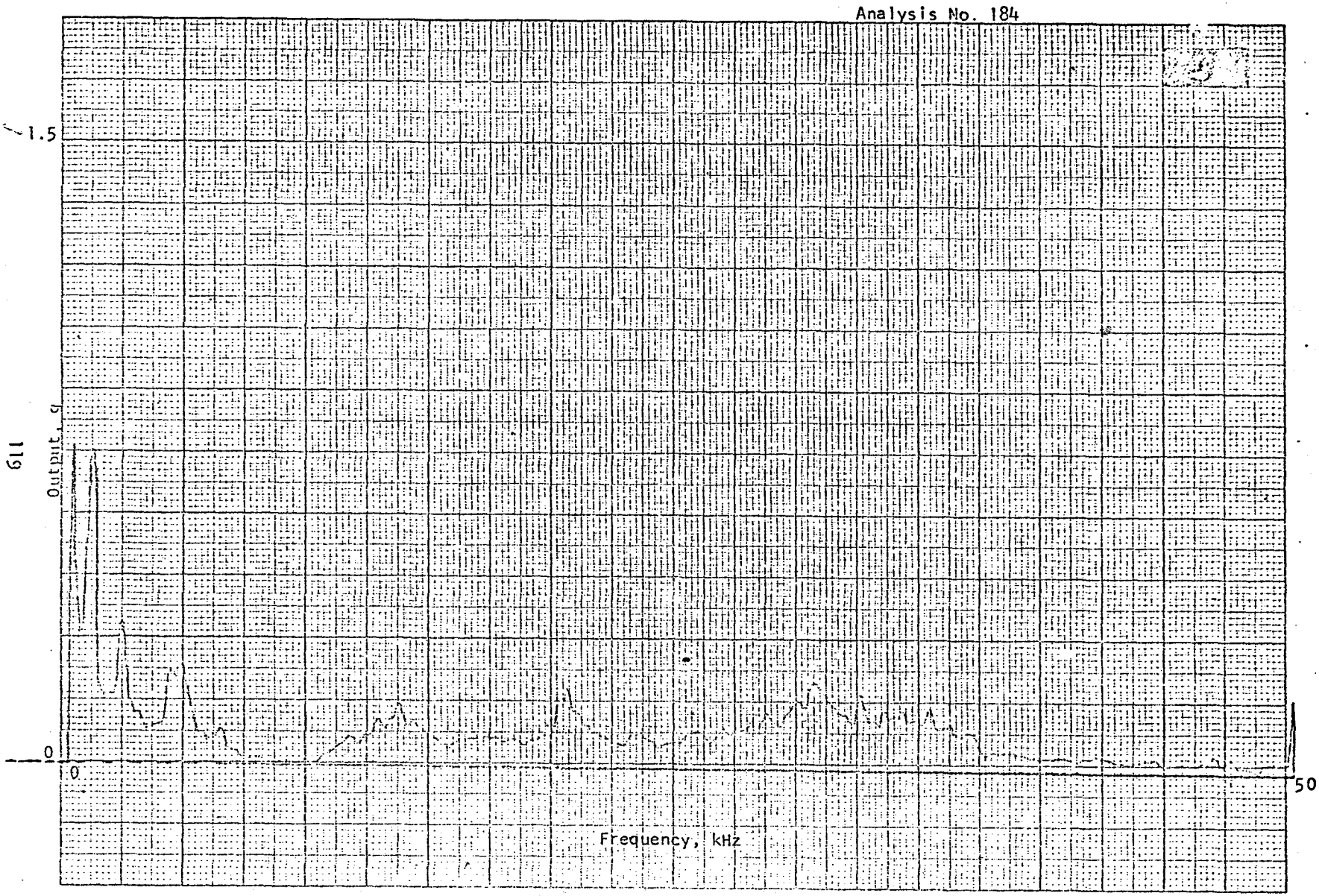

Figure 4-10 - Frequency Spectrum Analysis of Model 6230M8 on Run 4a.

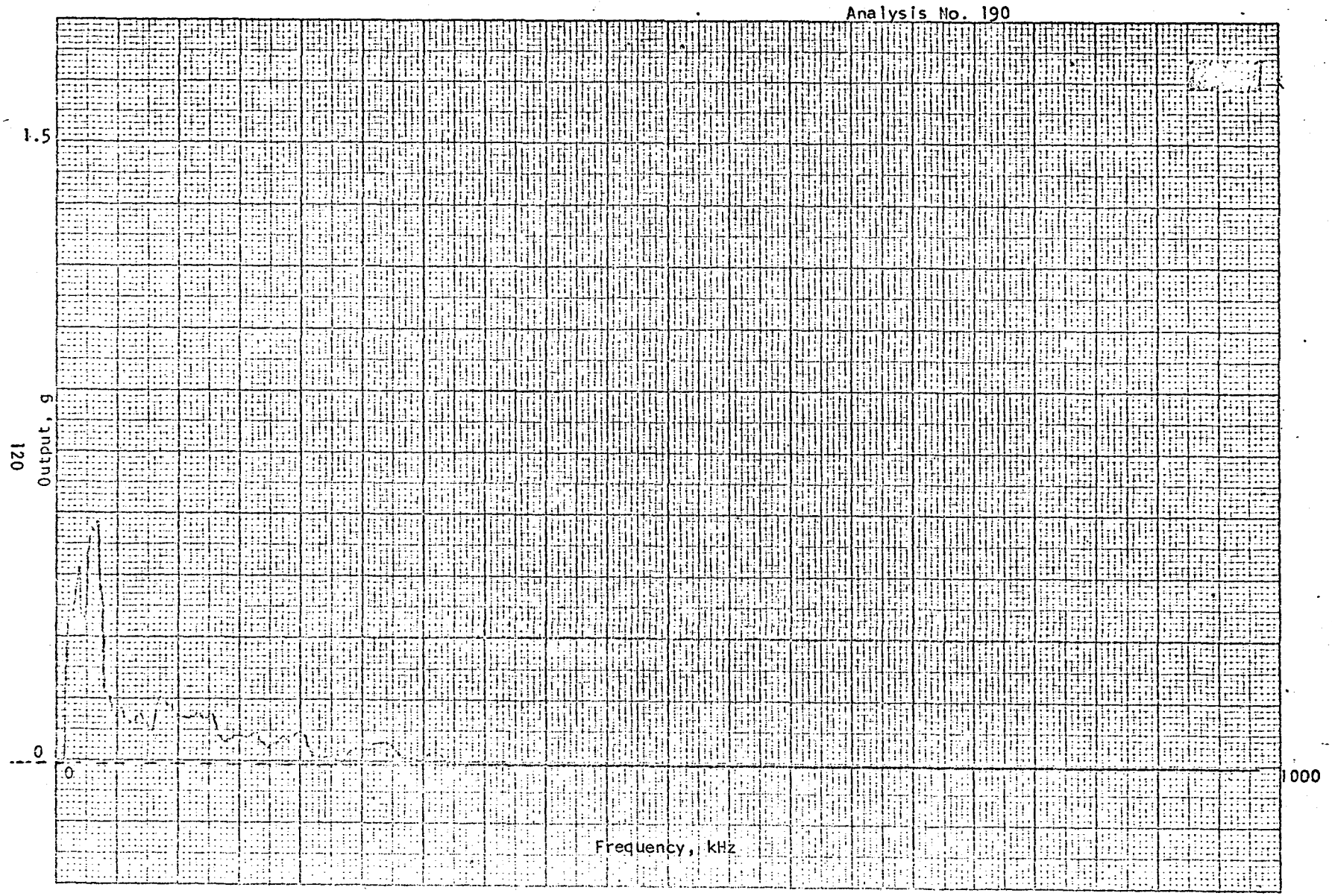

Figure 4-11 - Frequency Spectrum Analysis of Model 6230M8 on Run 4a.

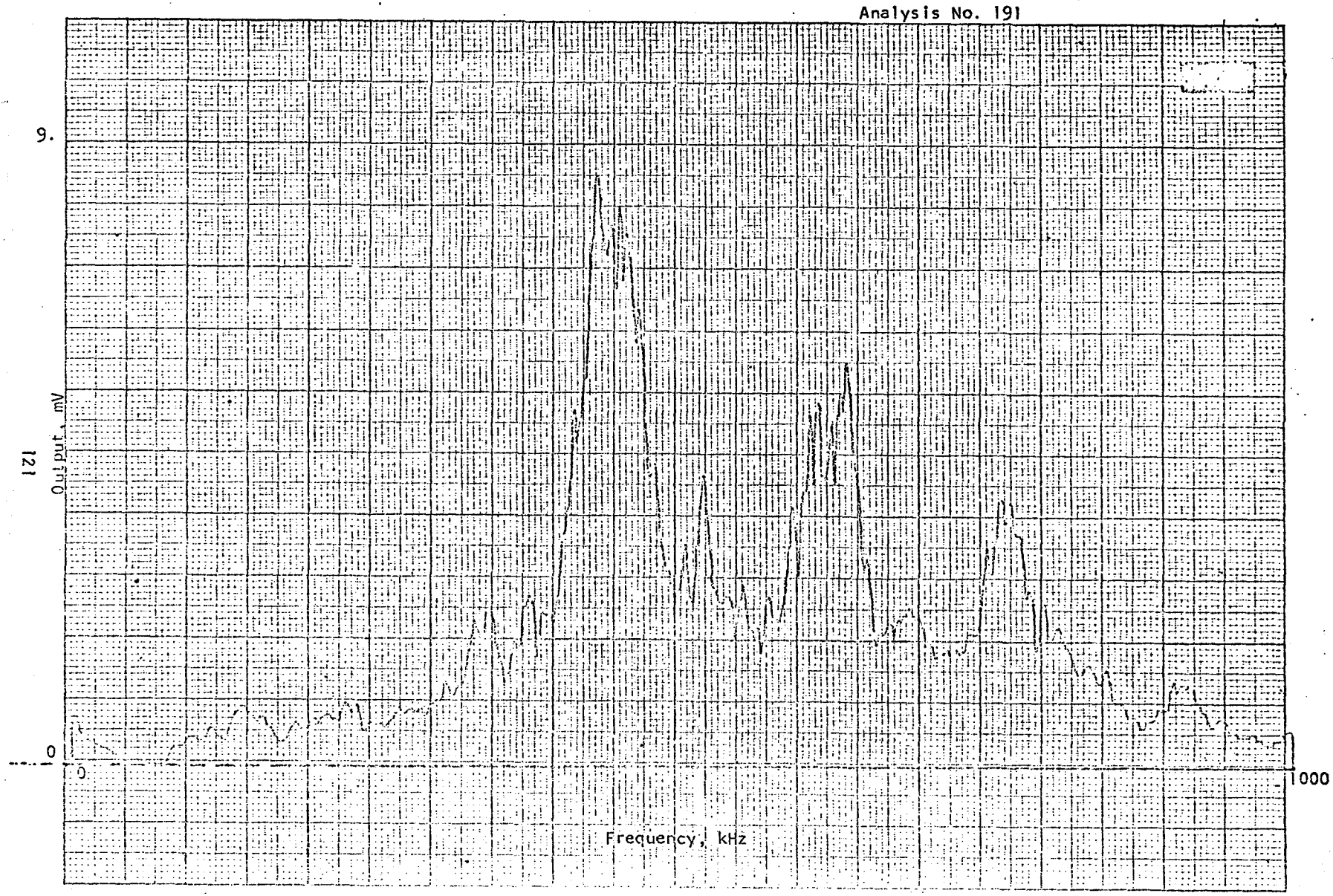

Figure 4-12 - Frequency Spectrum Analysis of Model D9202 with 40 db gain preamplifier on Run 4a.

Page intentionally left blank

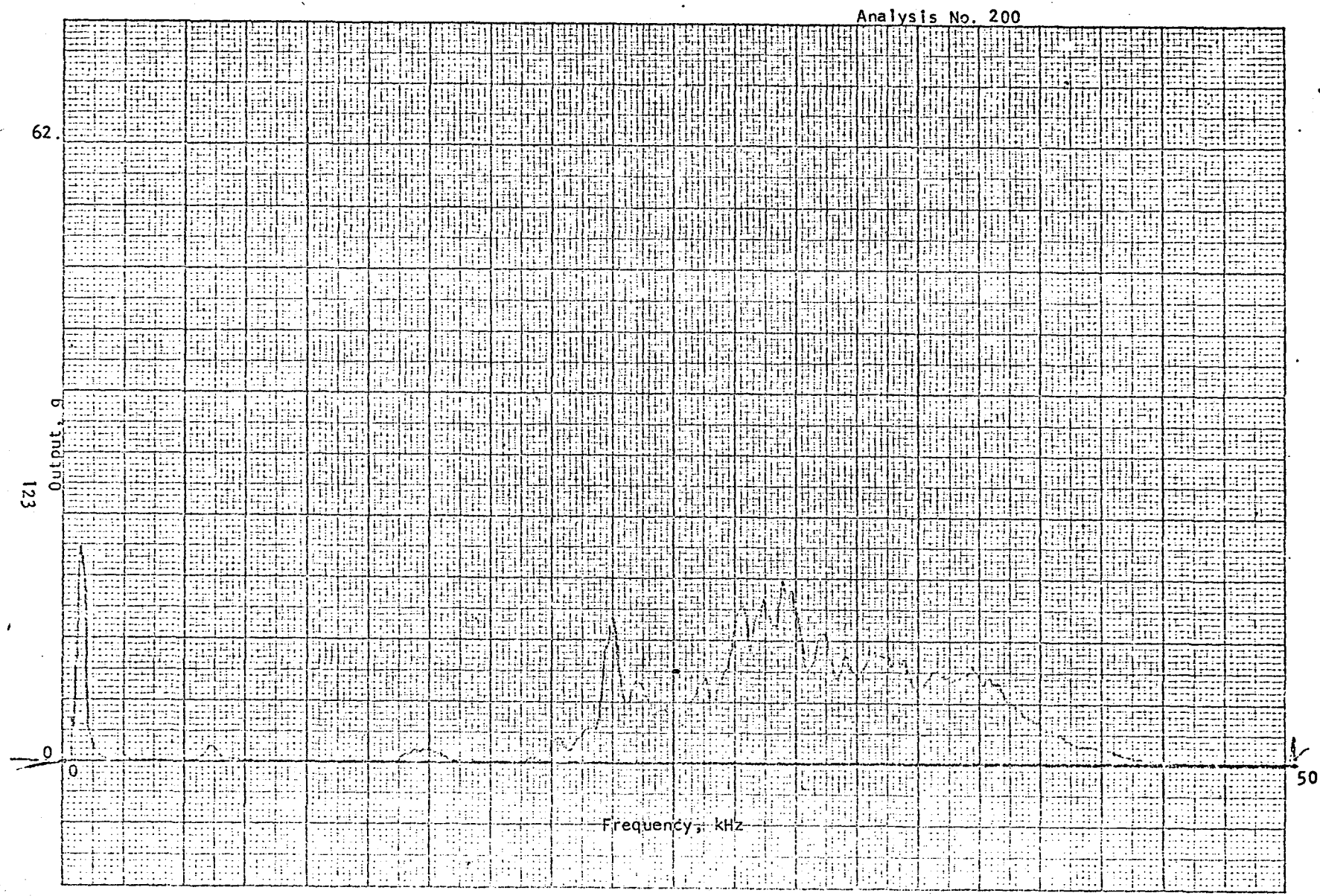

Figure 4-14 - Frequency Spectrum Analysis of Model 2236 on Run 5a.

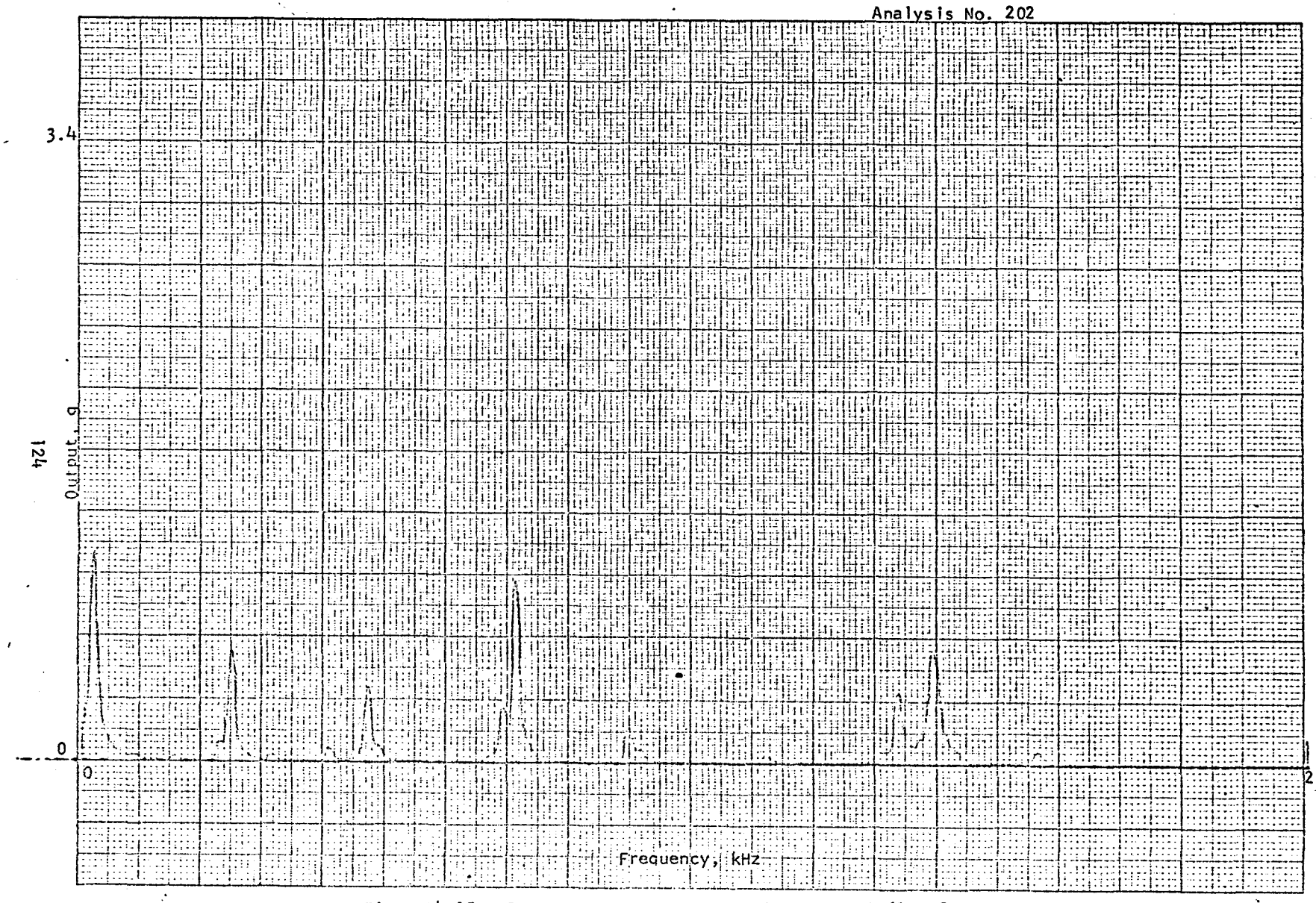

Figure 4-15 - Frequency Spectrum Analysis of Model 6230M8 on Run 5a.

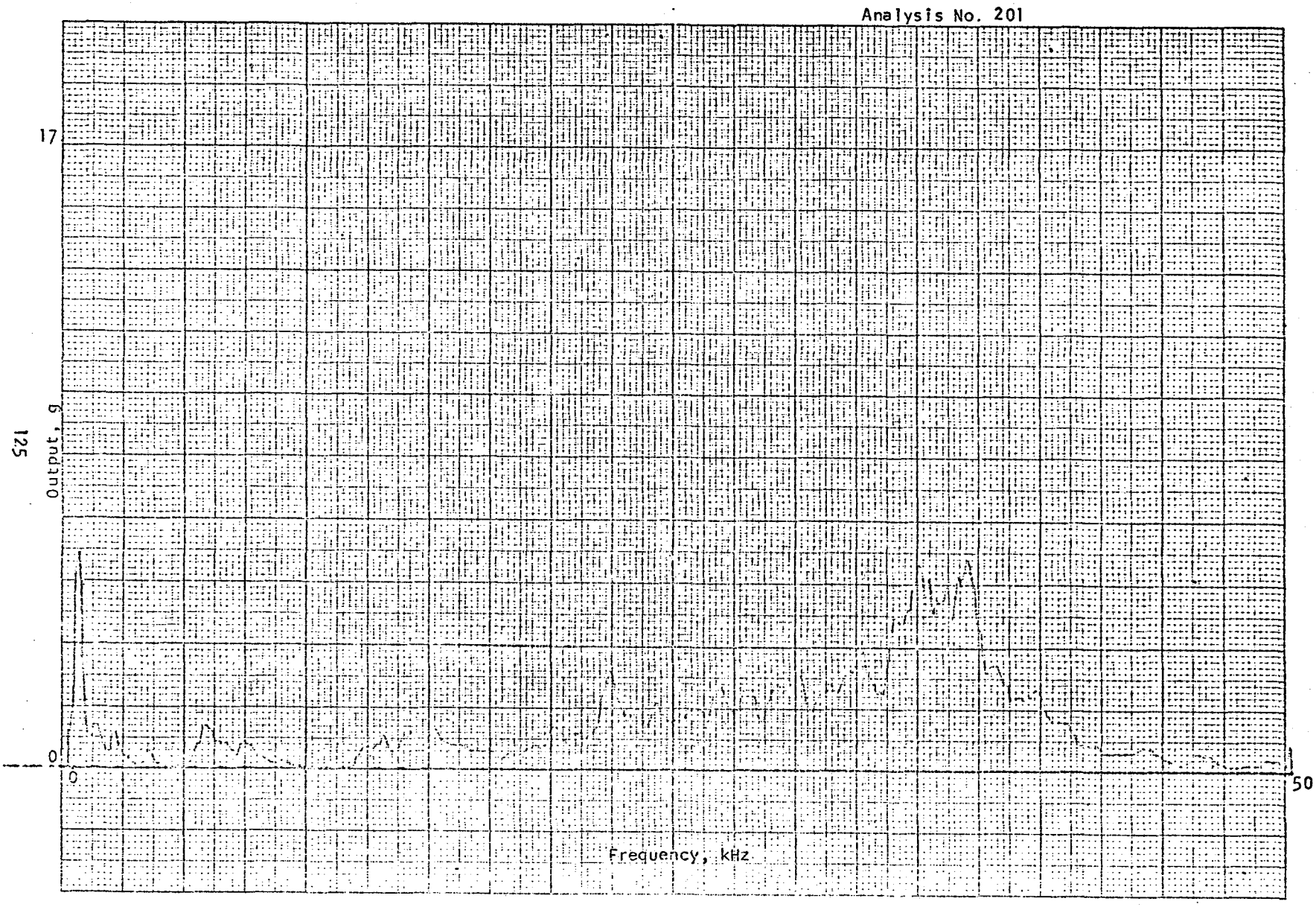

Figure 4-16 - Frequency Spectrum Analysis of Model 6230M8 on Run 5a.

46 1242

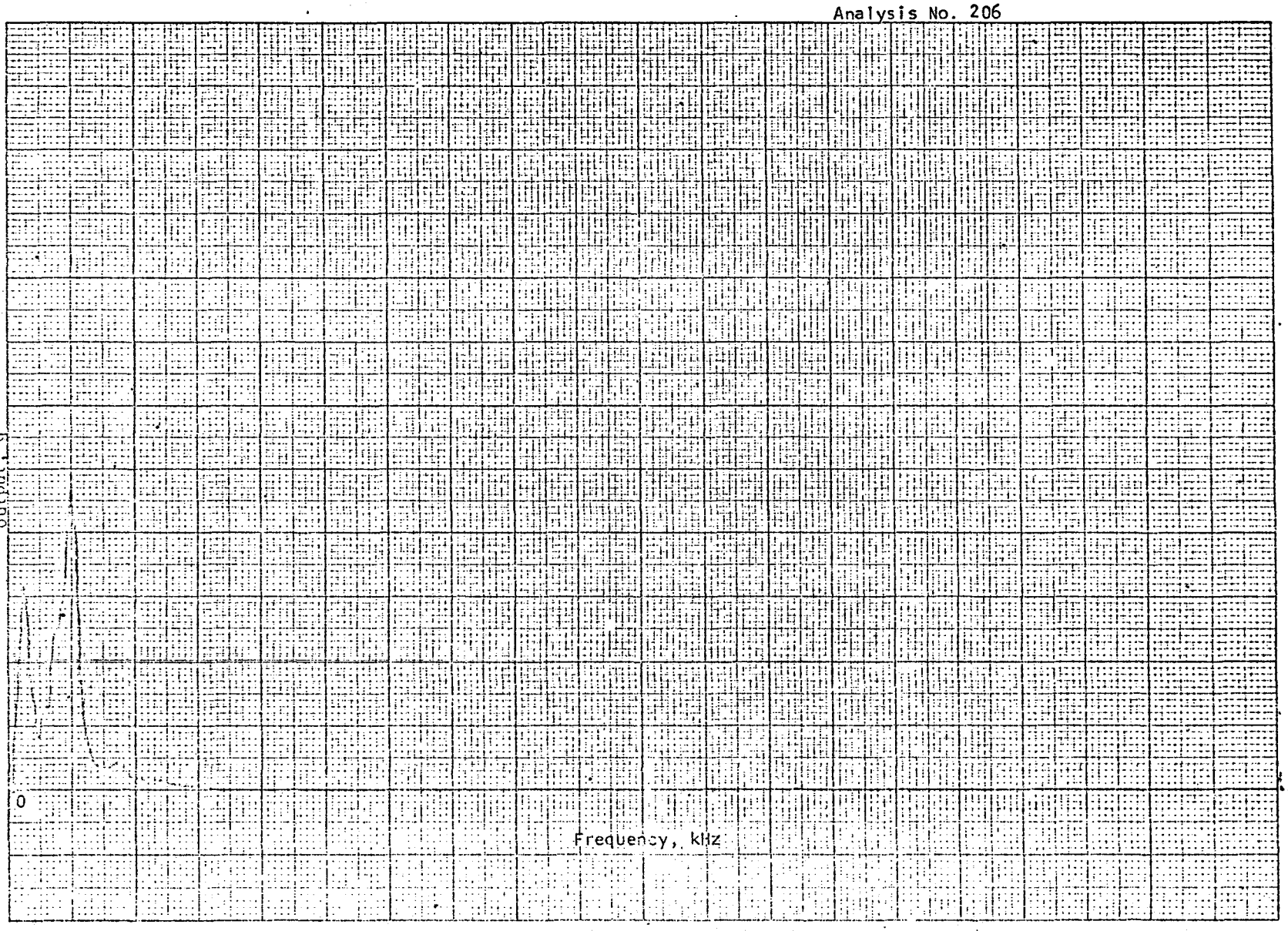

Figure 4-17 - Frequency Spectrum Analysis of Model 6230M8 on Run 5a.

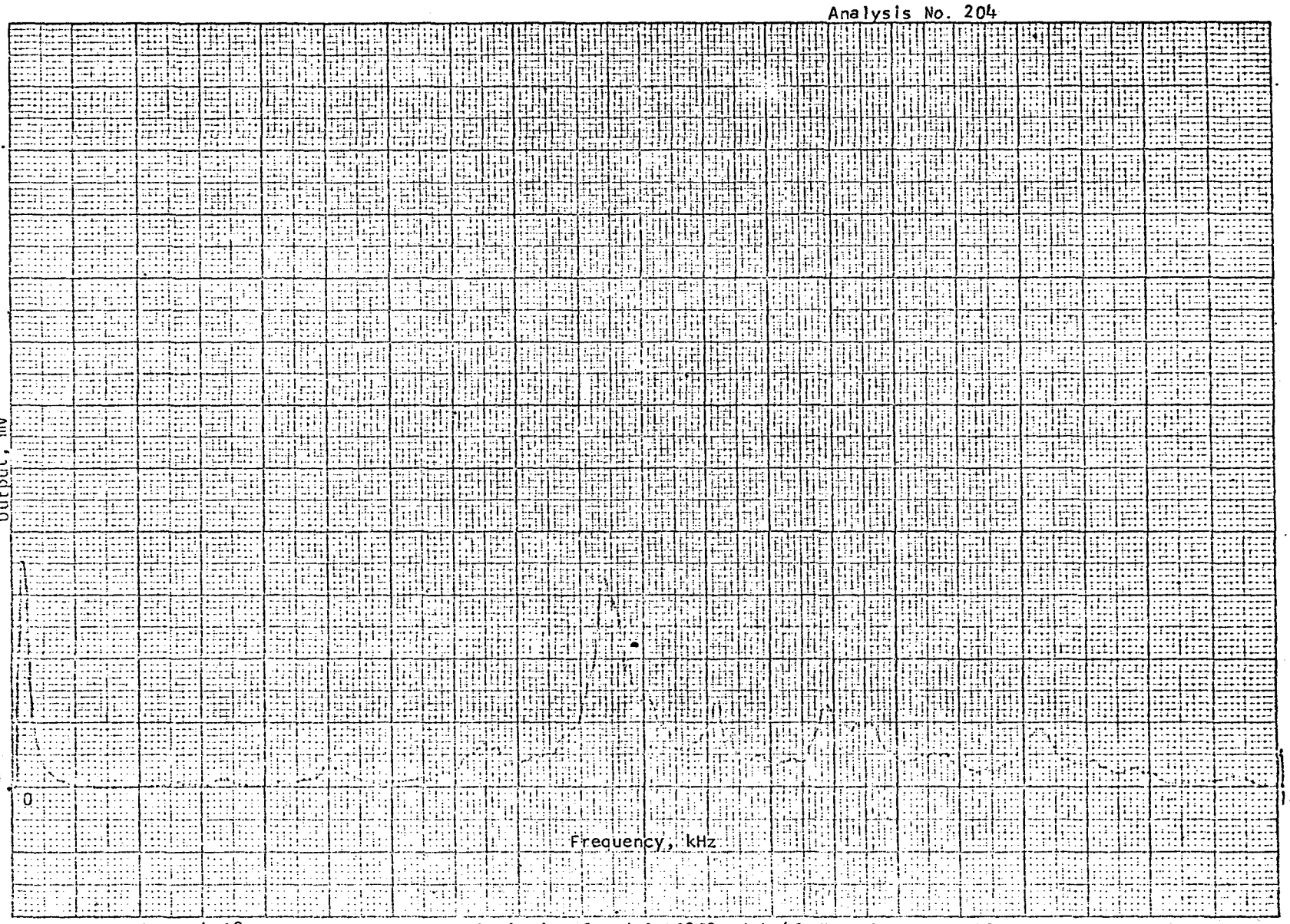

Figure 4-18 - Frequency Spectrum Analysis of Model D9202 with 40 db gain preamplifier on Run 5a.

Page intentionally left blank

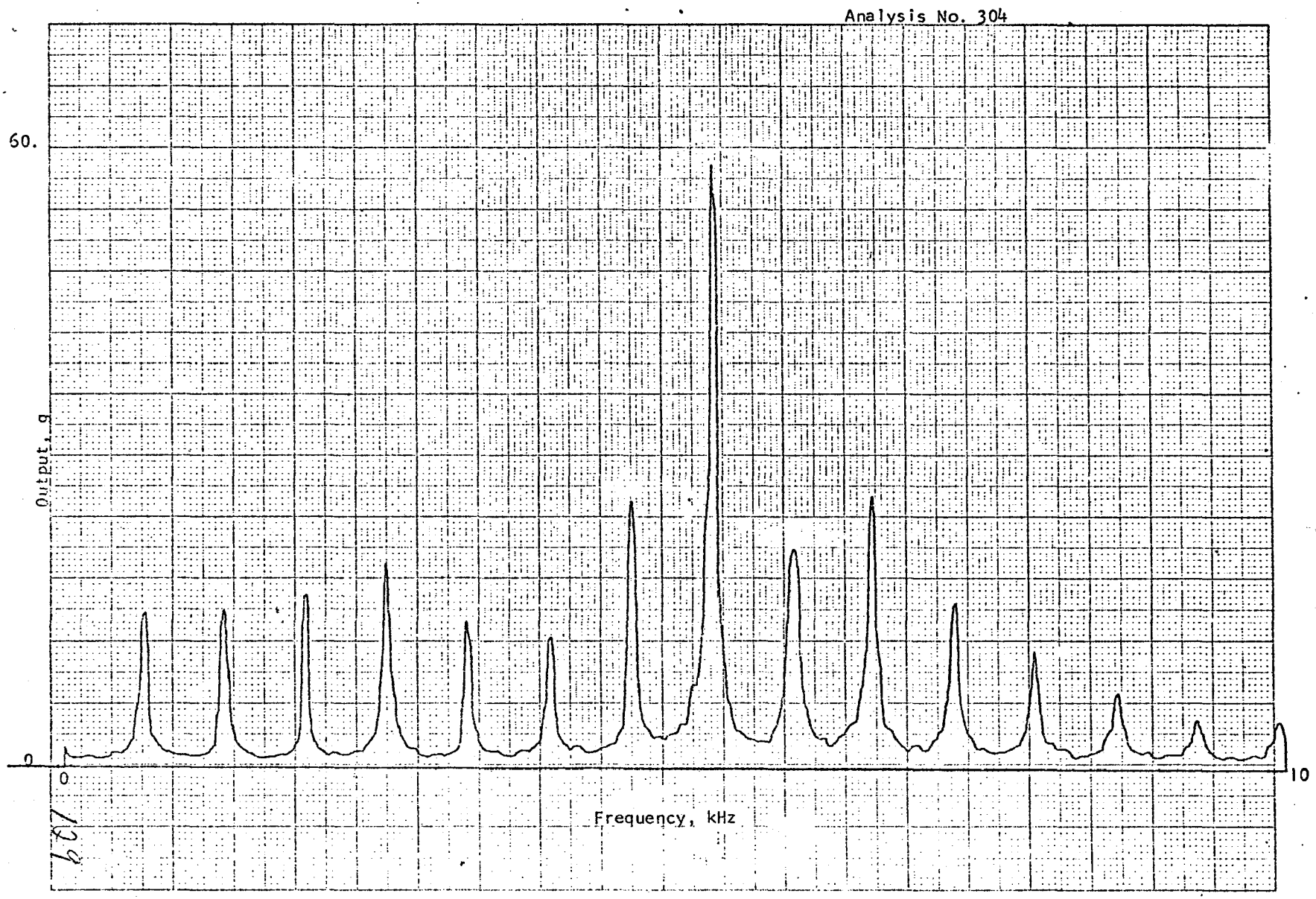

Figure 4-20 - Frequency Spectrum Analysis of Model 2236 on Run 8a.

46 1242

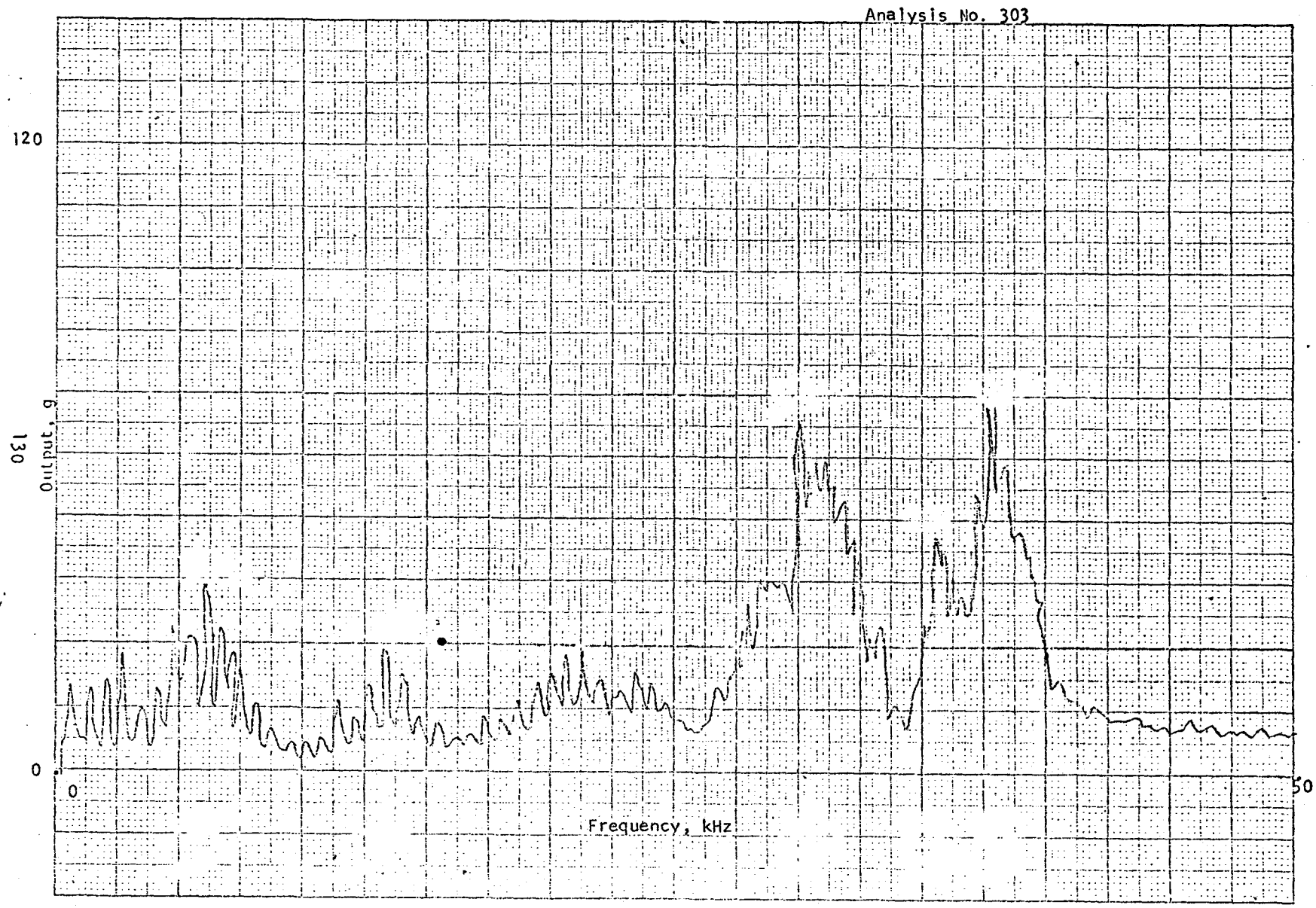

Figure 4-21 - Frequency Spectrum Analysis of Model 2236 on Run 8a.

Multiple Pages Missing from Available Version

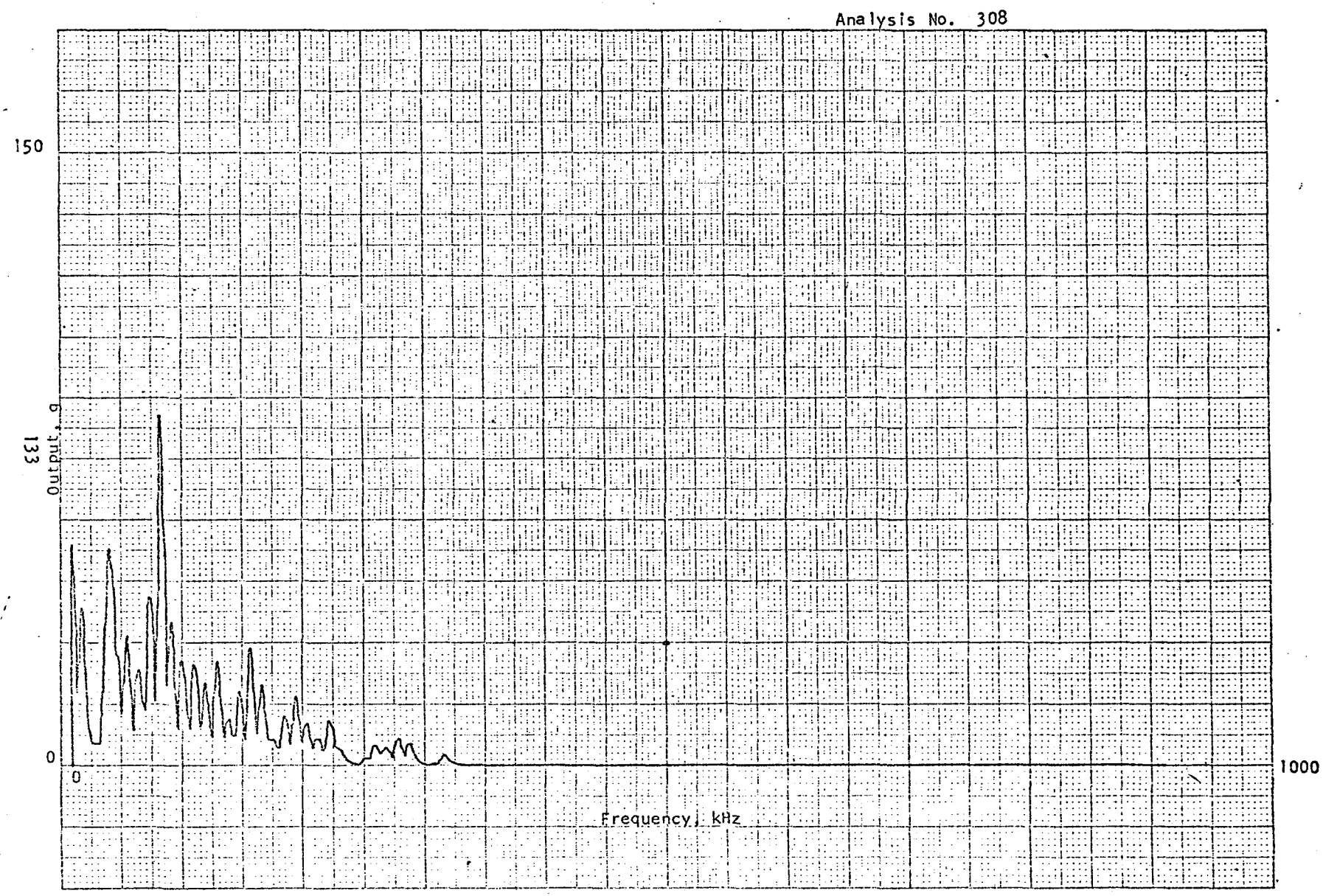

Figure 4-24 - Frequency Spectrum Analysis of Model 6230M8 on Run 8a.

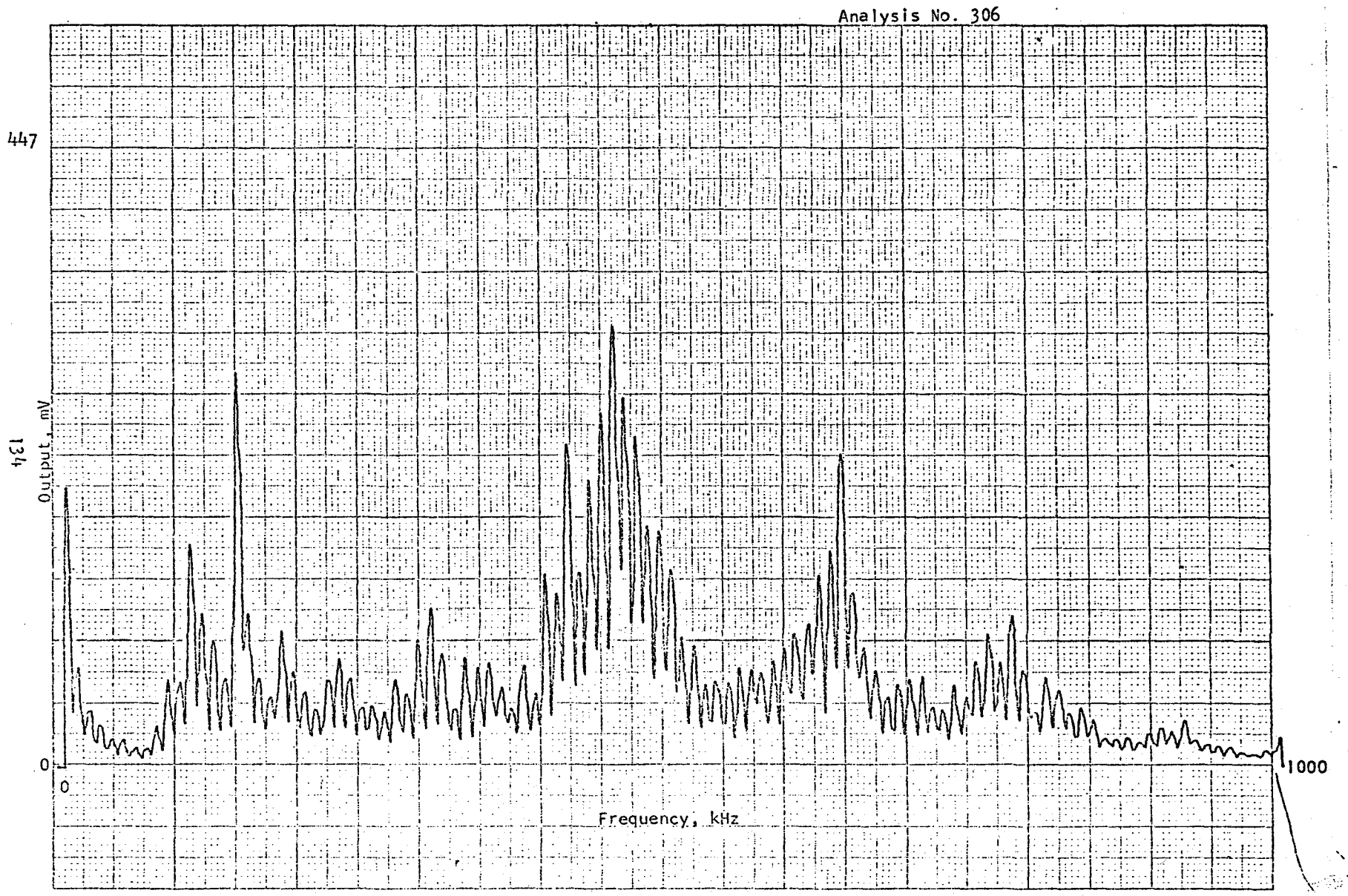

Figure 4-25 - Frequency Spectrum Analysis of Model D9202 with 40 db gain preamplifier on Run 8a.

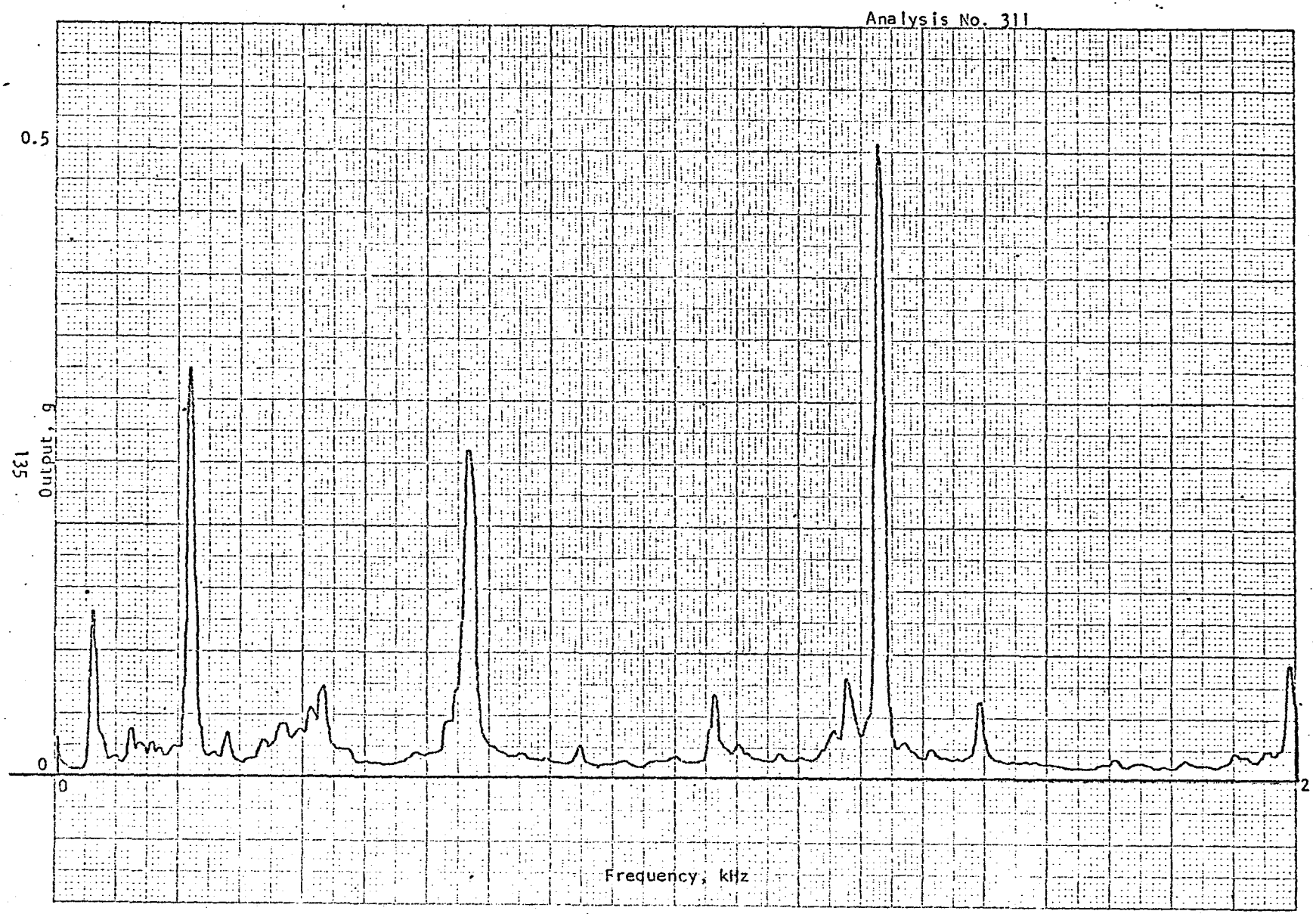

Figure 4-26 - Frequency Spectrum Analysis of Model 2236 on Run 9a.

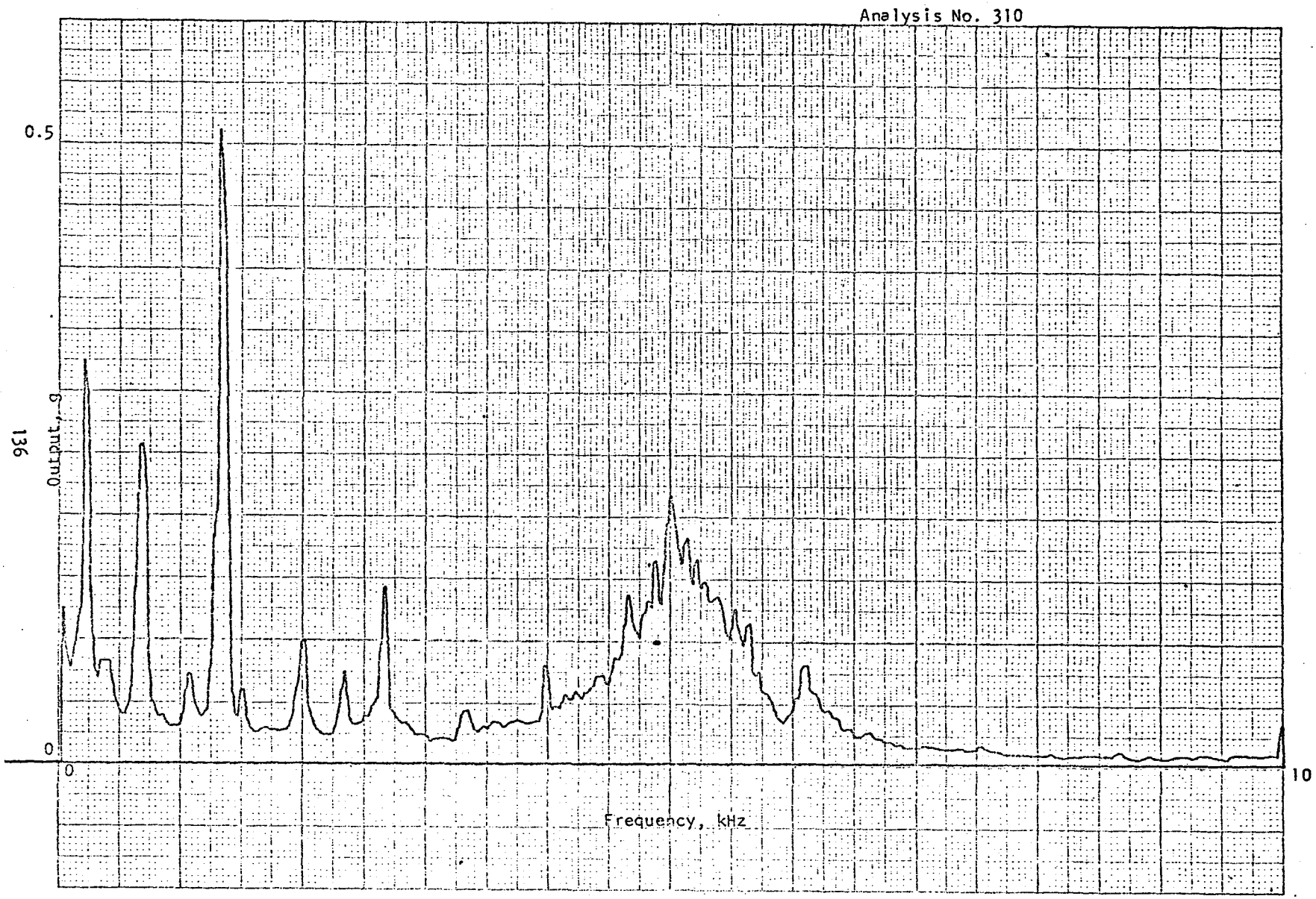

Figure 4-27 - Frequency Spectrum Analysis of Model 2236 on Run 9a.

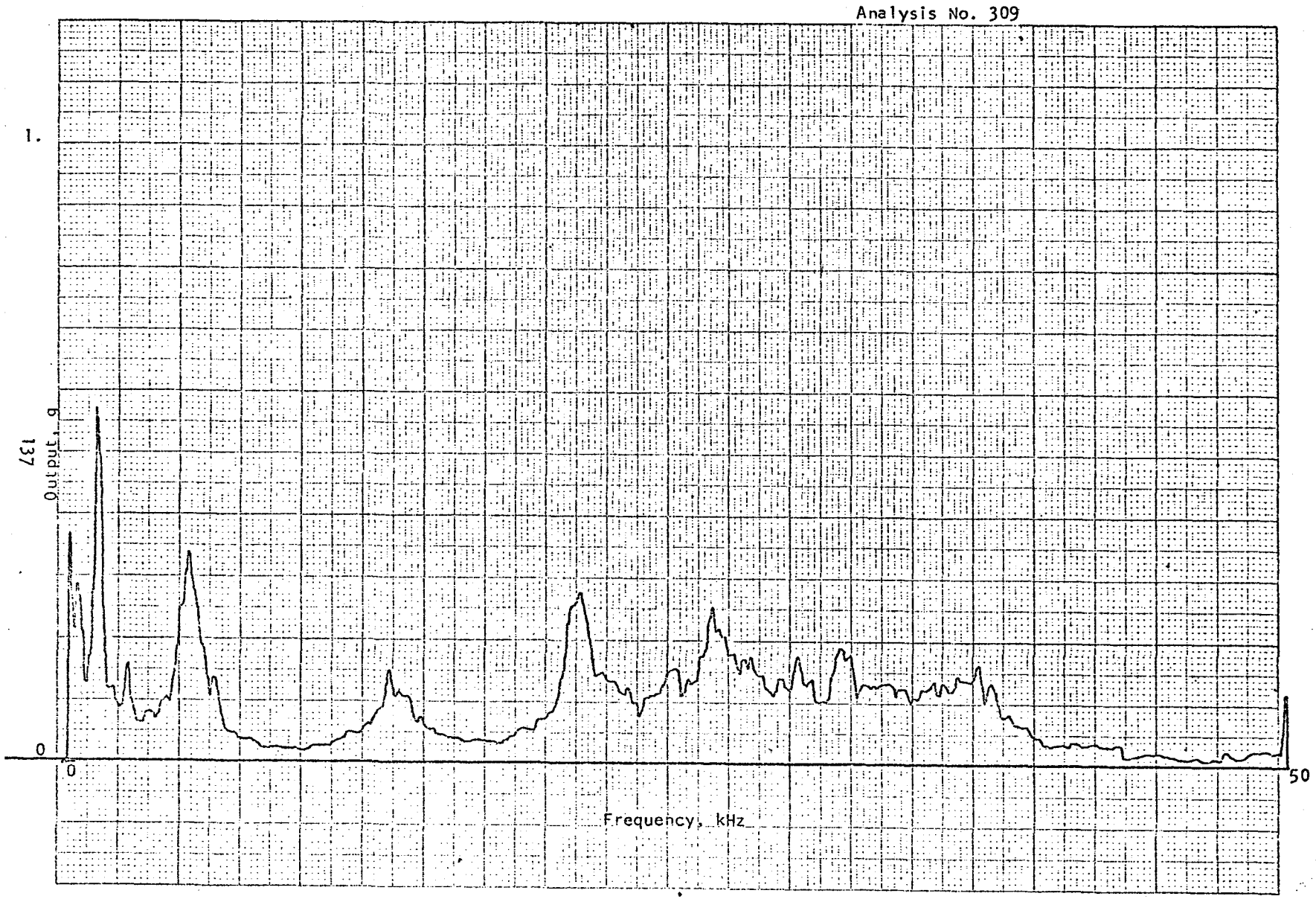

Figure 4-28 - Frequency Spectrum Analysis of Model 2236 on Run 9a.

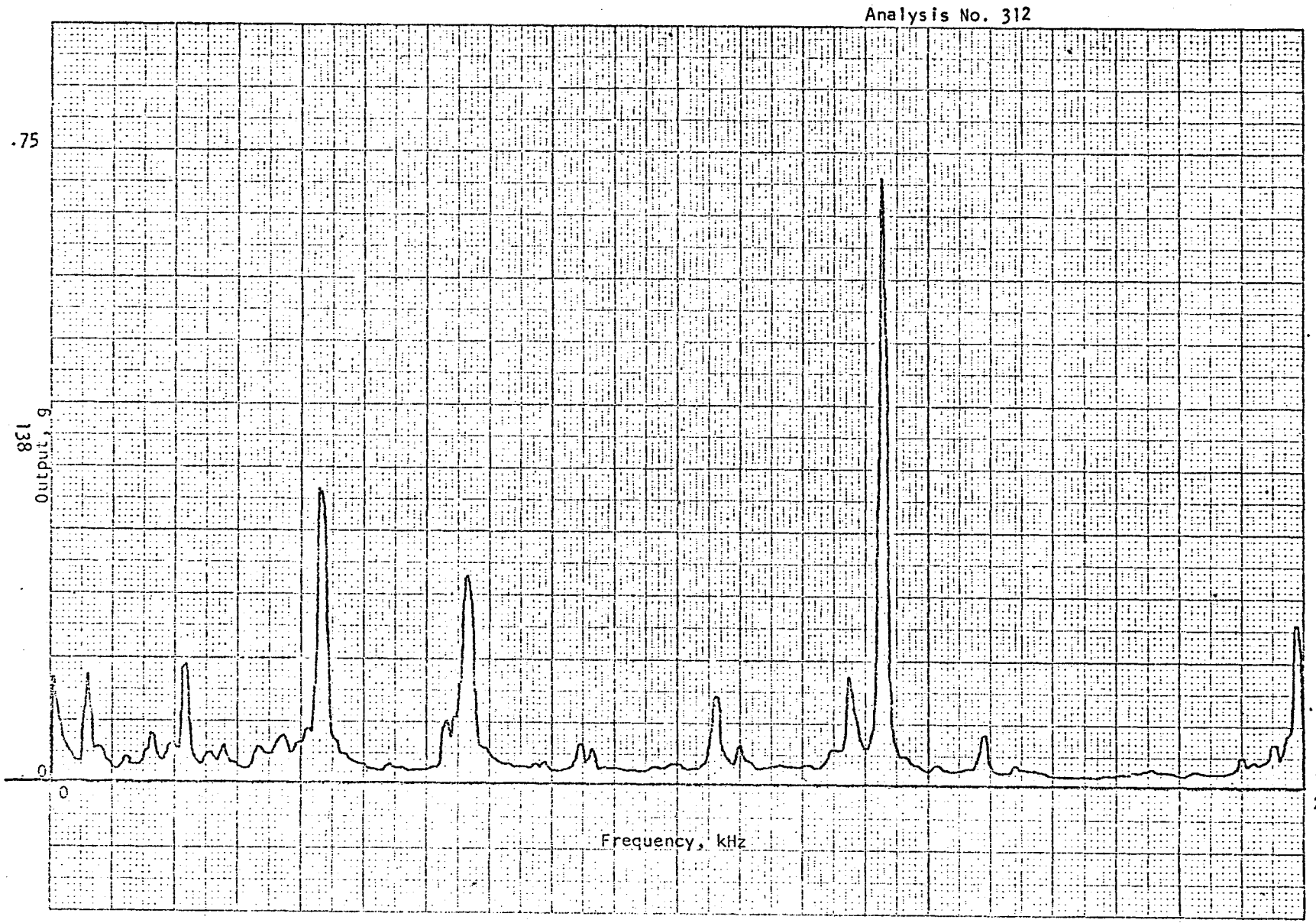

Figure 4-29 - Frequency Spectrum Analysis of Model 6230M8 on Run 9a.

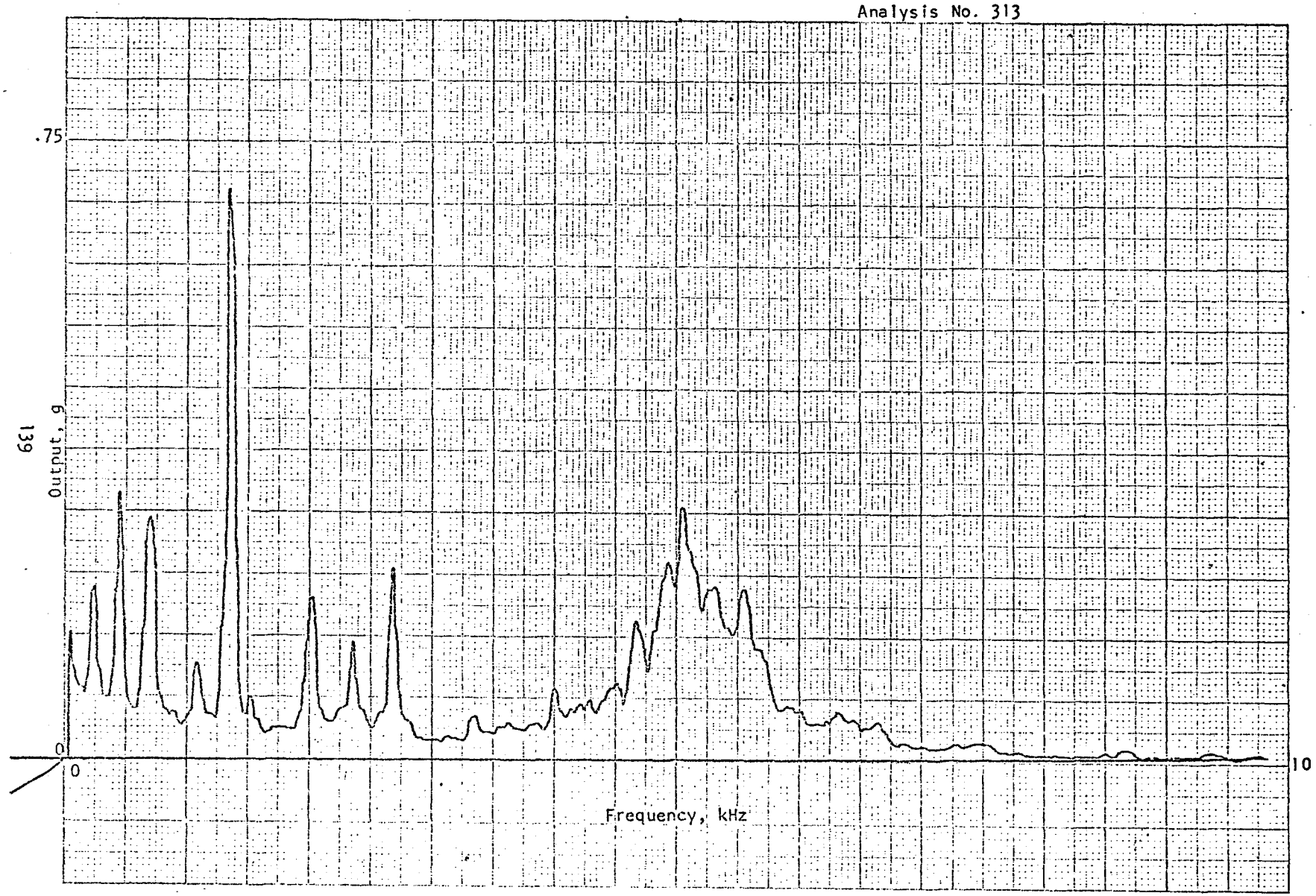

Figure 4-30 - Frequency Spectrum Analysis on Model 6230M8 on Run 9a.

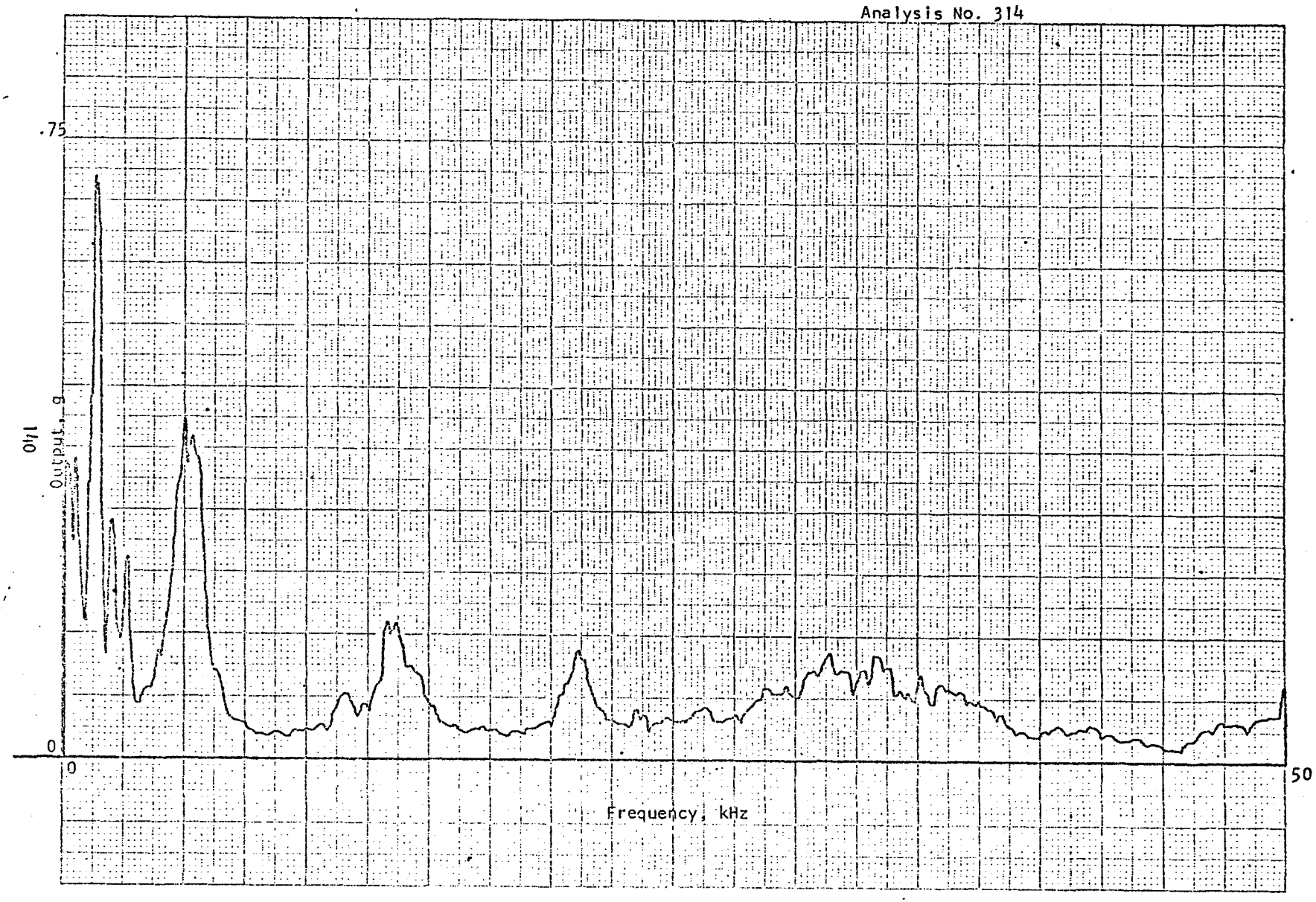

Figure 4-31 - Frequency Spectrum Analysis on Model 6230M8 on Run 9a.

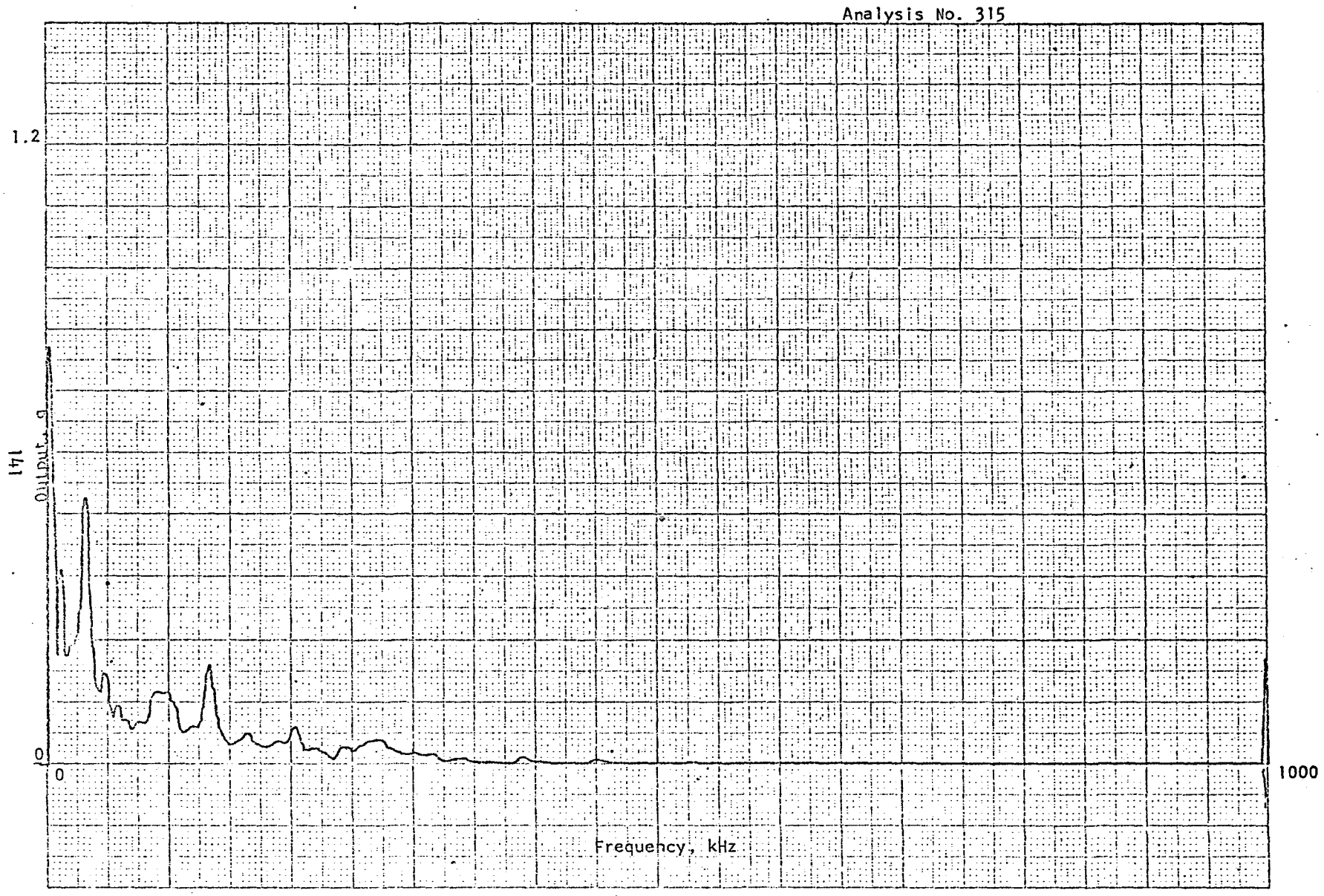

Figure 4-32 - Frequency Spectrum Analysis on Model 6230M8 on Run 9a.

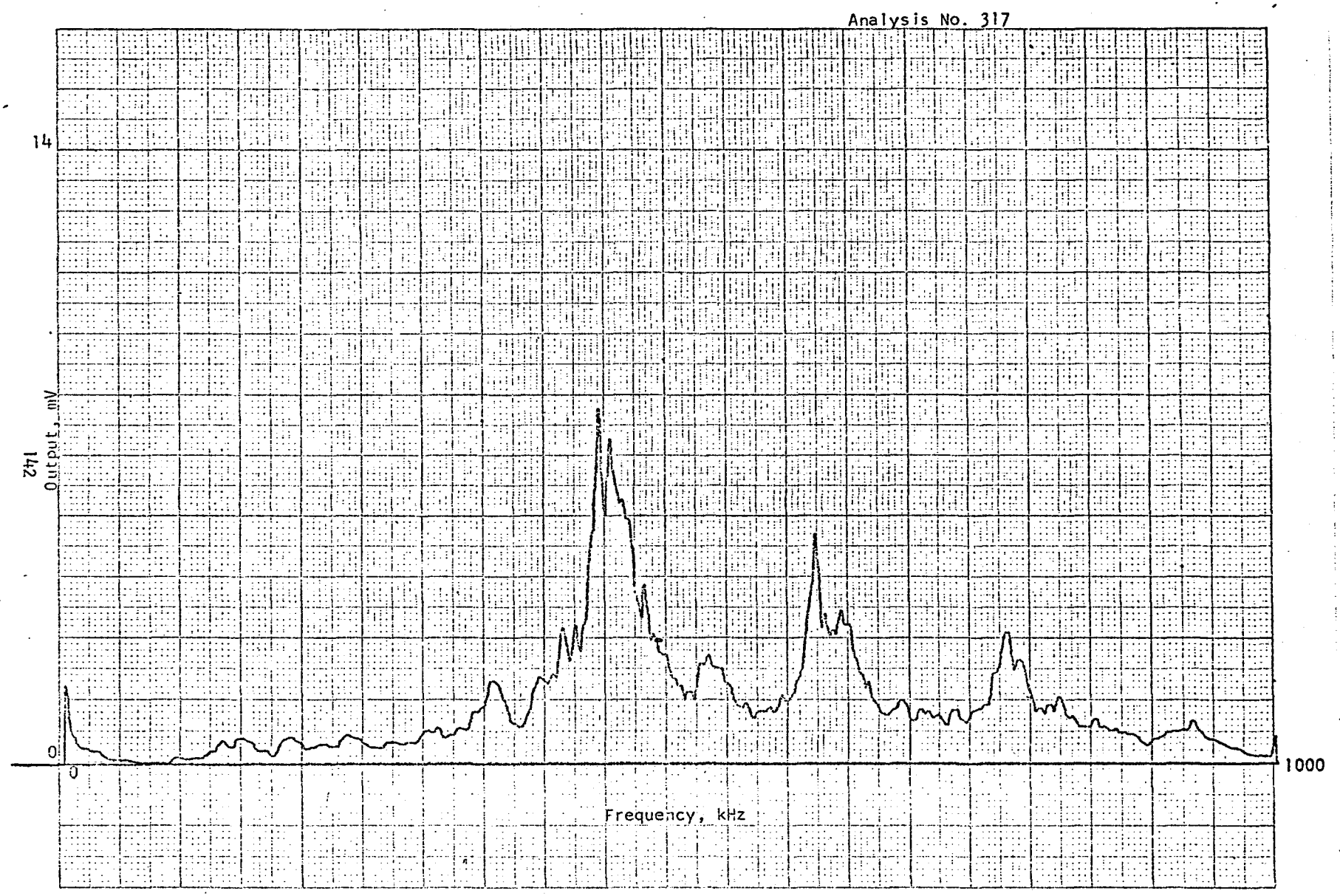

Figure 4-33 - Frequency Spectrum Analysis of Model D9202 with 40 db gain preamplifier on Run 9a.

APPENDIX V

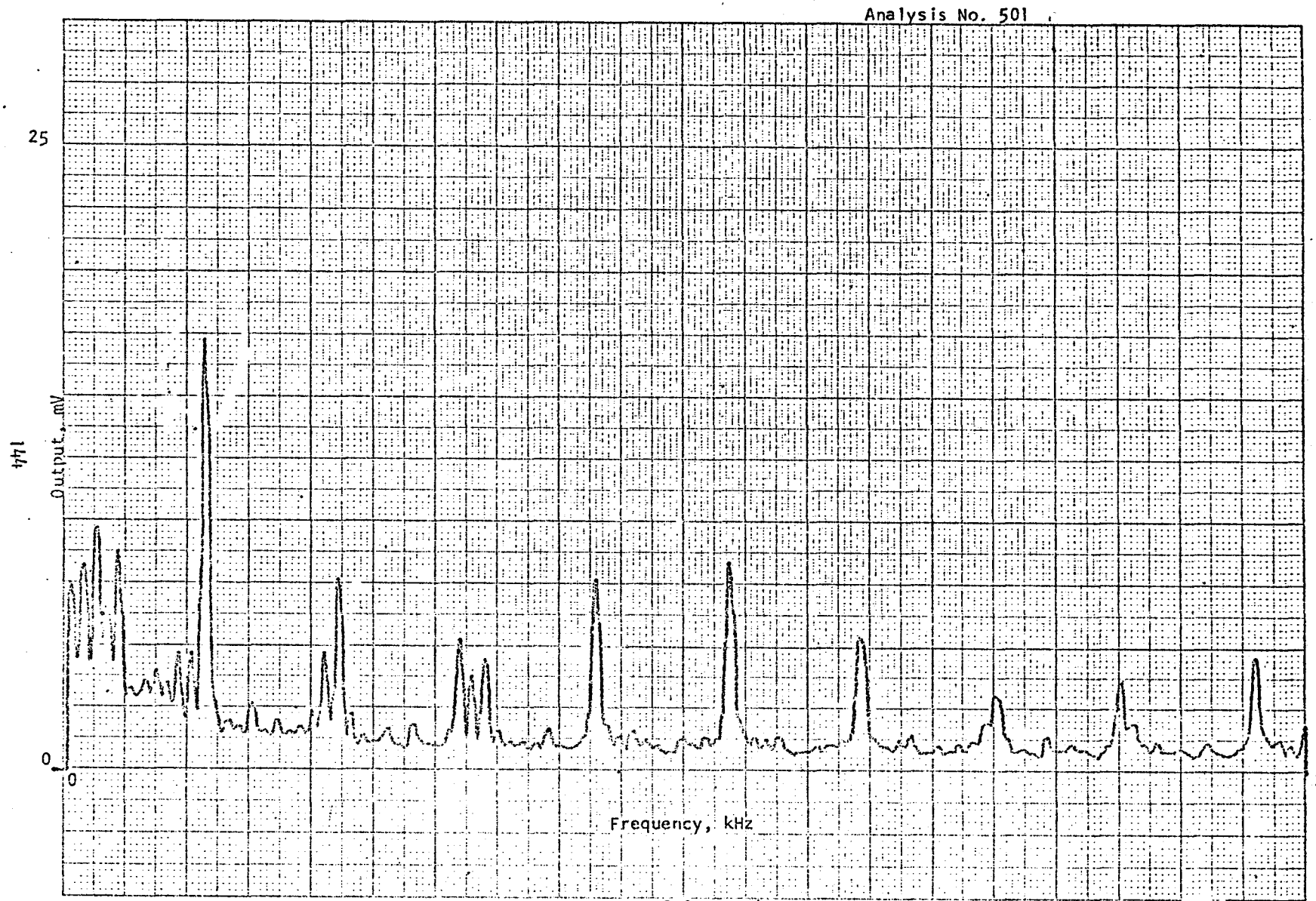

Figure 5-1 - Frequency Spectrum Analysis of Model D9202 with 40 db gain preamplifier obtained from envelope detected data at the beginning of fatigue test number one.

Multiple Pages Missing from Available Version

Figure 5-4 - Frequency Spectrum Analysis of Model 6230M8 obtained from broadband output data at the beginning of the fatigue test number one.

Figure 5-5 - Frequency Spectrum Analysis of Model 6230M8 obtained from envelope detected data at the conclusion of the fatigue test number one.

Figure 5-6 - Frequency Spectrum Analysis of Model 6230M8 obtained from broadband output data at the conclusion of the fatigue test number one.